15

THE IDENTIFICATION AND TRACKING OF AGULHAS RINGS USING SATELLITE ALTIMETRY

A thesis submitted to the
University of Cape Town
for the degree of
Master of Science in Oceanography
by
John Taunton-Clark

1993

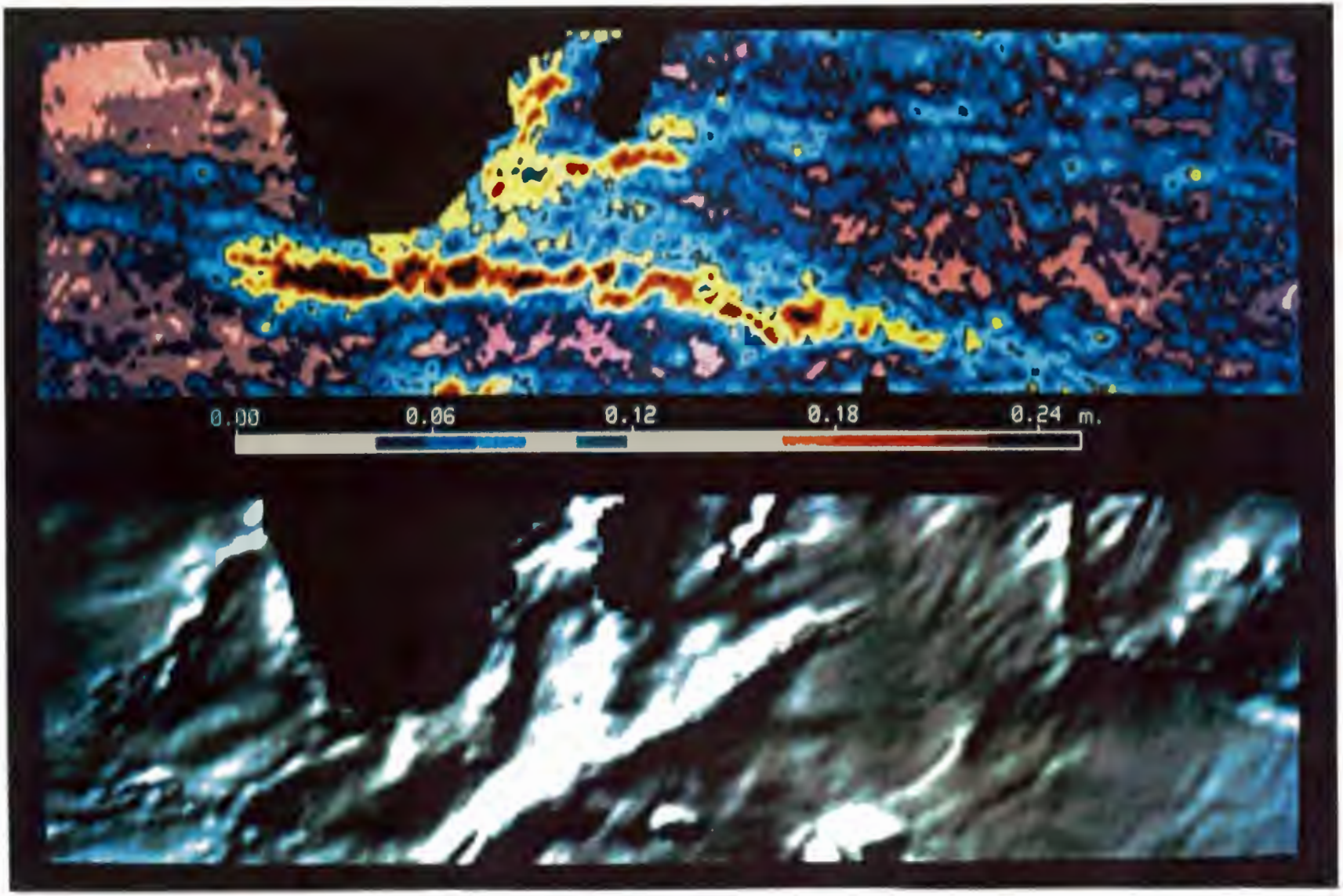

The mean sea surface and the mesoscale sea surface variability computed from an entire year of Geosat altimeter data. Main areas of variability coincide with the Agulhas Current, the Madagascar Current, and in particular with the Agulhas Return Current. Very low variabilities are observed in the South Atlantic north of the Walvis Ridge. (From TOPEX/POSEIDON Science Investigations Plan 1991)

ABSTRACT

The methods of analysing, interpreting and computing surface geostrophic currents from GEOSAT altimeter data are explained. These methods were implemented in an examination of GEOSAT altimeter data for the period 12 July 1988 to 13 May 1989 with application to the identification and tracking of Agulhas rings in the southeast Atlantic Ocean.

A population of as many as five anticyclonic (and cyclonic) circulation features of annular form consistent with that reported for Agulhas rings was identified from the altimeter data. The positive identification of the same feature in subsequent repeat cycles was, however, difficult.

The Vema ring was identified as it travelled approximately along the ground track of GEOSAT pass A158. Its horizontal (approximately 200 km diameter) and vertical (>30 cm sea surface elevation) dimensions confirmed its identity as an Agulhas ring. The translation speed of the Vema ring along pass A158 was determined as 6.8 $cm \cdot s^{-1}$ consistent with the speeds reported in the literature. Surface geostrophic speeds calculated from the altimeter-derived sea surface slopes showed maximum anticyclonic speeds of nearly 40 $cm \cdot s^{-1}$ toward the SW at the northern rim and 25 $cm \cdot s^{-1}$ toward the NE at the southern edge of the ring.

PREFACE

This project was undertaken in order to develop the ability within the Sea Fisheries Research Institute (SFRI) to archive, analyse and interpret altimeter data in preparation for our involvement in the Cape Basin Experiment component of the TOPEX/Poseidon mission which began with the successful launch from Kourou, French Guiana, on August 10, 1992.

The body of the thesis consists of five chapters. Chapter 1 provides a short introduction to the Agulhas retroflection region and briefly develops the rationale for interest in this region and the satellite altimetry techniques applied to the study of its mesoscale variability. An overview of the Agulhas retroflection, its associated rings, the responsible mechanisms and their characteristics is given in Chapter 2 so as to describe the features which will be sought in the altimeter data. Chapter 3 describes the altimetry measurement concept, the common techniques of analysis plus the specific details of the software package used. The results from these analyses are then interpreted and discussed with reference to other analyses of altimeter data for this region in Chapter 4. Concluding comments are given in Chapter 5.

Preliminary results of these analyses were published in Duncombe Rae *et al.* (1992b) and a copy of this manuscript is included as Appendix A.

ACKNOWLEDGEMENTS

My sincere thanks go to Dr.Marten L. Gründlingh of the Earth, Marine and Atmospheric Science and Technology (EMATEK) division of the CSIR at Stellenbosch. He kindly provided the Satellite Altimetry Data System (SADS) software and the preprocessed data which were used for this project as well as his ready assistance at all times. Louise Watt deserves a special note of thanks for handling the bulk of the routine data analyses and production of the original graphics.

I thank Dr.L.V. Shannon, Director: Sea Fisheries Research Institute (SFRI), for having had the foresight to involve the Institute in altimetry and for affording me this opportunity of becoming acquainted with the relevant techniques. My colleague Chris (Stretch) Duncombe Rae graciously tolerated my interminable questions and earns my gratitude. Lastly, I thank my supervisor, Dr.Frank Shillington, for his patience and guidance.

LIST OF CONTENTS

LIST OF TABLES

LIST OF FIGURES

CHAPTER 1

INTRODUCTION

The Agulhas Current retroflection region to the south of South Africa has long been known as one of active variability in the mesoscale current patterns (see Frontispiece), but only relatively recently has the potential importance of this feature and its associated rings or eddies been realised (e.g. Gordon 1985).

The path available for the circumpolar circulation around Antarctica is relatively wide between southern Africa and Antarctica and allows the exchange of warmer, more saline water from the southwest Indian Ocean into the southeast Atlantic. This may significantly influence the heat and salt balance of the Atlantic and may be, in part, responsible for this ocean's anomaly in having a net equatorward heat flux across 30°S (Gordon 1985, 1986). This transfer of heat and salt is thought to be an important part of the global thermohaline circulation and hence a vital link in understanding global climate and climate change.

Cold and very saline North Atlantic Deep Water (NADW) is formed in the North Atlantic and sinks to travel southwards, ultimately spreading into the world oceans at depth. After reaching the surface layers, mainly in the tropical regions of the Pacific Ocean, it returns via the Indian Ocean circulation (see Fig.1) (e.g. Broecker 1987 and 1991). A warm-water return path is

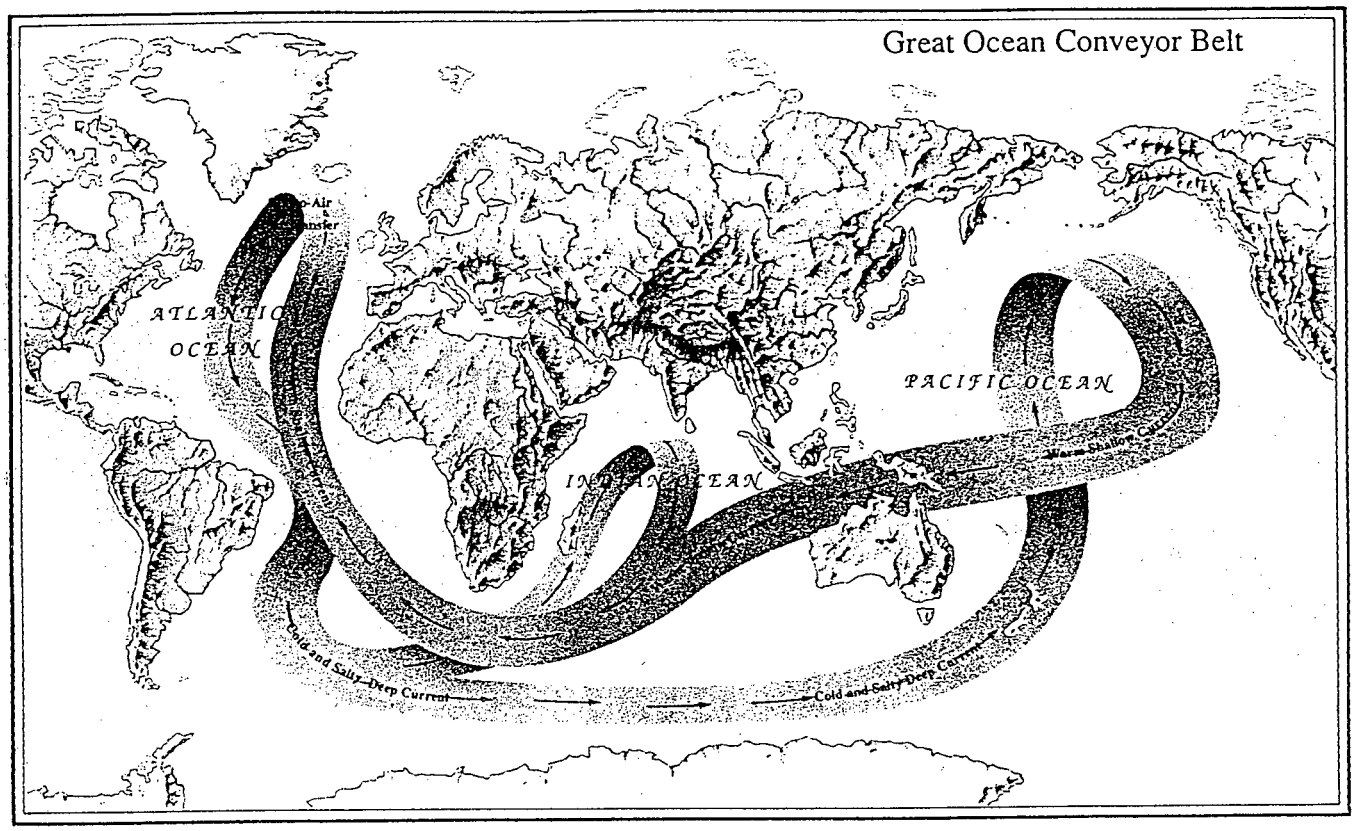

Figure 1. The great ocean conveyor logo (from Broecker 1987).

required for the intermediate and thermocline water which has to be returned to the North Atlantic to balance the production of the NADW there (Gordon 1986, Piola and Gordon 1986). The Agulhas Current provides the pathway and a significant proportion of this exchange takes place by way of ring shedding from the retroflection and by the intermittent direct leakage of Agulhas Current water into the southeast Atlantic (Gordon 1986, Olson and Evans 1986, Lutjeharms and Gordon 1987, Shannon 1985, Shannon *et al.* 1990, Gordon *et al.* 1992). Since Agulhas rings may be as much as four times as energetic as those in other western boundary currents (Olson and Evans 1986) they may, in addition to their heat and salt contributions, contribute significant quanta of energy into the relatively quiescent Benguela system (Holland 1978). The rate of production of these rings and their subsequent migration and decay are important inputs to the improvement of the understanding of regional and global ocean heat and mass balances (Van Ballegooyen *et al. in prep.*).

Intrusion of the retroflection westward into the South Atlantic and the passage of rings through the region may have significant effects on the local ocean environmental conditions and weather (Brundrit and Shannon 1989, Shannon *et al.* 1989, Duncombe Rae *et al.* 1992a,b). Large eddies of relatively warmer water may serve to modify atmospheric systems moving eastward toward the Cape, perhaps intensifying cyclonic low pressure systems or having larger-scale effects (Walker and Mey 1988, Mey *et al.* 1990, Shannon *et al.* 1990). Extensive positive sea surface temperature anomalies adjacent to the South African coast and of Agulhas

origin have been described (Shannon *et al.* 1989) and linked positively to increased rainfall over the subcontinent (Walker 1989, Walker 1990).

The dominant fish species which is exploited by the South African pelagic fishing industry is the anchovy (*Engraulis capensis*) which is spawned on the Agulhas Bank and recruits to the fishery on the west coast (Crawford *et al.* 1987). The shedding of Agulhas rings may influence the funnelling of Agulhas Bank water into the Benguela system and thereby assist in the transport of anchovy eggs and larvae into their recruitment area (Lutjeharms and Valentine 1988). The recent identification of phyllosoma larvae of what may prove to be an Indian Ocean rock lobster species (*Panulirus* spp.) in the eastern arm of the South Atlantic gyre (P.C.N. van der Byl and D.E. Pollock *pers.comm.*) suggests that ring shedding and translation may provide a mechanism for the inter-ocean and basin-wide distribution of biotic material (Duncombe Rae 1991).

Duncombe Rae *et al.* (1992b) have shown that Agulhas rings may interact with the Benguela upwelling system by the entrainment of filaments at the upwelling front. Significant volumes of water (offshore volume flux of $1.5*10^{-6}$ $m^3 \cdot s^{-1}$ - Lutjeharms *et al.* 1991) may be siphoned by this process from the Benguela frontal region, providing the potential for the loss of fish eggs and larvae from the Benguela upwelling system with the consequent impact on the recruitment potential of a fishery resource such as the anchovy (Duncombe Rae *et al.* 1992a).

An improved understanding of the interactions of the Agulhas retroflection and rings with the local environment and biota plus the ability to monitor them would be a valuable addition to the fisheries resource assessment toolbox as well as to the understanding of global climate mechanisms.

Satellite altimetric techniques offer cost-effective and relatively synoptic monitoring of the mesoscale circulation features of the Agulhas retroflection region and that influenced by their subsequent translation (Fu and Zlotnicki 1989). Altimetry, unlike thermal satellite imagery, is not defeated by the cloud cover prevalent in the region to the south of South Africa and can provide the sea surface topography and surface geostrophic current speeds on time and space scales capable of resolving Agulhas rings. The technique therefore provides a better means of determining the rate of shedding of rings and their migration than is possible with thermal imagery (where the surface thermal signal may be quite quickly masked or lost) or traditional shipborne survey methods (Gordon and Haxby 1990, Duncombe Rae *et al.* 1992b, Feron *et al.* 1992). The direct assimilation of altimetry data into numerical models is an added important benefit.

GEOSAT Exact Repeat Mission (ERM) altimeter data for approximately one year (12 July 1988 to 13 May 1989) and covering the region from 20°S to 40°S and 0°E to 20°E were analysed for the study reported in this thesis. The computer facilities available precluded the use of a longer data span, but one year was

considered to be adequate for the generation of a useful mean sea surface topography. The use of the GEOSAT altimeter results for the potential identification of Agulhas rings and tracking of their translation into the southeast Atlantic was examined, with particular reference to the "Vema" ring which had been identified from hydrographic survey data in April and May of 1989 (Duncombe Rae *et al.* 1989).

This project was undertaken in order to develop the ability within the Sea Fisheries Research Institute (SFRI) to archive, analyse and interpret altimeter data in preparation for our involvement in the Cape Basin Experiment component of the TOPEX/POSEIDON mission which began with the successful launch from Kourou, French Guiana, on August 10, 1992.

CHAPTER 2

An overview of the Agulhas Current retroflection and its associated rings

2.1 A brief description of the Agulhas Current system

The Agulhas Current is one of the world's large western boundary current systems and flows relatively close inshore along southern Africa's southeast coast between about 28°S and 35°S (see Fig.2) (Duncan 1968, Gründlingh 1983a,b and others).

The current is characterised by a relatively narrow ribbon of warm water some 90 to 100 km wide (Pearce 1977). Current speeds increase from both edges of this ribbon toward a maximum at the ($>1 m \cdot s^{-1}$) central current core which may be some tens of kilometres wide (Duncan 1968, Pearce op.cit., Grundlingh 1983a,b, Lutjeharms and Van Ballegooyen 1988). The inshore and offshore edges of the current are often convoluted and features such as shear-edge eddies may be seen from satellite thermal imagery (Harris and Bang 1974, Lutjeharms 1981a,b, Lutjeharms *et al.* 1989). The main body of the current is topographically steered, following the continental shelf slope approximately parallel to the coast (Gründlingh op.cit., Goschen and Schumann 1990). South of the southern Cape coast, at about 36°S, it exhibits meanders until eventually reaching an abrupt turnaround where it curves to the south and then flows back toward the east as the Agulhas Return Current to close the

Figure 2a. NOAA II AVHRR Ch4 thermal band image showing the Agulhas Current, its retroflection and return current (24/03/1992 from Satellite Applications Centre CSIR).

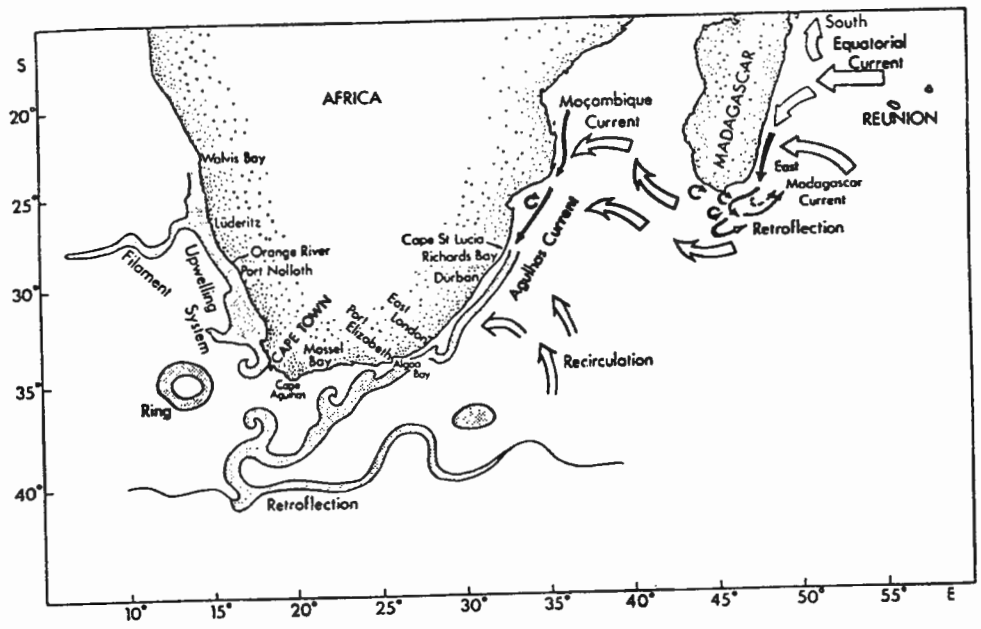

Figure 2b. A stylised view of the circulation features of the Agulhas Current (from Duncombe Rae 1991).

circulation of the South Indian Subtropical gyre (Bang 1970a,b, Gründlingh 1977, Gründlingh and Lutjeharms 1979, Lutjeharms and Van Ballegooyen op.cit., Duncombe Rae 1991). This recurvature is a consistent downstream circulation feature first documented by Dietrich (1935), named the "retroflexion" (sic) by Bang (1970a,b) and now popularly referred to as the Agulhas retroflection.

2.2 The Agulhas retroflection

2.2.1 The location and dimensions of the retroflection

Bang (1970a,b) noted from his analysis of sea surface temperatures for March 1969 that the main body of the current retroflected at about 22°E. Harris and Van Foreest (1978) and Harris *et al.* (1978) described, from their analyses of combined hydrographic data, ship's drift vectors and satellite infrared imagery, two extreme modes of final retroflection. One was at the longitude of Cape Agulhas at 20°E and the other as far west as 14°E. Although the analysis of satellite-tracked drifting buoys also showed retroflection to occur as far west as 14°E, satellite thermal (infrared) imagery did not suggest any preferred location within the range defined above (Harris *et al.* op.cit., Lutjeharms 1981b).

More recently, analyses of larger data sets based on satellite thermal imagery and hydrographic observations have allowed the compilation of some descriptive statistics for the retroflection, some of which are given in Table 1.

Table 1. Locations and dimensions of some features of the Agulhas retroflection from satellite thermal imagery (after Lutjeharms and Van Ballegooyen 1988).

	1978	1979	1982	1983	All years
Total number of image days	337	361	318	95	1 111
Number of cloudpoor days	47	53	44	31	175
Cloud poor days as percentage	14%	15%	14%	33%	16%
Retroflection position for each event (B, Fig. 3)	17°26′	18°25′	18°36′	18°27′	18°15′°E
Maximum easterly retroflection position (B, Fig. 3)	19°45′	20°50′	25°30′	20°40′	20°30′°E
Maximum westerly position of warm features	9°40′	10°00′	12°00′	10°00′	9°40′°E
Mean diameters of retroflection loop (AC, Fig. 3) (km)	374	310	332	370	342
Standard deviation of loop diameter (km)	54	78	71	53	66

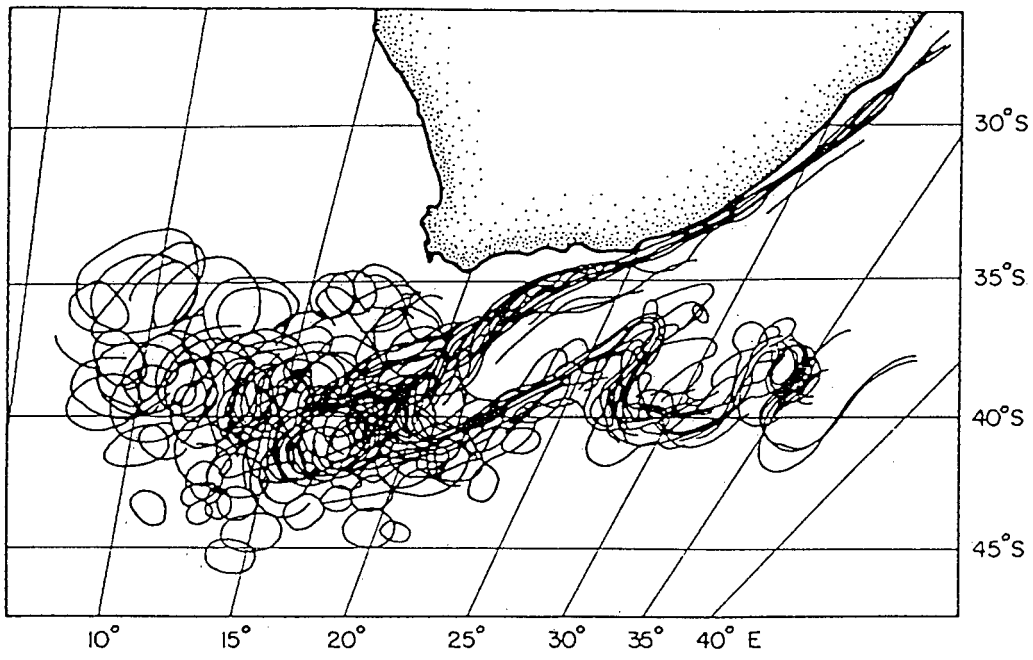

Figure 3. The variable positions of the retroflection and rings deduced from satellite thermal imagery (from Lutjeharms and Van Ballegooyen 1988).

Although the position of the retroflection was found to be highly variable, its most consistent easterly position was identified at 20°E, coincident with the location of the highest current speeds (>100cm·s^{-1}) inferred from drifters (Gründlingh 1979, Patterson 1985, Lutjeharms and Van Ballegooyen 1988)(see Fig.3). A maximum easterly retroflection position at 20° 30'E, in agreement with earlier observations, and a mean position over the four years at 18° 15'E was noted. Retroflection has, however, been seen to occur on a few occasions each year as far upstream as 25°E, perhaps induced by the downstream propagation of a "Natal pulse" (Lutjeharms 1981a,b, Lutjeharms and Roberts 1988). A secondary location of the retroflection seemed to lie at about 16°E, but its exact western extent was often obscured by the rings radiating from it. The farthest westward extent of the retroflection was observed from the declouded Meteosat imagery to be at 9° 40'E and is somewhat farther west than previous estimates (Lutjeharms and Van Ballegooyen op.cit.) although Lutjeharms (1988b) did report the possible presence of the retroflection as far west as 8°E.

The average retroflection loop diameter was found to be relatively constant from year to year with a mean of 341 ± 72 km over the period January 1978 to November 1979 (Lutjeharms 1981b) and 342 ± 66 km for the years 1978, 1979, 1982 and 1983 (Lutjeharms and Van Ballegooyen 1988) (see Table 1).

The dynamic topographies associated with Agulhas rings have been calculated from the temperature and salinity fields to give

surface relief relative to the general background of some 30 to 70 dyn cm (Harris and Van Forreest 1978 - 30 dyn cm relative to the 1000 db level; Gordon *et al.* 1987 - 50 and 70 dyn cm relative to the 1500 db level; Gordon and Haxby 1990 - 30 dyn cm relative to 3000 db; Van Ballegooyen *et al. in prep.* - 20 to 75 dyn cm relative to 1500 db). Surface topographies from satellite altimetry have yielded similar results of 30 cm or more suggesting only weak barotropic modes associated with rings (Gordon and Haxby op.cit., Van Ballegooyen *et al. op. cit.*).

2.2.2 The mechanism for retroflection

Attempts at mathematically modelling the Agulhas Current have commonly considered it as a free inertial jet where the conservation of potential vorticity and the influence of bottom topography were important in determining the course of the current (Harris 1970, Darbyshire 1972, Harris and Bang 1974, Gill and Schumann 1979, Lutjeharms and Van Ballegooyen 1984).

A net poleward flow in such a model can be sustained if the planetary vorticity change on moving southward (the ß effect) is balanced by increasing depth of the current (Robinson and Niiler 1967, Niiler and Robinson 1967). Because the depth is limiting, the current must change direction. However, since no substantial topographic feature exists in the retroflection region, it has been considered doubtful that topography is the main steering effect on the current (Lutjeharms and Van Ballegooyen 1984, Ou and De Ruijter 1986). De Ruijter (1982) modelled the current as

part of the large scale wind-driven ocean circulation incorporating inertia and showed that the model retroflection was critically dependent on the position of the zero of the wind stress curl south of South Africa. Later models incorporating baroclinicity showed the retroflection to result from an adjustment to the change in vorticity balance as the current separates from the shelf (De Ruijter and Boudra 1985, Boudra and De Ruijter 1986). After separation, potential vorticity is conserved and the gain of relative vorticity is expressed in the retroflection toward the east. Ou and De Ruijter (op.cit.) incorporated current inertia, the beta effect and the curvature of the bathymetry in their model and produced current separation at 35°S and a southernmost retroflection position at 41°S which are consistent with observations. Although their modelled retroflection was unstable, it did point to the importance of changes in the volume flux of the current in determining the current path. Varying the volume and momentum transport of the modelled current showed earlier (i.e. farther east) retroflection under conditions of increased transport (Lutjeharms and Van Ballegooyen op.cit.). Although no evidence for seasonality in the surface velocity of the current was noted by Pearce and Gründlingh (1982), seasonal changes in the volume transport may be related to changes in the subsurface velocity field (Duncan 1970). Retroflection positional shifts due to volume transport changes are consistent with the hypothesis of Gründlingh (1978) which stated that retroflection may occur farther west in summer when the flow of the Agulhas Current is assumed to be weakest.

Coastal friction may act as a sink for the latitude-induced gain of positive vorticity and was included with inertial and ß effects in the model of Boudra and Chassignet (1988). They determined that the vertical stretching component (due to bathymetric changes) was as important as the planetary vorticity component in producing the model retroflection.

More recently, Holland *et al.* (1991) have used a 5 layer, eddy-resolving, quasi-geostrophic model to investigate the time-dependant flow in the Agulhas retroflection region. They showed the value of assimilating satellite altimeter (GEOSAT) data for realistically initialising models and "to keep their forward integration on track". Although detailed modelling of the oceans around southern Africa is scarce, the retroflection of the Agulhas Current and the shedding of rings from it are features of sophisticated large scale and global eddy-resolving ocean circulation models such as those reported by the FRAM (Fine Resolution Antarctic Model) Group (1991) and Semtner and Chervin (1992).

In summary, one may see the retroflection as being governed by the total change in vorticity (due to changes in the curvature of the current path, changes in the planetary vorticity with changing latitude and changes related to bathymetry) coupled with the effects of changes in the volume transport of the Agulhas Current and possibly the curl of the wind stress south of the continent. The Agulhas is unique among western boundary currents in that it reaches the southern tip of the continent at a lower

latitude than that at which it would naturally separate and this results in its somewhat different behaviour compared to other western boundary currents (Veronis 1973, De Ruijter 1982).

2.2.3 The behaviour of the retroflection and consequent ring shedding

Lutjeharms and Van Ballegooyen (1988) showed how variable the features of the Agulhas Current are downstream of about 20°E (see Fig.3). They used the strong thermal gradients (some 4°C per 10 km) which were visible from thermal imagery to delineate the westward extremes of the retroflection position (Lutjeharms and Van Ballegooyen op.cit.). They noted that the intrusion of warm Agulhas water may extend some 500 km westward into the southeast Atlantic, but that it was not always possible to distinguish whether an intact retroflection loop or closely spaced series of rings was responsible.

Figure 4 shows a stylised view of the general behaviour of the retroflection according to which Lutjeharms and Van Ballegooyen (1988) determined their "consistent characteristics in the progradation behaviour of the retroflection". They identified consistent events wherein the retroflection exhibited progradations toward the west. The rate of westward movement was seen to increase over time until being terminated by a "sudden discontinuous jump" toward the east (Lutjeharms and Van Ballegooyen op.cit.). This is graphically displayed in Figure 5.

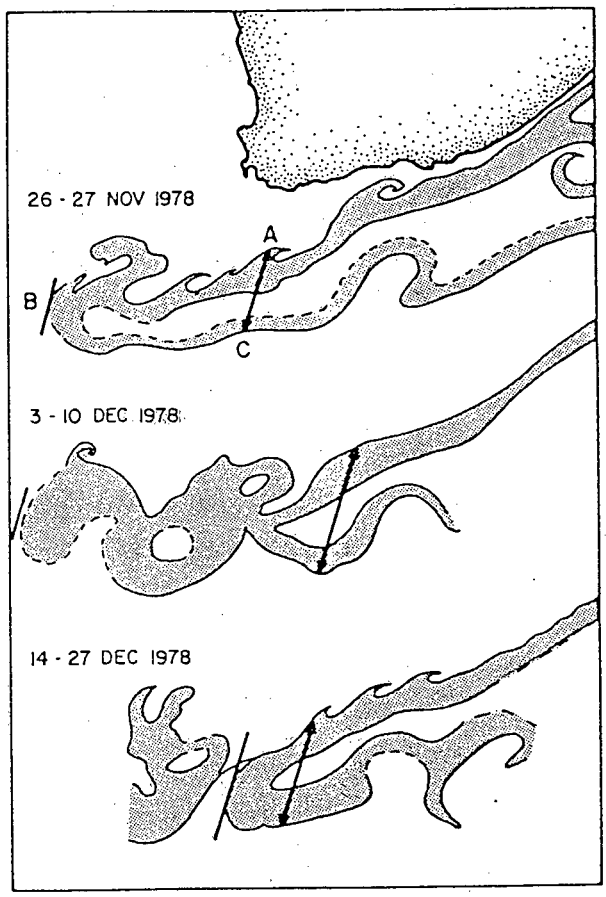

Figure 4. The typical westward progradation, current coalescence and ring-shedding behaviour of the Agulhas retroflection in 1978 (from Lutjeharms and Van Ballegooyen 1988). AC denotes the retroflection loop diameter and B the farthest westward intrusion of an intact retroflection loop.

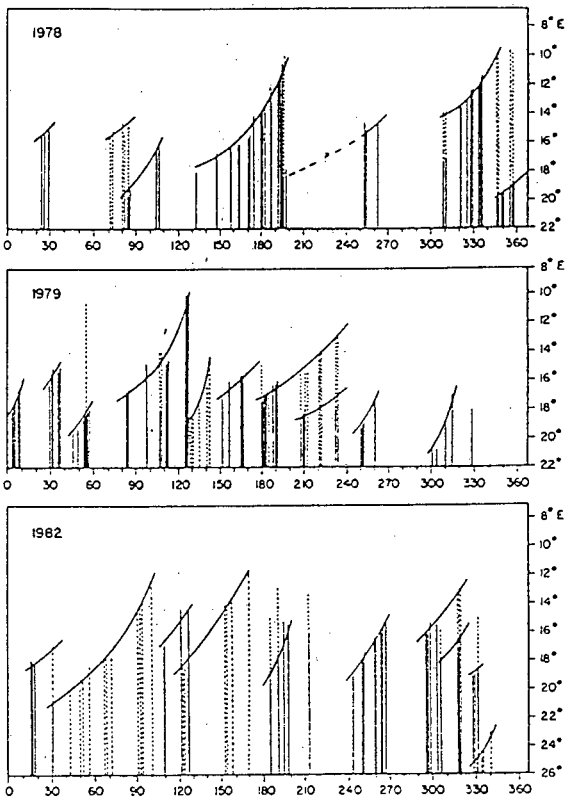

Figure 5. Zonal location of the westernmost limit of the Agulhas Current retroflection for three full years from METEOSAT thermal infrared imagery. Abscissas are in year days. Solid lines denote an intact retroflection loop. Where rings had become detached or where cloudiness made it difficult to establish the unbroken nature of the retroflection loop, represented by dotted lines (from Lutjeharms and Van Ballegooyen 1988).

Table 2. Statistics of prograding events of the Agulhas retroflection determined from satellite thermal imagery (from Lutjeharms and Van Ballegooyen 1988).

	1978	1979	1982	1983	All years
Number of cloud poor days	47	53	44	31	175
Mean period of each event (days)	55	37	32	30	39
Mean rate of westward progradation (cm s^{-1})	7	13	14	15	12

Lutjeharms and Van Ballegooyen (1988) determined a mean westward progradation rate of 12 $cm \cdot s^{-1}$ and a mean event duration of some 39 days, neither of which exhibited any seasonal variation (see Table 2). They also proposed that each progradation event culminated in the shedding of an Agulhas ring. From three years of data (1978, 1979 and 1982) they calculated an average of nine rings shed per year at just more than one month intervals.

Satellite altimetry results have indicated that at least five rings are shed per year (Gordon and Haxby 1990). Van Ballegooyen *et al.* (*in prep.*) report 14 rings over the two years 1987 and 1988 which they convert to a shedding rate of one every two months. Feron *et al.* (1992) produced a correlation matrix showing the time delays (average of four weeks) over which sea surface height anomaly features (from GEOSAT altimeter data for November 1986 to September 1989) within the Agulhas retroflection region become decorrelated (see Fig. 6). The "small islands of high correlation" observable in Figure 6a show that after several weeks the current again asumes its earlier position. Figure 6b and 6c shows the correlation matrix transformed so that the y axis represents time relative to the x axis time. The peaks apparent in Figure 6b and 6c represent periods of stability in the Agulhas retroflection pattern. Feron *et al.* (op.cit.) suggest that the relatively rapid changes toward less stable patterns which occur after these peaks indicate the shedding of a ring and the subsequent return of the retroflection to a previous location. This seems to be consistent with the behaviour described by Lutjeharms and Van Ballegooyen (1988). Figure 6c

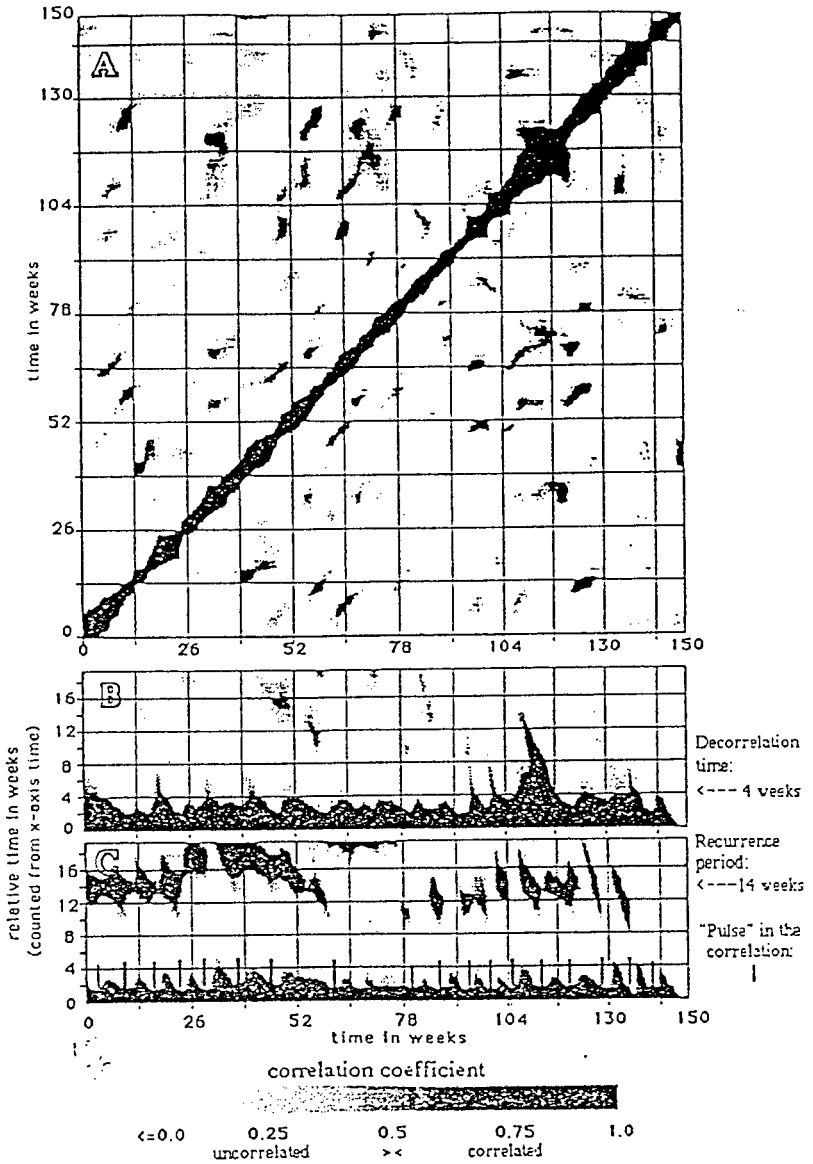

Figure 6. a. The correlation matrix in the Agulhas retroflection area showing the return of the sea surface anomaly field to a previous pattern after some time period.
b. The correlation matrix transformed so that the y axis represents time relative to that on the x axis. This shows an average decorrelation time of four weeks.
c. The matrix transformed via principle components analysis and harmonic analysis to contain 80 % of the normalized variance.
18 pulses in the correlation time suggests that is how many rings were shed over the three years (from Feron *et al.*1992).

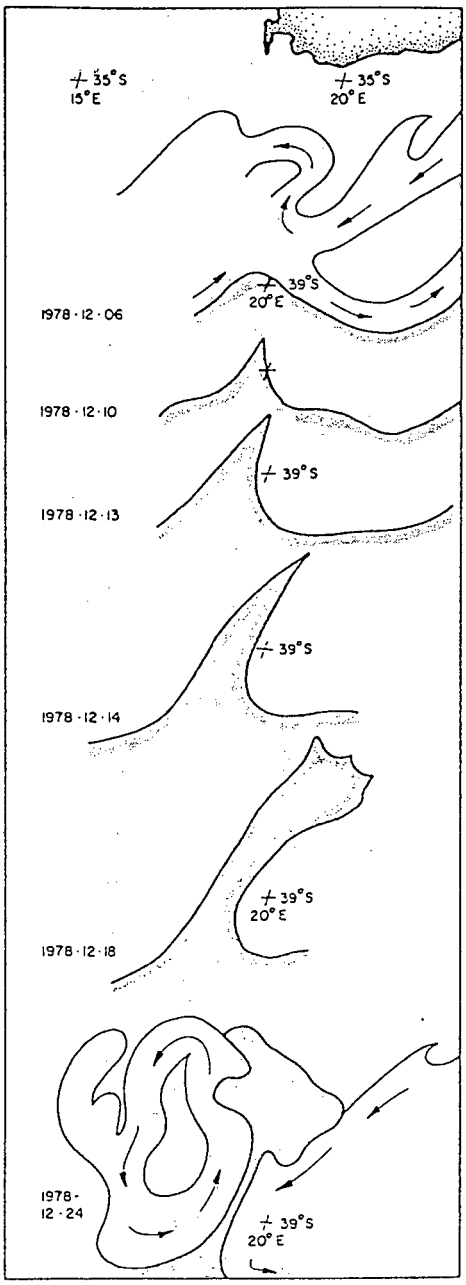

Figure 7. The characteristic development and shedding of an Agulhas ring as observed from satellite thermal imagery (from Lutjeharms and Van Ballegooyen 1988).

shows some 18 of these peaks over the three year period of observation which confirms an average ring-shedding rate of 6 per year. Contrasted with the reported ring-shedding rates of two per year for the East Australian Current (Nilsson and Creswell 1981), the rate for the Agulhas is quite high, but not as high as the one per week reported for the Brazil Current (Legeckis and Gordon 1982).

In their analysis of satellite thermal imagery, Lutjeharms and Van Ballegooyen (1988) showed how most cases of ring shedding were preceded by the genesis and growth of a cold wedge of Subantarctic Surface Water at the subtropical convergence as shown in Figure 7. They proposed a mechanism, revealed in Figure 8, whereby closure of the retroflection loop onto itself results in this cold wedge being drawn equatorwards and finally separating the ring from the retroflection (see also Lutjeharms and Gordon 1987, Gordon *et al.* 1992). This is consistent with the wind-driven, baroclinic model of Boudra and De Ruijter (1986) from which it was concluded that ring formation was dependant on the closure of the retroflection onto itself and the interaction with the cold, low potential vorticity, eastward currents to the south. Such a mechanism for ring spawning may be influenced or precipitated directly by perturbations in the Agulhas Current itself. Changes in volume transport may influence the location of the retroflection and perhaps the downstream growth of current meanders may be agents of ring shedding (Lutjeharms 1981b, Lutjeharms and Van Ballegooyen 1984).

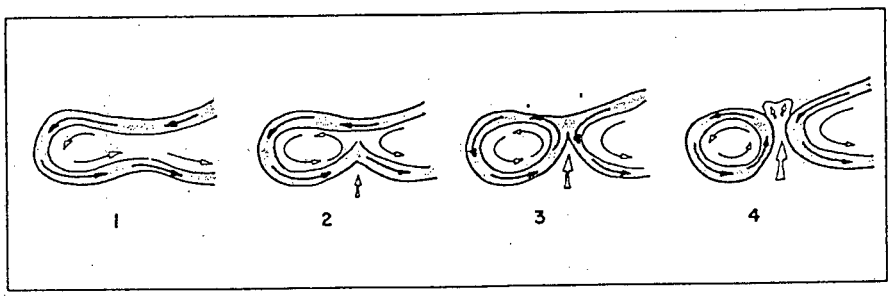

Figure 8. A conceptual image of the initiation (2), development (3) and separation (4) of an Agulhas ring from the retroflection (from Lutjeharms and Van Ballegooyen 1988).

Table 3. Parameters measured for some of the rings listed in Table 5. Radius is the radius of the maximum radial velocity, with values in parentheses indicating estimates; h_{10} is the depth of the 10°C isotherm at the ring centre; δh_{10} is the difference between the depth of the 10°C isotherm at the centre and at the edge of the ring; v_t and v_r refer to the translation and maximum radial speeds respectively (negative speeds indicate anticyclonic flow); APE is the available potential energy; KE is the kinetic energy.

Ring	Radius (km)	h_{10} (m)	δh_{10} (m)	v_t (cm·s^{-1})	v_r (cm·s^{-1})	APE (×10^{-15}J)	KE (×10^{-15}J)
R83.1	115	750	370	4.8	−60	30.5	6.2
R83.2	130	740	420	8.5	−90	51.4	8.7
R83.3	90	560	140	?	−29	?	?
R87.1	(130)	425	145	?	?	?	?
R87.2	(150)	700	350	?	?	?	?
R87.3	(100)	650	300	?	?	?	?
R87.4	(115)	770	455	?	?	?	?
R87.5	(140)	520	370	?	?	?	?
R87.6	145	520	300	8.3	−43	?	?
R89b	145	600	300	6.4	−55	38.8	2.3
R90.4	90	870	510	?	−60	26.2	2.6

Table 4. Some characteristics of Agulhas rings deterined from hydrographic and GEOSAT altimeter data (from Van Ballegooyen *et al. in prep.*).

Eddy	Altimetric Height[1] (cm)	Initial dimension[2] (km)	Dimension[3] from individual pass (km)	Period	Drift speed ($cm.s^{-1}$)	Hydrographic dimensions[4] (km)	Max Dynamic Height anomaly[5] (cm)
A1	<20	-	-	Jan 87 - Apr 87	4.7	260	20
A2	30-40	130	230	Jan 87 - Apr 87	6.0		50
A3	<20	-	-	Feb 87 - Aug 87	4.0	310	45
A4	50-60	190 x 300	250 x 280	Dec 86 - Sep 87	9.0	245 x 280	60
A5	35-40	100	200	Jan 87 - May 87	3.7	190	31
A6	30	80 x 160	-	Jan 87 - Nov 88	5.4	220 x 290	31
A7	40-50	240 x 550	-	Dec 86 - Nov 87	6.4	-	65-75
A8				Dec 86 - Jun 87	6.4		
				Jun 87 - Dec 87	1.0		
				Dec 87 - Jun 88	1.6		
				Jun 88 - Dec 88	2.1		
C1	-40	160	-	Jan 87 - Dec 87	4.6	-	

[1] Taken from interpolated altimeter data above the altimetric mean sea level
[2] Taken from the interpolated snapshots at the + 20 cm contour
[3] Taken from individual passes at the 0 cm contour (background)
[4] Taken from the 10°C/300 m intercept contour
[5] Determined as the anomaly of the dynamic height (calculted relative to 1500 dB) with respect to reference dynamic height of 153 cm

2.2.4 The characteristic dimensions and flow velocities associated with Agulhas rings

Satellite thermal imagery suggests that typical ring diameters are similar to those for the retroflection loop at about 340 km (see Tables 3 and 4) (Lutjeharms and Van Ballegooyen 1988). GEOSAT altimeter data have defined eddy diameters of 350 km (for May 1987 - Gordon and Haxby 1990), 100 to 300 km (July 1987 to July 1988 - Wakker *et al.* 1990b), while that for 1989 showed diameters in the range 200 to 300 km (Duncombe Rae *et al.* 1992b). Hydrographic data on Agulhas Current rings have shown diameters from about 180 km to 300 km (see Table 3), but these values will vary according to the criteria chosen to define the edges of the rings. Table 4 gives the characteristics of the eight eddies tracked by Van Ballegooyen *et al.* (*in prep.*) from GEOSAT altimetry and verified by hydrographic results.

Although a range of eddy-like features may be shed from the retroflection and propagate into the southeast Atlantic, rings were specifically defined as having "definitive annulus characteristics" by Lutjeharms and Van Ballegooyen (1988). The "retroflection ring" reported by Gordon *et al.* (1987a,b) and the "Vema" ring reported by Duncobe Rae *et al.*(1992b) were shown to be highly elliptical in shape with major to minor axis ratios of approximately 2:1. This is reiterated by Van Ballegooyen *et al.* (in prep.) who suggest that recently shed rings or those that have in some way interacted with the parent current will have irregular shapes.

The surface thermal signature of rings may be relatively quickly masked as a result of the large sea/air temperature differences causing a rapid transfer of heat from the ocean to the atmosphere (Walker and Mey 1988, Lutjeharms and Gordon 1987, Duncombe Rae 1991). The subsurface signature of rings, however, extends to depths as great as 4000 m (Gordon and Haxby 1990). A central, mixed isothermal core is evident in some rings extending to a depth of about 100 m (Van Ballegooyen *et al. in prep.*) or to 300 m in the case of a "winter" ring which suffered greater heat loss to the relatively colder winter atmosphere and hence deep convective mixing (Duncombe Rae 1991). Isotherm depression at the ring centre relative to its edge may be between 140 m and 510 m with typical depressions of 300 m to 400 m (see Fig. 9) (Duncombe Rae op.cit.) The salinity structure generally follows that of the temperatures (see Fig. 9). Surface salinities within Agulhas rings are higher than those typical of Agulhas surface waters and may be increased by evaporative losses (Van Ballegooyen *et al.* op.cit.).

Olson and Evans (1986) reported thermocline (10°C isotherm) depression of 400 m and 700 m for their northern and southern rings respectively (see Fig. 10). They noted greater scatter in the depth of this isotherm at the outer edges of the ring as a consequence of a tilt in the large scale thermocline. This slope of the background thermocline suggests that the rings were embedded in a large scale background flow.

Agulhas rings are characterised by an anticyclonic sense of

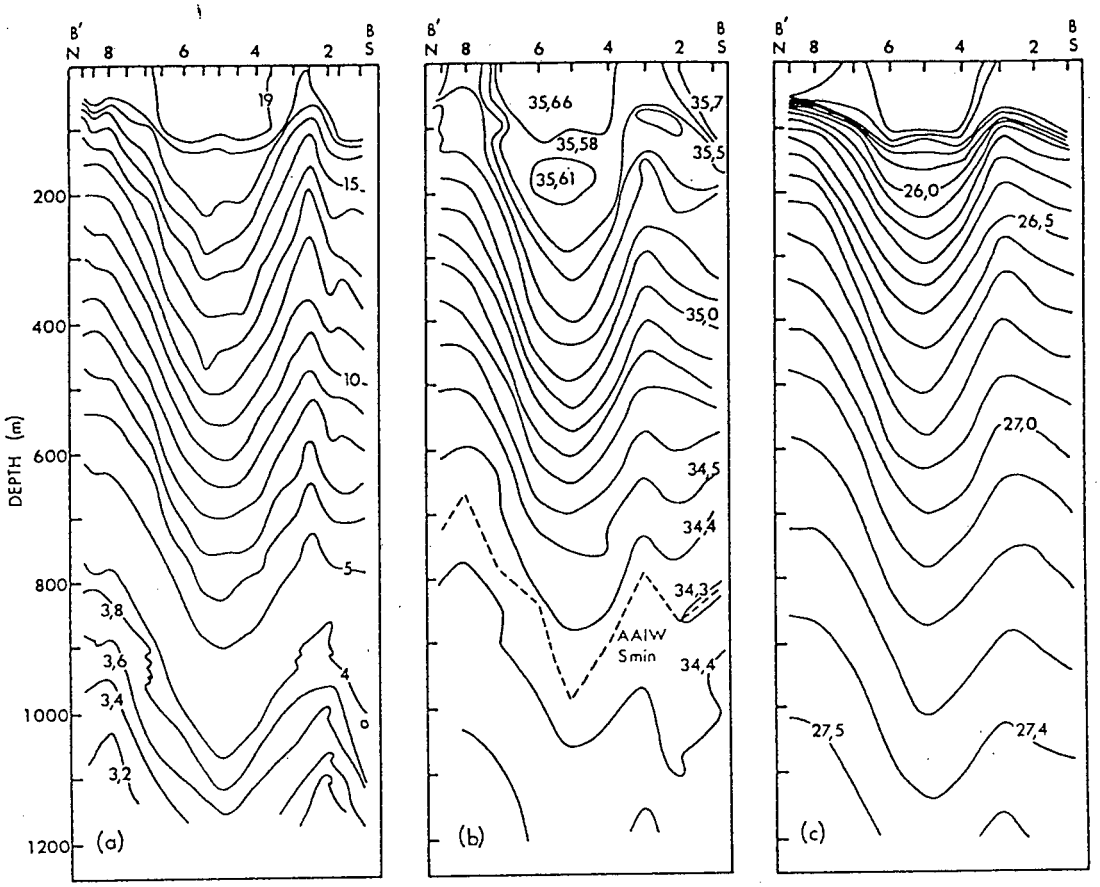

Figure 9. South/north section across the Vema ring (May 1989) a. temperature (°C), b. salinity (x 10^{-3}), c. density ($kg \cdot m^{-3}$) (from Duncombe Rae *et al.* 1992b).

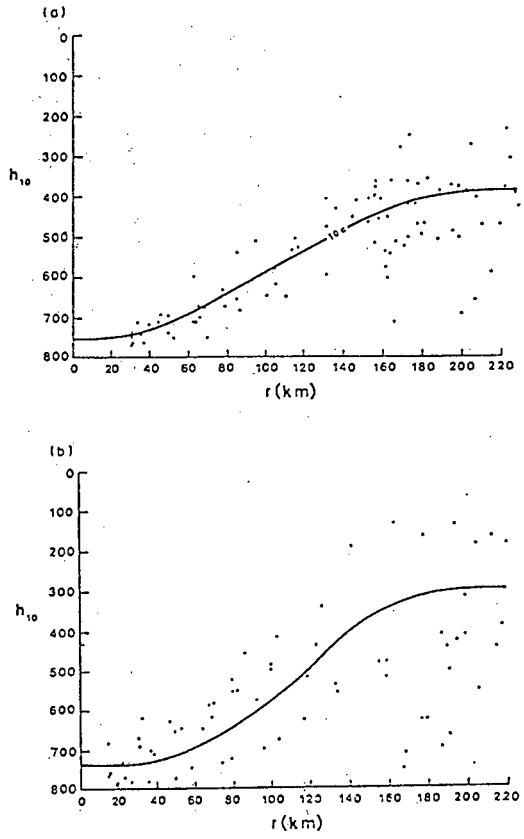

Figure 10. Azimuthal mean distribution of the depth of the 10°C isotherm in (a) the northern and (b) southern Agulhas rings studied by Olson and Evans (1986). Individual measurements of the 10°C depth are given by dots. The mean is hand drawn and is forced to have zero slope at r = 0 or at very large radii consistent with the boundary conditions on a symmetric vortex (from Olson and Evans 1986).

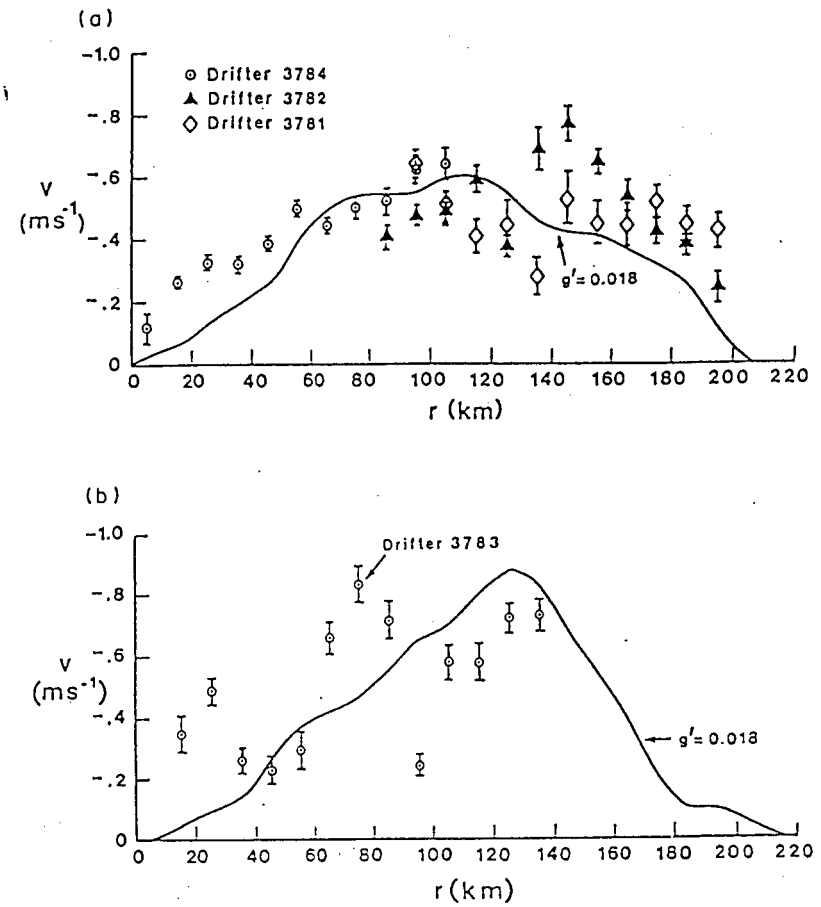

Figure 11. The azimuthal velocity around the (a) northern and (b) southern rings described by Olson and Evans (1986) as a function of radius from the ring centre. Solid curves are based on the 10°C isotherm depths (see Fig. 10) and the gradient balance equation with an empirical g' (from Olson and Evans 1986).

rotation with velocity maxima toward the outer edges of the rings (Olson and Evans 1986). Table 3 shows the radial speeds encountered to range from some 29 $cm \cdot s^{-1}$ to 90 $cm \cdot s^{-1}$. Azimuthal velocities calculated as a function of radius from the ring centre for the two rings investigated by Olson and Evans (op.cit.) are illustrated in Figure 11. Excess momentum inside the radius of maximum velocities which has been measured by drifters may indicate a coherent barotropic mode superimposed on the ring interior. Olson and Evans (op.cit.) reported that this excess momentum relative to that inferred from the baroclinic field may be a common feature of anticyclonic rings.

The range of translation speeds of hydrographically detected rings lies between 4.8 $cm \cdot s^{-1}$ and 8.5 $cm \cdot s^{-1}$ (Olson and Evans 1986, Duncombe Rae 1991). GEOSAT altimeter results showed translation rates of 5 to 8 $cm \cdot s^{-1}$ (Gordon and Haxby 1990), 4 to 8 $cm \cdot s^{-1}$ (Wakker *et al.* 1990b) and 1 to 9 $cm \cdot s^{-1}$ (Van Ballegooyen *et al. in prep.*). The last authors reported initial rates of ring translation of 3 to 9 $cm \cdot s^{-1}$ which decreased as a consequence of reaching the Walvis Ridge where the rings were delayed and also decayed to some extent. These rates exceed those predicted from theory for the ß-induced propagation (about 2 $cm \cdot s^{-1}$ - Olson and Evans op.cit.) and suggest further evidence for a large component of their translational motion coming from the background flow in which they are embedded.

2.2.5 The translation paths of rings

Early hydrographic data have revealed large rings probably of Agulhas origin in the region to the south and southwest of the Cape, although their true nature, mechanism and consequences were not initially appreciated (Duncan 1968, Bang 1970a,b; Harris and Van Foreest 1977). The analysis of satellite infrared imagery led Lutjeharms (1981a,b) to describe the development and shedding of Agulhas rings and their subsequent translation both to the north and south of the retroflection. Similarly, Lutjeharms and Van Ballegooyen (1988) described how the retroflection and surrounding regions may at any time be populated by a number of rings of various ages and in various stages of decay (Lutjeharms and Valentine 1988). Their suggestion is that these represent rings spawned earlier and then displaced from the retroflection by their subsequent translation. Duncombe Rae (1991) compiled a table (see Table 5) and a map (see Fig. 12) giving the postions of rings in the south Atlantic detected by hydrographic survey.

These data are further supported by the evidence for the consistency in the position of rings to the SW of Cape Town identified from the locations of warm filaments seen in infrared imagery (Lutjeharms and Valentine 1988). These authors inferred the presence of rings at this location for about thirty percent of the time, but could relate no specific dynamic reason such as bathymetric features to explain the persistence. Gordon *et al.* (1987a,b) noted from hydrographic results, the presence of two rings simultaneously, one recently shed near the retroflection, the other located to the WSW of Cape Town. The data suggest that there is a preferred translation path of these rings to the NW,

Table 5. A list of rings encountered hydrographically in the South Atlantic Ocean. The rings are named chronologically according to the year encountered. The position refers to the time at which hydrographic measurements were made.

Ring	Vessel	Voyage	Date	Lat. (°S)	Long. (°E)	Source	Comment
R64.1	*Africana II*	?	64–3	40,5	15	Duncan 1968	Wide station spacing. Reversing bottles
R69.1	*Africana II*	?	69–3	35	15	Harris & Van Foreest 1978	Wide station spacing. Reversing bottles
R83.1	*Knorr*	104–5	83–11	35,5	15,4	Olson & Evans 1986	ARC (Cape Town eddy)
R83.2	*Knorr*	104–5	83–11	38,9	18,3	Olson & Evans 1986	ARC (Retroflection eddy)
R83.3	*Oceanus*	133	83–2	23,0	–5,0	McCartney & Woodgate-Jones 1991	Detected on CTD line along 23°S
R85.1	*Thomas Washington*	?	85–3	35	15,5	Bennett 1988	CTD line (Cape Town eddy 85)
R87.1	*S.A. Agulhas*	48	87–2	34,8	15,8	Lutjeharms 1987, Valentine *et al.* 1988	2 lines SCARC (ring Susan)
R87.2	*S.A. Agulhas*	48	87–2	35,9	11,6	Lutjeharms 1987, Valentine *et al.* 1988	1 line SCARC (ring Rosemary)
R87.3	*S.A. Agulhas*	48	87–2	37,7	9,5	Lutjeharms 1987, Valentine *et al.* 1988	2 lines SCARC (ring Mariaan)
R87.4	*S.A. Agulhas*	48	87–2	38,0	15,0	Lutjeharms 1987, Valentine *et al.* 1988	2 lines SCARC (ring Erina)
R87.5	*S.A. Agulhas*	48	87–2	40,9	14,4	Lutjeharms 1987, Valentine *et al.* 1988	1 line SCARC (ring Helen)
R87.6	*Discovery*	?	87–4	27,0	7,5	Gordon and Haxby 1990	1 CTD line
R89a	*Africana*	71	89–4	32,1	10,8	Duncombe Rae *et al.* in press a	1 XBT line (Vema ring)
R89b	*Benguela*	246	89–5	30,5	9,2	Duncombe Rae *et al.* in press a	R89a revisited, 3 lines (Vema ring)
R90.1	*Melville*	?	90–1	30	2	Gordon *et al.* in prep.	CTD line SAVE-4
R90.2	*Melville*	?	90–1	30	6	Gordon *et al.* in prep.	CTD line SAVE-4
R90.3	*Africana*	81	90–5	36,3	14,3	Personal observation	Feature on return from South America. Ring?
R90.4	*Africana*	85	90–7	35,3	11,7	Duncombe Rae and Shillington in prep.	Search for ring (Winter ring)

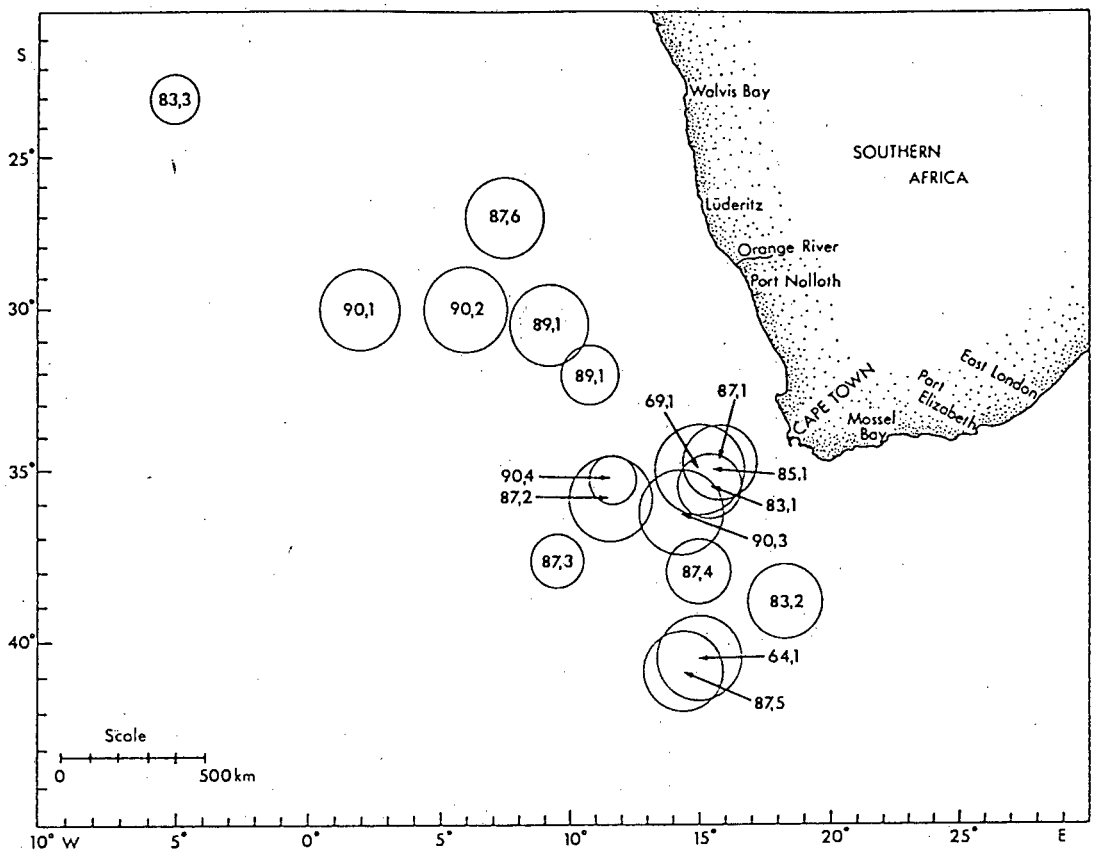

Figure 12. The positions of Agulhas rings detected hydrographically in the South Atlantic Ocean. Rings are numbered according to Table 5. The circles indicate the diameter of the maximum azimuthal velocity for each ring in Table 3. Estimated diameters are shown for rings for which no data appear in Table 3. Data sources for the rings are given in Table 5 (from Duncombe Rae 1991).

passing relatively close to Cape Town (Olson and Evans 1986, Wakker *et al.* 1990b).

Although there is some evidence to suggest that rings may propagate southwards across the Subtropical Convergence (Colton and Chase 1983, Lutjeharms 1988b), reports show translation after shedding into the south Atlantic in a generally WNW to NW direction (Olson and Evans 1986, Gordon and Haxby 1990). Analysis of GEOSAT data for 1987 and 1988 revealed that only one of the fourteen eddies identified moved southwards across the Subtropical Convergence (the same eddy reported by Wakker *et al.* 1990b) (Van Ballegooyen *et al. in prep.*).

This process of ring shedding and translation may play an important role in the local and basin scale heat balance. The rings may translate far into the South Atlantic although this was difficult to observe from satellite thermal imagery due to the relatively rapid loss of the surface thermal signature (Walker and Mey 1988). McCartney and Woodgate-Jones (1991) described a positive Agulhas ring east of the mid-Atlantic ridge in the eastern south Atlantic subtropical gyre at 5°W and 23°S. It was still an energetic feature distinguishable in the hydrographic data some 3000 km and two years distant from its shedding at the Agulhas retroflection region. The rings may cross the Cape Basin embedded in the Benguela arm of the gyre and may be delayed on encountering the Walvis Ridge before moving farther westwards.

Van Ballegooyen *et al.* (*in prep.*) mapped the paths of their eight

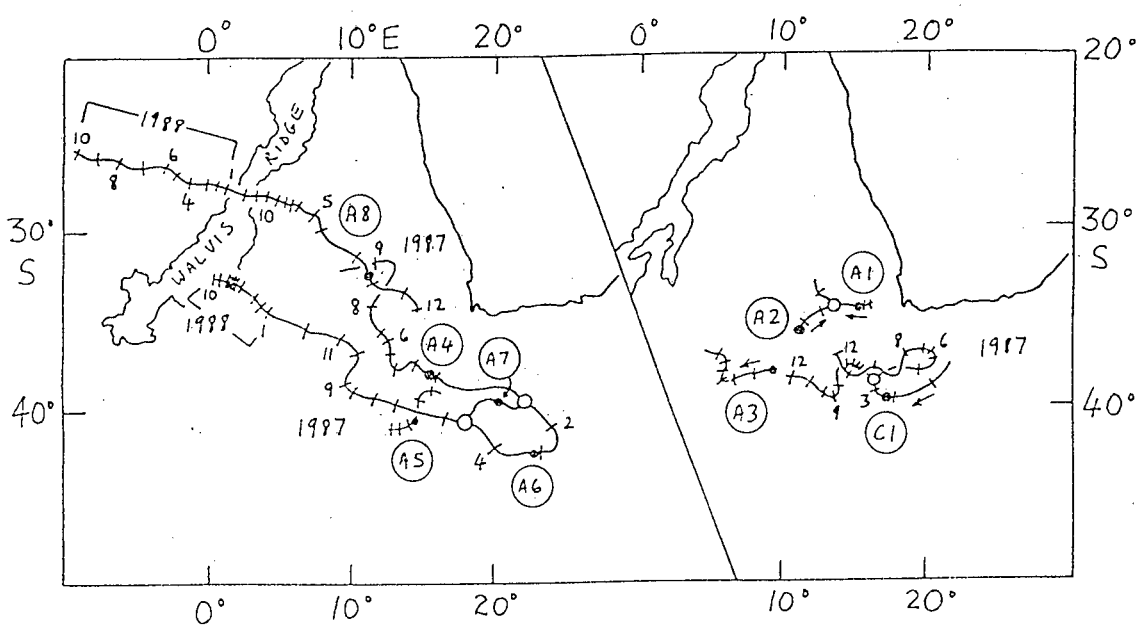

Figure 13. Movement of rings observed during the SCARC cruise and the altimetric study performed by Van Ballegooyen *et al. (in prep.)*. Dashes indicate the position at the first of each month, dots give the positions of the rings at the time of the SCARC cruise (Feb/Mar 1987) and circles show the positions of separation or coalescence (from Van Ballegooyen *et al. in prep.*).

eddies (see Fig. 13). They concluded that at short time scales the eddies may interact and move in any direction, leading to a "spaghetti-like migration pattern", but that on longer time scales they generally moved towards the west or northwest. Wakker *et al.* (1990b) and Gordon and Haxby (1990) identified the presence of numerous "densely packed" anticyclonic and cyclonic eddies in the Cape Basin. Gordon and Haxby (op.cit.) showed translation paths within an envelope of 1000 km north-south dimension and stretching towards the northwest from the retroflection (see Fig. 13). Wakker *et al.* (op.cit.) alluded to two "channels of increased variability west of South Africa in the vicinity of the Walvis Ridge", indicated from their root mean square (rms) sea surface height variability map, and in broad agreement with the results of Gordon and Haxby (op.cit.).

Wakker *et al.* (1990b) noted that the translation velocities of rings in the SE part of the Cape Basin is rather chaotic, but that equatorward of 35°S the rings begin to move with the subtropical gyre in a NW to W direction. The topography to the south and southwest of Cape Town appeared to influence the passage of rings in the south where Wakker *et al.* (op.cit.) suggested that rings preferred passage to the north of the Schmidt-Ott seamount. These authors reported that farther north the Walvis Ridge has a marked effect on the passage of rings. They further reported that rings may be delayed for some time at the Walvis Ridge and that relatively deeper pathways across the Ridge were favoured (Wakker *et al.* op.cit.).

From GEOSAT altimetry, Gordon and Haxby (1990) traced rings into the western South Atlantic between latitudes 20°S and 30°S and reaching to 30°W. These authors suggested that the rings may be entrained by the Brazil Current and so rejoin the gyral circulation and contribute to the northward flow across the equator to feed the production of North Atlantic Deep Water. It may be possible for them to be entrained by the North Brazil Current and translate more directly across the equator (Stramma 1989, Duncombe Rae 1991).

CHAPTER 3

Satellite Altimetry

3.1 The measurement of sea surface topography by altimetry

3.1.1 The altimeter measurement scheme

The first direct physical oceanographic measurements in the form of sea level and its variability were made in the 1970s by radar altimeters aboard the GEOS3 (1975-1978) and SEASAT (1978) satellites. Although GEOS3 data provided poor spatial coverage and SEASAT failed after a short lifetime, the potential of satellite altimetric techniques was clear (Douglas and Cheney 1990, Wakker *et al.* 1990a, Ray *et al.* 1991).

Satellite altimetry may be simply described as the measurement of the satellite altitude above the point on the ocean surface directly beneath it (the sub-satellite point) (Calman 1987, Smith *et al.* 1987, Fu *et al.* 1990). The GEOSAT altimeter radar antenna emitted a short pulse (102.4 μs duration) downward every 980 μs and determined the time taken, Δt, for this signal to travel down to the sea surface, reflect and return to the antenna. The radial distance between the altimeter antenna and the ocean surface, or its height above the sea, h_s, can then be calculated by:

$$h_s = c \frac{\Delta t}{2} \qquad (1)$$

where c = the speed of light (Fu *et al.* 1988, Fu and Zlotnicki 1989, Nerem *et al.* 1990, Fu *et al.* 1990 and others). This measurement, h_s, contains errors resulting from various instrumental and environmental sources which are summarised by the model below (after Nerem *et al.* 1990):

$$h = h_s+h_c+h_{iono}+h_{wet}+h_{dry}+h_{baro}+h_{otide}+h_{etide}+h_{EM}+b+\varepsilon \qquad (2)$$

where

h is the geometric distance between the satellite centre of mass and the ocean surface at the subsatellite point;

h_s is the instantaneous distance between the altimeter antenna and the ocean surface;

h_c is the correction for the displacement of the altimeter antenna from the spacecraft centre of mass;

h_{wet} is the wet troposphere correction;

h_{dry} is the dry troposphere correction;

h_{iono} is the ionosphere correction;

h_{baro} is the inverse barometer correction;

h_{otide} is the ocean tide correction;

h_{etide} is the solid Earth tide correction;

h_{EM} is the EM bias or sea state correction;

b is the correction for a possible bias in h;

ε is the contribution of random and systematic

errors to the altimeter measurement.

Corrections for signal propagation delays resulting from atmospheric dry air mass (h_{dry}), water vapour content (h_{wet}) and ionospheric influences (h_{iono}) were provided with the Geophysical Data Records (GDRs). For GEOSAT, corrections for h_{dry}, h_{wet} and h_{baro} were derived from the relevant climatology fields provided by the United States Fleet Numerical Oceanography Center (Douglas and Cheney 1990). Ionospheric retardation of the radar signal was corrected using a model scaled by the monthly average sunspot numbers (Smith *et al.* 1987). Corrections for the solid Earth and ocean tide effects were also provided with the GDRs.

The correction for the EM (electromagnetic) or sea state bias results from the tendency of the altimeter to over-read its altitude relative to a 'rough' sea surface. Surface wave troughs, because of their cusp-like shape (departure from a sinusoidal profile), reflect radar signals better than peaks (Gründlingh 1988) and this leads to underestimation of the sea surface elevation above the reference ellipsoid. Douglas and Agreen (1983) suggested corrections of some 6 to 7 percent of the significant wave height (SWH or $H_{1/3}$), but uncertainty still exists as to the preferred correction algorithm (Wakker *et al.* 1990a, Fu and Glazman 1991, and others). For this reason no corrections for sea state bias were made in this analysis (Van Ballegooyen *et al. in prep.*). Aspects of this data reduction procedure are portrayed in Figure 14.

The orbit height, h_o, is obtained by a global ground-based network of Doppler tracking stations and represents the height of the centre of mass of the satellite above an arbitrary reference, usually a standard oblate spheroid fit to the earth's shape (Calman 1987, Smith *et al.* 1987, Wakker *et al.* 1988) (see Fig. 15). The geoid height, h_g, represents a level surface or surface of equal geopotential and may be derived from historical ground or satellite-based gravity data. The sea surface would coincide with this geoid if the ocean were at rest and would vary in height, h_{sea}, relative to the reference surface by up to 100m (some say 200 m, e.g. Chelton *et al.* 1990) as a result of bathymetry and irregular mass distribution of the solid earth beneath the sea (Calman op.cit., Nerem *et al.* 1990, Wakker *et al.*1990a). Bathymetric features such as seamounts, deep ocean trenches and faults are revealed in the sea level variations (see Frontispiece). The much smaller departures from the geoid (about 1 metre) caused by geostrophic flow and other dynamic processes are termed the dynamic ocean topography η (Fu *et al.* 1990, Nerem *et al.* op.cit. and others).

Thus η may be related to h_g and h_{sea} as :

$$\eta(x) = h_{sea}-h_g(x) \qquad (3)$$

and

$$h_{sea} = h_o(x)-h(x) \qquad (4)$$

at any position x, as is shown in Figure 15.

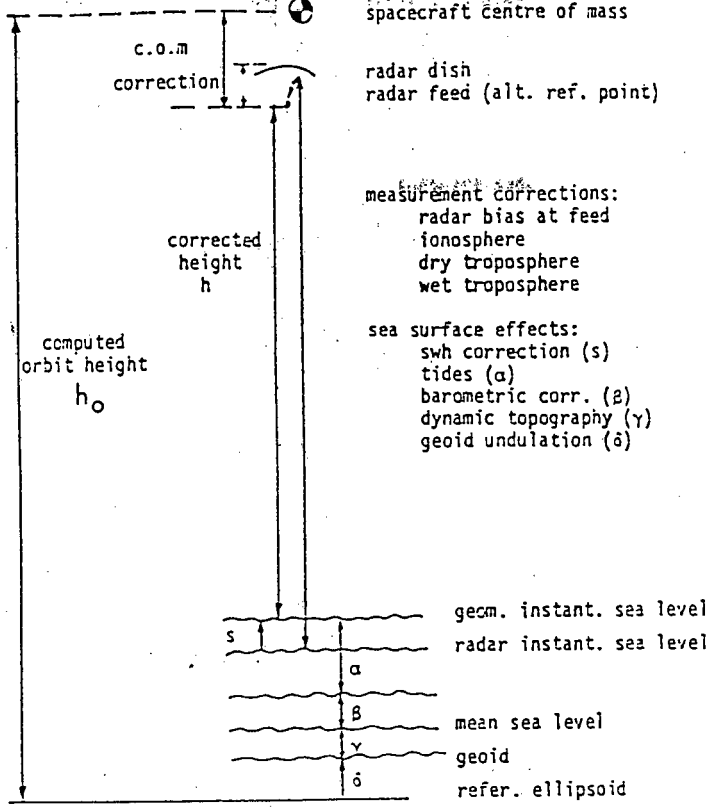

Figure 14. Altimeter data reduction scheme. Abbreviations and contractions are: c.o.m., centre of mass; alt. ref. point, altimeter reference point; corr., correction; geom., geometric; instant., instantaneous; refer., reference (from Wakker *et al.* 1988).

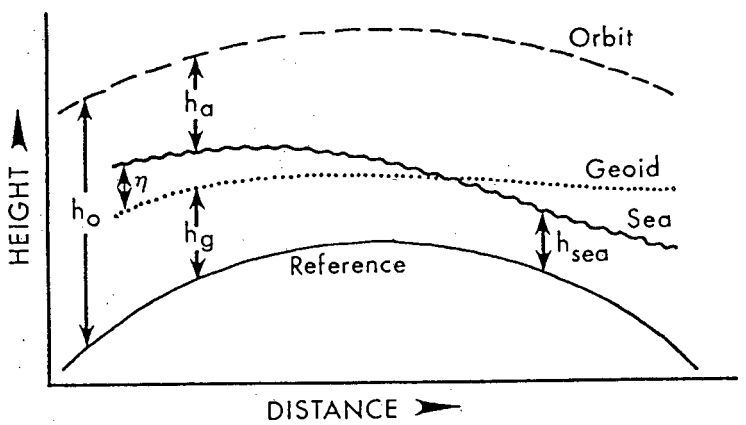

Figure 15. A definition sketch for the altimeter measurement system (from Calman 1987).

Only h is measured directly by the satellite, so much data must come from elsewhere and accuracy problems result from differences in the relative scales of observation. Satellite orbit heights are typically about 800km, while η has a maximum of just more than 1 metre. The quantity $((h_o-h)-h_g)$ represents a small difference between large numbers and is therefore sensitive to small errors in each of the terms. Since orbit height determinations were reported as the largest source of errors (random errors of about 3 m globally), this is an important point to note (Smith *et al.* 1987 and others). Fortunately, errors associated with the orbit determination vary on time and length scales much greater than the mesoscale surface topography.

Radial orbit errors are essentially long-wavelength compared to the oceanic mesoscale eddies (O(300 km)) and may be assumed to vary linearly over length scales up to 3000 km. In the method of collinear analysis used here, relative errors between subsequent exact repeat orbits are almost eliminated by removing linear trends from the altimeter measurements. This detrending also removes components of other errors remaining in the altimeter profiles (Wakker *et al.* 1988). This process is sensitive to deviations in the collinearity of exact repeat tracks of more than two kilometres, especially in areas of steep bathymetry. In the case of GEOSAT, where collinearity within one kilometre was achieved, this linear detrending is successful (Wakker *et al.* op.cit., Brenner *et al.* 1990).

Linear detrending of orbital arcs which form crossing ground

tracks is also used in the crossover differences minimization technique. The trends within the area of study are adjusted so as to minimize the crossover residuals. A potential problem is that the residuals contain no information about the slope or elevation of the sea surface as a whole (Wakker *et al.* 1988).

Numerical techniques for the removal of long-wavelength errors thus successfully remove most of the orbit error as well as the influence of the general large scale ocean circulation, leaving the mesoscale features of interest (Cheney et al. 1989 and others).

Although the geoid is relatively poorly known over many parts of the globe and geoid models may induce their own errors, it is possible to derive time-dependent currents without a geoid. Since geoidal effects are relatively time-invariant over the dominant time scales of ocean currents (<1 year), mean surface elevations may be calculated from exact repeat orbits which are substituted as a geoid (Calman 1987, McConathy and Kilgus 1987, Smith *et al.* 1987, Grundlingh 1988). Exact repeat ground tracks to collinearity of within 2 km are required, particularly in the vicinity of steep geoid gradients, in order to eliminate sea surface height variations (unrelated to ocean dynamics) which could otherwise arise (Wakker *et al.* 1988). By considering the measured sea heights and deduced η to be the sum of the time dependent and time independent or mean components of η :

$$\eta(x,t) = \bar{\eta}(x)+\eta'(x,t) \qquad (5)$$

$$h_{sea}(x,t) = \overline{h_{sea}}(x)+h_{sea}'(x,t) \qquad (6)$$

therefore the time-varying component of η is given by

$$\eta'(x,t) = h_{sea}'(x,t)-\overline{h_{sea}}(x) \qquad (7)$$

The fluctuating part of the sea surface topography (SST) can then be derived purely from satellite altimetric measurements and orbit height data by equation 5. The mean sea surface $\overline{h_{sea}}(x)$ can be computed by averaging equation 5 using repeated measurements over the same point. This effectively eliminates the need for a gravitational geoid to study ocean variability and is particularly suited to regions of high variability such as where rings and current meanders dominate (e.g. the Agulhas retroflection region). Knowledge of mean flows is unfortunately lost since the mean dynamic topographies are combined with the geoid in determining the mean sea surface, which, following equation 3, is given by:

$$\overline{h_{sea}}(x) = \overline{\eta}(x)+h_g(x) \qquad (8)$$

This seperation into mean and fluctuating components is the basis of the crossover and collinear methods of studying ocean variability (see Chapter 3.1.2).

Analyses of the altimeter return signal also yield ocean surface wind speeds and significant wave heights (SWH or $H_{1/3}$). Wind

speeds are related to the radar backscatter power or cross section and SWH to the slope of the leading edge of the return signal (e.g. MacArthur *et al.* 1987). Global measurement of these wind and wave parameters in conjunction with the ocean surface topography should also prove to be very useful to a large number of maritime organisations.

Many of the errors inherent in altimetric determination of SST occur at vastly different scales, allowing the use of filtering and other numerical methods for the separation of signal from noise. The mean values of any errors in the altimeter height measurements are included in the mean sea surface derived so only the time-varying components of these errors will affect the ultimate accuracy. The time-varying components of these errors is generally much smaller than the the mean error (Chelton *et al.* 1990). The most problematic of the atmospheric errors is that caused by atmospheric water vapour whose scales of variability can closely match those of the mesoscale ocean circulation and may result in the reduced accuracy of altimeter-measured SST. Spatial water vapour gradients in the Agulhas retroflection region may differ significantly from the climatology of the region (Mey *et al.* 1990) and may serve to reduce the elevations recorded for rings. However, since the signal from Agulhas rings is a relatively large one, this factor should not have proved problematic (Monaldo 1990). Altimeter missions following GEOSAT (i.e. TOPEX/POSEIDON) will have onboard microwave radiometers to enable accurate corrections for atmospheric water vapour to be made to the altimeter data. Generally, however, most corrections

will provide a significant reduction in the variance of SST (Ray *et al.* 1991). Further details of errors, their scales and the effectiveness of corrections are given by Wakker *et al.* (1988), Nerem *et al.* (1990), Ray *et al.* (op.cit.).

3.1.2 The crossover and collinear techniques

The crossover and collinear techniques are the two commonly used methods of deriving SST and its variability from satellite altimetric data.

The crossover technique uses the difference in measured sea surface height at two different times from locations where the satellite ascending and descending pass tracks cross each other (Calman 1987, Douglas *et al.* 1987 and others) (see Fig. 18). Because the geoidal component contained within the altimeter height measurements will be the same for all height measurements at the crossover point, the crossover difference contains no error due to the geoid. In addition to corrections for altimeter measurement errors, a reduction to the dominant radial orbit error is achieved by a correction to the ephemeris which is derived from minimising the height measurements at crossover points (Douglas *et al.* op.cit., Wakker *et al.* 1988, Leben *et al.* 1990, Nerem *et al.* 1990). Since radial orbit errors may be assumed to vary linearly over length scales of < 3000 km (Wakker *et al.* op.cit.), linear trends for each orbit segment within the region of interest may be adjusted to minimise the root mean square (rms) crossover differences. The variability of the

residual sea heights at crossovers can then be calculated and combined to produce a field of topographic variability. The crossover method was not used in the analyses presented in this thesis.

The collinear method was provided by the Satellite Altimetry Data System (SADS) (see Chapter 3.3) package and is the technique used for the analysis presented here. This method depends on the collinearity or geographical superposition of individual ascending or descending repeat passes. GEOSAT collinear ground tracks varied by ± 1 km at the equator crossing nodes from their nominal paths (Brenner *et al.* 1990). Other than in regions of extremely steep gravitational gradients (such as where very steep bathymetric gradients occur at the edge of subsea canyons, etc.) this contributed generally small errors of 1 to 2 cm (Brenner *et al.* op.cit.) and collinear tracks were assumed to be perfectly aligned (Wakker *et al.* 1988, Van Ballegooyen *et al. in prep.*).

Again it may be assumed that the geoidal component of the measurements will be identical for each collinear pass. Therefore their differences will be free of this error (Douglas *et al.* 1987). Only residual errors caused by orbit level changes, instrument error and sea level variability will be reflected by the differences (Gründlingh 1988). Much of the residual orbit error may be removed by linearly detrending the along-track height measurements (Douglas *et al.* op.cit., Gründlingh op.cit.).

The individual measurements at 1 second intervals are slightly

offset between repeat passes. Data were therefore interpolated along-track so that they co-registered spatially (Wakker *et al.* 1988, Van Ballegooyen *et al. in prep.*, and others).

The variability of the SST may be derived from the collinear differences in similar fashion to that described previously for the crossover technique. The SST for a given 17 day cycle, for example, may be derived as the departure of the collinear measurements for individual passes from the mean topographic profile computed over a nest of a number of repeat passes, thereby effectively removing the geoid and large spatial- and long time-scale components. The SST remaining represents features of the mesoscale circulation like rings and current meanders (Douglas *et al.* 1987, Gründlingh 1988, Fu *et al.* 1990, and others).

Blaha and Lunde (1992) suggest caution in the use of this time averaged representation of the geoid. Apart from the geoid and relatively time-invariant components of the SST, this mean contains a smoothed realization of the transient SST due to rings and current meanders. Several years of data may be required before adeqately smoothing out mesoscale variability in the mean. Furthermore, should the period of the repeat cycle fall within that of the mesoscale circulation, aliasing may present a problem (Tournadre 1990, Blaha and Lunde *op.cit.*). The latter authors propose the use of a selected reference pass as a way of eliminating the influence of the geoid. This approach also has drawbacks, however, since the reference pass will contain signals

related to the geoid as well as dynamic processes and may therefore induce spurious features in the departures from the reference.

3.1.3 Geostrophic flow and sea surface topography

Geostrophic flow in the ocean is defined as a balance between the horizontal pressure gradient force and the apparent Coriolis force, assuming that frictional and boundary effects may be neglected, that flow is non-accelerated and occurs in straight lines (Neumann and Pierson 1966 and others). This geostrophic approximation is applicable to ocean current systems with length scales greater than 50 km and time scales greater than 1 day (Wells 1986, Calman 1987).

Vertical pressure changes in the ocean, excluding atmospheric pressure effects, are due only to the weight of water above a given point and thus independent of water motion. This is illustrated by the vertical hydrostatic equation:

$$-\frac{1}{\rho}\frac{dp}{dz} = -g \qquad (9)$$

where ρ is water density, p is pressure, g is the gravitational acceleration and z is positive upward.

Horizontal pressure gradients exist and depend on the mass or density distribution within the ocean. These gradients are related to ocean surface slopes which may be set up by winds, for example, and to the spatial variability in the temperature and salinity of sea water. If the effects of atmospheric pressure are excluded, the sea surface may be considered to be an isobaric surface. In a well-mixed, homogeneous ocean, density will increase with increasing depth as the water is affected by the weight of water above. Isobars representing surfaces of equal pressure will be parallel to the sea surface and to the isopycnals (or surfaces of equal density). Horizontal pressure gradients within the ocean will be determined only by the sea surface slope in such barotropic conditions (Neumann and Pierson 1966 and others). Spatial variability in the density of sea water also affects the mass distribution within the ocean resulting in horizontal pressure gradients. Under these baroclinic conditions, the isopycnals and isobars will intersect. As soon as a parcel of water begins to move under the influence of a horizontal pressure gradient, the Coriolis force will act towards the left (southern hemisphere) until balancing the pressure gradient force to produce steady motion perpendicular to the gradient. The geostrophic equation defines this force balance in the x-direction as:

$$-\frac{1}{\rho}\frac{dp}{dx} = v\,2\Omega\sin\phi \qquad (10)$$

where v is velocity perpendicular to the pressure gradient, Ω is

where v_s is the surface velocity and η is the sea surface elevation with respect to the geoid and x is horizontally perpendicular to v_s (Calman 1987, Wakker *et al.* 1990a). The sea surface elevations measured by the altimeter are the sum of the barotropic and baroclinic components (Blaha and Lunde 1992). Hydrographic data on the temperature and salinity distributions can provide the relative baroclinic flows down the water column. Referencing these relative currents to the altimeter-derived surface currents will yield absolute results.

Complete derivations of the geostrophic relationship and methods are given in standard texts like Neumann and Pierson (1966), Pond and Pickard (1978) and many others.

3.2 The GEOSAT mission

The U.S. Navy Geodetic Satellite (GEOSAT) mission was initially conceived as a means of improving knowledge of the earth's gravitational field (Jensen and Wooldridge 1987, McConathy and Kilgus 1987, Douglas and Cheney 1990). The dense coverage of altimeter data which the satellite could provide would enable more accurate determination of the marine geoid necessary for the improved navigation requirements of the United States Navy. GEOSAT flew two consecutive missions known as the Primary Mission and the Exact Repeat Mission. In addition to the geodesy applications of the Primary Mission, the U.S. Oceanographer of the Navy devised the Global Ocean Applications Program (GOAP) in

order to optimise the environmental and oceanographic uses of data from both the Primary Mission and the Exact Repeat Mission (ERM).

The Primary Mission began when the satellite was launched on 12 March 1985 into an 800 kilometre altitude, 108 degree inclination orbit that provided near repeat ground tracks every three days. This mission lasted 18 months, whereafter, beginning on 1 October 1986, the satellite orbit was changed to a 17.05 day exact repeat cycle optimised for oceanographic applications. The satellite was declared operational in this ERM orbit on 8 November 1986 (Douglas and Cheney 1990). Although this mission was scheduled to end in April 1989, the satellite continued to operate until tape recorder failure in October 1989 ended the global data set (Douglas and Cheney op.cit.). The mission finally ended on 5 January 1990 when the altimeter output power dropped below acceptable limits (Wakker *et al.* 1990a). During the Primary Mission, the accuracy of measuring mesoscale sea surface topography was limited by errors in the known marine geoid which contaminated the oceanographic measurements. The exactly repeating orbit of the ERM allowed the long-term averaging of local mean sea surface along tracks which may then be subtracted from the altimeter heights to reduce the effect of errors in the geoid.

The ERM orbit provided an equatorial ground track separation of 164 kilometers, decreasing with increasing latitude to the limit of coverage at about 70° latitude north and south. In the region

of our interest in the south east Atlantic, ground track separation varies from about 110 to 140 kilometers (see Fig. 18). The spatial resolution provided coupled with the repeat cycle period of 17 days is likely to adequately resolve mesoscale eddies (Fu and Zlotnicki 1989), although this period may allow aliasing of the eddy signals. The ascending nodes, or positions where the ascending passes cross the equator as the satellite travels from south to north, of the exact repeat orbits are approximately at 1.05 + n(1.475)°E longitude, where n=0 to 244 (244 orbits of the earth within one 17 day period or cycle) (see Fig. 18) (Descending passes represent the ground track of the satellite on the same orbit, but during that period of its travel from north to south). These nodes were chosen to coincide with those of the earlier Seasat, since collinearity within about 10 kilometers (at the equator) of the Seasat tracks was a condition of the availability of the data to general users. Neighbouring passes are not completed consecutively (i.e. they are not adjacent in time), but are occupied irregularly over each cycle (see Fig. 18). This pattern is, however, exactly repeated for all cycles.

GEOSAT was equipped with a 13.5 GHz nadir-looking pulse compression radar altimeter emitting pulses of 102.4 μs duration every 980 μs (MacArthur *et al.* 1987, Sailor and LeSchack 1987, Frain *et al.* 1987 and Jones *et al.* 1987 give full details of the altimeter configuration and operation). The instrument provides three basic measurements with errors as follows:

1. satellite height to ± 3.5 cm at SWH of 2 m;
2. SWH to ± 10 percent of the SWH or 0.5 m, whichever is the greater;
3. wind speed to 1.8 ms^{-1} over the range 1 to 18 ms^{-1}.

The GEOSAT data from the ERM period were distributed on a monthly basis by the U.S.A. National Aeronautics and Space Administration's (NASA) National Oceanographic Data Center (NODC) as Geophysical Data Records (GDR). Each GDR contained the 1-second along-track averaged height measurements (see Chapter 3.4) and the various accompanying corrections. Details of these corrections and the compilation of the GDRs may be found in the "GEOSAT Altimeter Geophysical Data Record: User Handbook" (Cheney *et al.* 1987).

3.3 The Satellite Altimetry Data System

3.3.1 Introduction to the package

The software package employed for the analysis of the GEOSAT data was provided by Dr.M.L.Gründlingh of the Division for Earth, Marine and Atmospheric Science and Technology (EMATEK) of the CSIR at Stellenbosch. The Satellite Altimetry Data System (SADS) emanated from a project initiated by Dr.Gründlingh. This project entailed the development of a computer data management and analysis system for satellite altimetry data based on the standard processing methods.

The design, development and implementation of the SADS package is described in detail by three volumes. "Part 1: The Design of SADS" contains design information and hardware requirements as well as describing data flows through the system (Lewis 1990a). "Part 2: Programmer's Reference Manual" details the software written for implementing the design and may be referred to in conjunction with the "Satellite Altimetry Data System Report: The NOAA GEOSAT Programs" which describes the software developed by NOAA for altimetry applications (Lewis 1990(b), 1990(c)). The use of the SADS is covered in "Part 3: User's Manual" which leads the user through the menu-driven system (Lewis and von St.Ange 1990).

3.3.2 Application

Stepwise details of the procedure through the SADS are given in the User Manual so only brief descriptions of the processing options which were used for this analysis will be given here.

The initial Geophysical Data Records (GDRs) are read from their distribution medium and converted into formats compatible with personal computers (PC). The original data are obtained as large, sequential, time-ordered collections of measurements where any one measurement is identifiable by its time and global position (latitude and longitude). These data are separated into user-selected passes which represent data along individual ground tracks of the satellite, either ascending (travelling south to north) or descending. The corrections for atmospheric effects and tidal influences which are included in the GDRs are applied.

Observations were not corrected for the slight non-colinearity (of < 1 km) of repeat orbits, but were interpolated in the along-track direction to co-register the 1 second observations from repeat orbits (Van Ballegooyen *et al. in prep.*). The orbital model used did not correct for orbital undulation, but tilt-and-bias corrections were applied over 10°latitude intervals in order to minimise these errors (van Ballegooyen *et al.* op.cit.). No correction for sea state bias was applied since uncertainty exists concerning the correction which should be used, but this is not considered to have had a significant impact on the results (Wakker *et al.* 1990a and others in Van Ballegooyen *et al.* op.cit.). Passes which crossed the geographical window of interest over the time period required (Cycles 37 to 54 - see Table 6) were then nested together according to their ascending or descending sense.

At the time of analysis, only the collinear method had been implemented in the SADS. Following this method it is possible to produce the profiles of sea height along track for each pass by two methods. One method involves normalising the variability with respect to a selected reference pass, but is therefore dependant on the characteristic topography at the time of the reference pass. The other method, which was used for this analysis, first determines the mean along-track sea height profile for each nest of passes over a given time period. This mean signal is then removed from that for individual passes to produce the along-track residual sea heights as departures from the mean topography over the time period chosen (about one year in the case of this

analysis). If this period is sufficiently long, the SST due to the geoid and the relatively time-invariant effects of the large-scale ocean circulation will be effectively removed. The residual heights then reveal the mesoscale, short-term features like eddies and current meanders which are of interest.

These residual heights can be treated as xy data pairs of height values and accompanying latitude/longitude coordinates and plotted for inspection as the topographic profiles along track (see Fig. 22). The residuals can also be grouped into a compound file representing all values for all passes within the geographical window for each 17 day cycle. These values can then be interpolated onto a uniform grid and contoured using a proprietry package such as SURFER (Golden Software, Inc. 1989,1990) to produce the SST anomaly over that cycle. Since neighbouring passes within any cycle are irregularly spaced with respect to time, a degree of spatial and temporal blurring occurs in these contour maps. Furthermore, since the region under inspection is highly variable at time scales shorter than 17 days, these contours are dificult to interpret.

To reduce the temporal distortion described above, the "snapshot" facility of the SADS was used. Residual heights were linearly interpolated at weekly intervals between the times of consecutive observations of individual passes (Van Ballegooyen *et al. in prep.*). These interpolated values were then gridded and contoured as above. The linearity of the interpolation in the snapshot procedure tends to reduce the sea heights and the contouring,

using the method of inverse distance squared, results in some smoothing which means that the contour values only approximate the true dimensions of the features revealed (Van Ballegooyen *et al.* op.cit.).

Table 6. Start dates of GEOSAT repeat cycles 37 to 54

Cycle 37	12 Jul - 28 Jul 1988
Cycle 38	29 Jul - 14 Aug 1988
Cycle 39	15 Aug - 31 Aug 1988
Cycle 40	01 Sep - 17 Sep 1988
Cycle 41	18 Sep - 04 Oct 1988
Cycle 42	05 Oct - 21 Oct 1988
Cycle 43	22 Oct - 07 Nov 1988
Cycle 44	08 Nov - 24 Nov 1988
Cycle 45	25 Nov - 11 Dec 1988
Cycle 46	12 Dec - 28 Dec 1988
Cycle 47	29 Dec - 14 Jan 1989
Cycle 48	15 Jan - 31 Jan 1989
Cycle 49	01 Feb - 17 Feb 1989
Cycle 50	18 Feb - 06 Mar 1989
Cycle 51	07 Mar - 23 Mar 1989
Cycle 52	24 Mar - 09 Apr 1989
Cycle 53	10 Apr - 26 Apr 1989
Cycle 54	27 Apr - 13 May 1989

CHAPTER 4

The analysis of the GEOSAT altimeter data

4.1 Data selection and processing

Hydrographic data collected on board FRS *Africana* during April of 1989 revealed the presence of an Agulhas ring near the Vema seamount (31° 40'S, 8° 20'E) (see Fig. 16) (Duncombe Rae *et al.* 1992b). A more intensive hydrographic survey of this feature was conducted by the RS *Benguela* during May of the same year. Conductivity-temperature-depth (CTD) and Expendable bathythermograph (XBT) stations were occupied along lines which crossed the Vema ring approximately SE to NW (line BB') and NE to SW (line CC') (see Fig.16). CTD stations were spaced at 30 nautical mile (approximately 55 km) intervals with XBTs deployed midway between them.

The horizontal thermal structure of the ring as indicated by the temperature field at a depth of 200 m is shown in Figure 16. The ring appeared to have been elliptical in shape with its major axis aligned approximately east-west and having a diameter of some 330 km (with respect to the 16° C isotherm)(Duncombe Rae *et al.* 1992b). Its minor axis of approximately 165 km diameter was aligned north-south (Duncombe Rae *et al.* 1989, Duncombe Rae *et al.* op.cit.). A vertical temperature section from the FRS *Africana* cruise in April suggests a horizontal diameter of about 240 km along a WNW-ESE axis

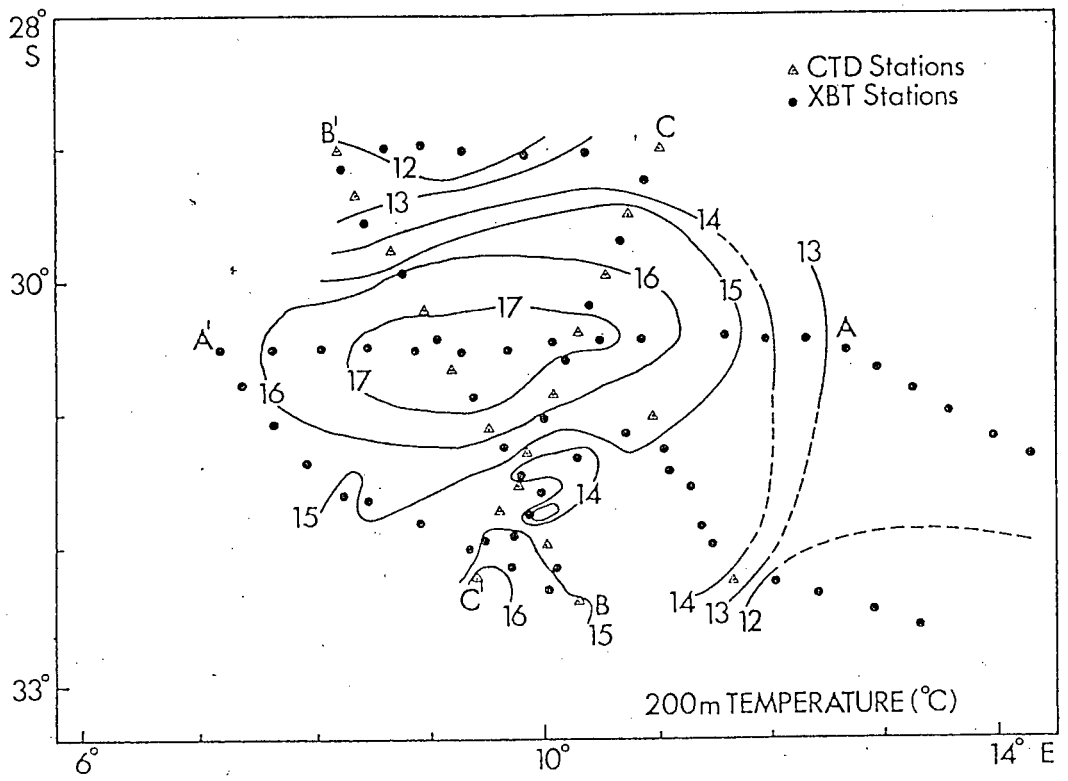

Figure 16. The Vema ring indicated by the isotherms (°C) contoured at 200 m depth from CTD (triangles) and XBT (circles) data collected by FRS *Benguela* during May 1989 (from Duncombe Rae *et al.* 1992b).

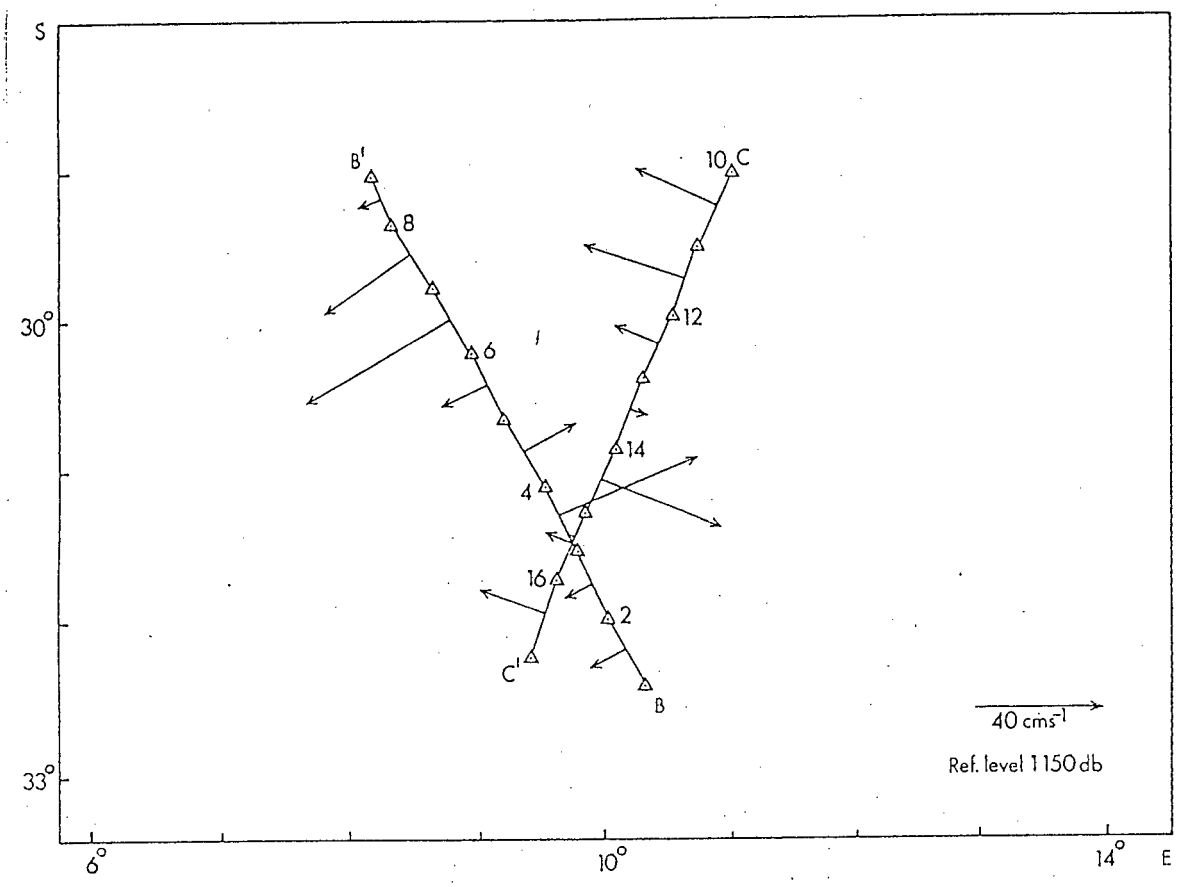

Figure 17. Surface geostrophic current vectors ($cm \cdot s^{-1}$) referenced to 1150 db. The lengths of the vectors are proportional to current speed. Even numbered CTD stations are annotated (from Duncombe Rae *et al.* 1992b)

(Duncombe Rae *et al.* 1992b). In May, the RS *Benguela* data describe an E-W ring diameter of about 530 km and a N-S diameter of some 180 km with respect to the 10° C isotherm.

The surface geostrophic velocities calculated from the CTD data and referenced to a level of no motion at 1150 db are shown in Figure 17. The anticyclonic circulation of the ring is clear with maximum speeds of 55 $cm \cdot s^{-1}$ to the SW between stations 6 and 7 on line BB' and 46 $cm \cdot s^{-1}$ to the NE between stations 3 and 4 on line CC'. Ship drift observations from SATNAV fixes while on station confirmed the anticyclonic flow (Duncombe Rae *et al.* 1992b).

In order to provide spatial congruence with the hydrographic observations, GEOSAT data within the geographic window from 20° to 40° S and 0° to 20° E were selected (see Fig. 18). This region includes the Agulhas retroflection and rings quite recently shed from it. The time period from 12 July 1988 to 13 May 1989, covered by GEOSAT cycles 37 to 54 (see Table 6), was selected to allow the earlier identification and tracking of the ring to its ultimate position of hydrographic detection.

No GEOSAT data were available for cycles 39, 45, 50 and 51. Data quantity and quality were unfortunately declining during this period and none were available after mid-May 1989 for true temporal overlap with the hydrographic detection of the ring. The deterioration of electromechanical components of the altimeter coupled with the increased solar activity and resulting spacecraft attitude variability caused severe data

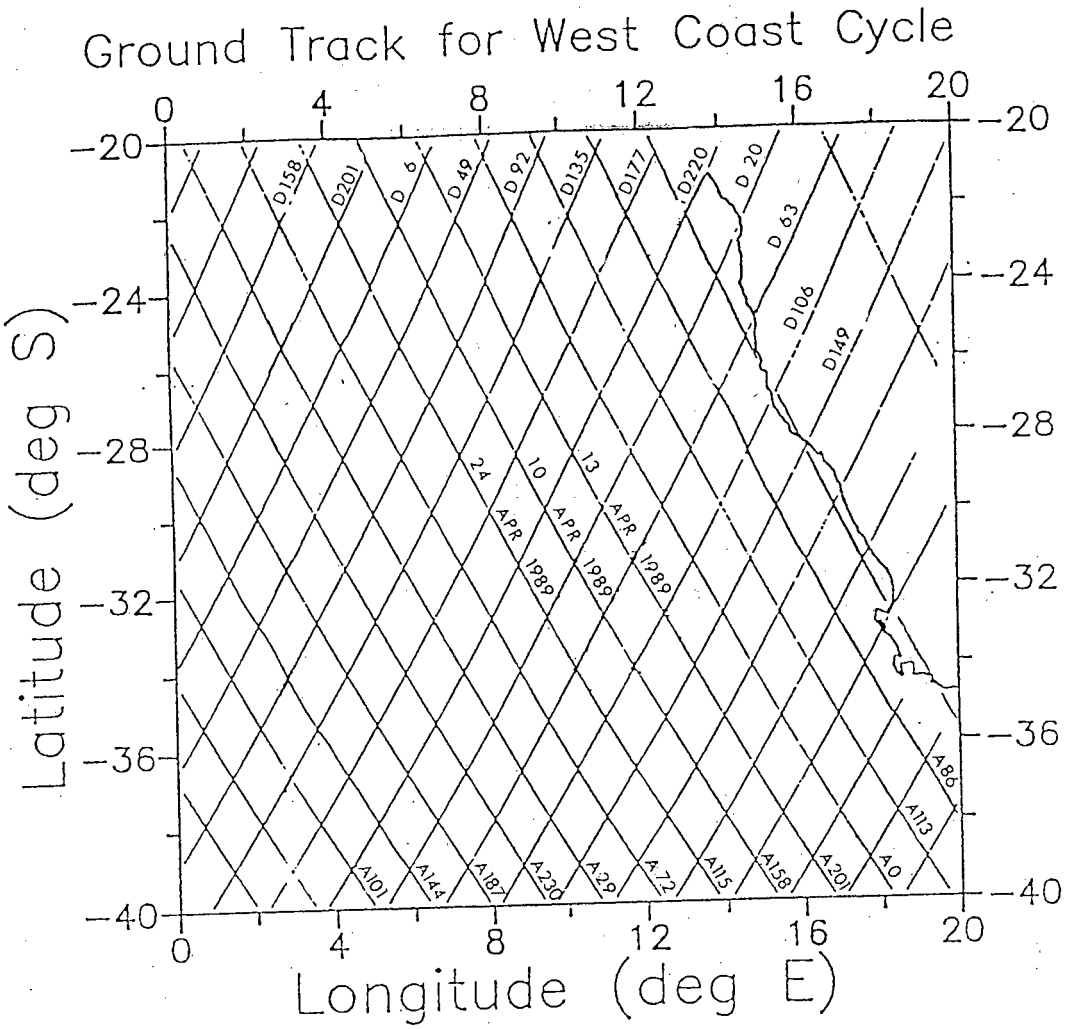

Figure 18. Map showing the west coast of South Africa and including the nominal ground tracks of the GEOSAT ERM orbits from which altimeter data were used in the analysis presented in this thesis. Ground tracks are numbered with the prefix A denoting an ascending pass and D a descending pass. The irregular timing of adjacent passes is indicated by the start dates shown for ascending passes A115, A158 and A201.

dropouts after this time (Chelton *et al.* 1990).

A local geoid approximation was modelled by the average sea surface topography within the window for the one year period selected. The average sea surface profile for each pass crossing the window over cycles 37 to 54 was computed and subtracted from the individual passes to leave the residual sea heights. This subtraction should remove the effects of the true geoid plus those components due to the relatively time-invariant circulation features.

4.2 Results

4.2.1 Contours of the sea surface topography

Contours of the residual sea surface heights representing a time series over cycles 37 to 54 are shown in Figures 19(a) to 19(n). Data for each pass and within each cycle were combined and gridded onto a uniform grid before contouring in 10 cm levels. Red shaded areas represent sea surface elevations higher than 10 cm referenced to the zero or mean background level. The zero line is annotated and should represent no departure from the mean background sea surface topography (SST) which combines the geoidal component and those due to semi-permanent features of the circulation. All other contours represent sea surface depressions.

In general, the contours reveal that the SST is most variable in

the SE corner of the region which is consistent with the analyses reported in the literature (as an example see Frontispiece). This may be expected from the influence of the variable behaviour of the Agulhas retroflection, the frequent shedding of rings from it and the interactions at the subtropical convergence. Root mean square variances were not calculated here as this exercise has been performed repeatedly and reported widely in the literature (see Shum *et al.* 1990 for example).

The region is populated by a number of features representing both sea surface depressions and elevations. It is clear that the shape of these features is determined to some extent by the distribution of available data and the consequent contouring. It is therefore important to view the data availability overlays simultaneously when interpreting the contours. Each cycle represents a period of 17 days over which the data are temporally smoothed. Neighbouring ascending or descending passes are not necessarily adjacent in time, but follow an irregular sequence over the cycle (e.g. cycle 53: passes A115 on 24/04/1989; A158 on 10/04/1989; A201 on 13/04/1989; see Fig. 18). This sequence is, however, duplicated from one cycle to the next. This may result in the spatial distortion of features which may shift significantly over 17 days. An Agulhas ring, for example, may move some 100 km in that time thus blurring its representation by the contours.

It was anticipated that these contour plots of SST would provide a means of identifying and tracking Agulhas rings from their

shedding to their translation westwards or northwestwards through the SE Atlantic as has been achieved by other researchers (e.g. Gordon and Haxby 1990, Van Ballegooyen *et al. in prep.*).

From the hydrographic data and other altimetric results we expect Agulhas rings to be annular in shape and of about 150 to 500 km in diameter (see Chapter 2). They should be characterised by sea surface elevations in their centres of about 30 cm or more above the background. Van Ballegooyen *et al.* (*in prep.*) report that side lobes of opposite sign to an intense SST feature are generated by the altimeter process. The assessment of true topographic relief should therefore be relative to the depth or height of theses lobes in preference to the zero reference. An examination of the contours for cycles 37 to 54 (Figs. 19(a) to 19(n)) shows that the identification of annular features with elevations of at least 30 cm above the zero reference which may be Agulhas rings is relatively easy for any given cycle. It appears that the region may generally be populated by as many as 6 rings at any time which is consistent with the literature to date (see Lutjeharms and Valentine 1988, Duncombe Rae 1991, Van Ballegooyen *et al. in prep.*). There seems to be a preferred position for a region of sea surface elevation in the vicinity of the Vema seamount at about 31° 40'S, 8° 20'E which may be related to a delay in their passage caused by interaction with the Walvis Ridge (Duncombe Rae 1991, Van Ballegooyen *et al. in prep.*).

Inspection of the data availability overlays shows that many data

gaps existed, particularly in the area closest to the west coast of South Africa, for most cycles. Cycles 40 and 53 were selected for more detailed inspection because of their relatively complete data coverage. Five Agulhas rings may be identified from cycle 40 (see Fig. 19(c)), their centres located approximately as given in Table 7 which also gives their diameters and maximum surface elevations. Four annular shaped depressions are also evident which would suggest cyclonically rotating eddies. These are identified on Figure 19(c) by numbers C40.1 to C40.4. They have surface depressions ranging from 70 cm to 40 cm and have diameters of approximately 140 km to 340 km.

Similarly, several Agulhas rings may possibly be identified from cycle 53 and are detailed in Table 8 (see Fig. 19(m)). In addition to the anticyclonic rings, several areas of topographic depression suggestive of cyclonic rings are also evident on Figure 19(m). Their maximum depressions range from 20 cm to as much as 90 cm and their maximum diameters from 130 km to 310 km. The very intense features such as those at about 21°S, 5.5°E and 23°S, 6.5°E (indicated on Fig. 19(m) by ↗) are considered to be artefacts of the data distribution and contouring problems and are ignored.

Inspection of the contour plots for consecutive cycles did not allow for the positive identification of the same feature in subsequent cycles and hence it was not feasible to track the progress of a ring over time. Without concomitant hydrographic confirmation it is not possible to positively identify any

features as Agulhas rings (see Tournadre 1990). The estimation of shedding rates for rings can therefore only be crudely derived as follows. Assuming a mean translation rate towards the west or northwest of some 5 $cm \cdot s^{-1}$ (Duncombe Rae 1991, Van Ballegooyen *et al. in prep.*) one may conclude that any features visible in the SST for cycle 40 (start:1 September 1988) should have drifted beyond a radius of some 1000 km from their shedding location (centered say at 38°S, 20°E) by the time of cycle 53 (start:10 April 1989). An assessment of those features evident within this radius may then be assumed to be the production rate over the seven months elapsed. On this basis, perhaps 4 rings can be identified within the 1000 km radius in cycle 53 yielding a rate of about 6 or 7 rings per year which is consistent with other reports (e.g. Olson and Evans 1986, Van Ballegooyen *et al.* op. cit.).

Figure 19. Sea surface topography anomalies (departures from the mean sea surface topography for cycles 37 to 54). Regions of elevation >10 cm are indicated by pink shading. The zero contour is annotated and others refer to regions of sea surface depression. The overlays for each figure show the data availability for each altimeter pass for each cycle. Figures 19a to 19n refer to cycles 37 to 54 respectively, but note that no altimeter data were available for cycles 39, 45, 50 and 51.

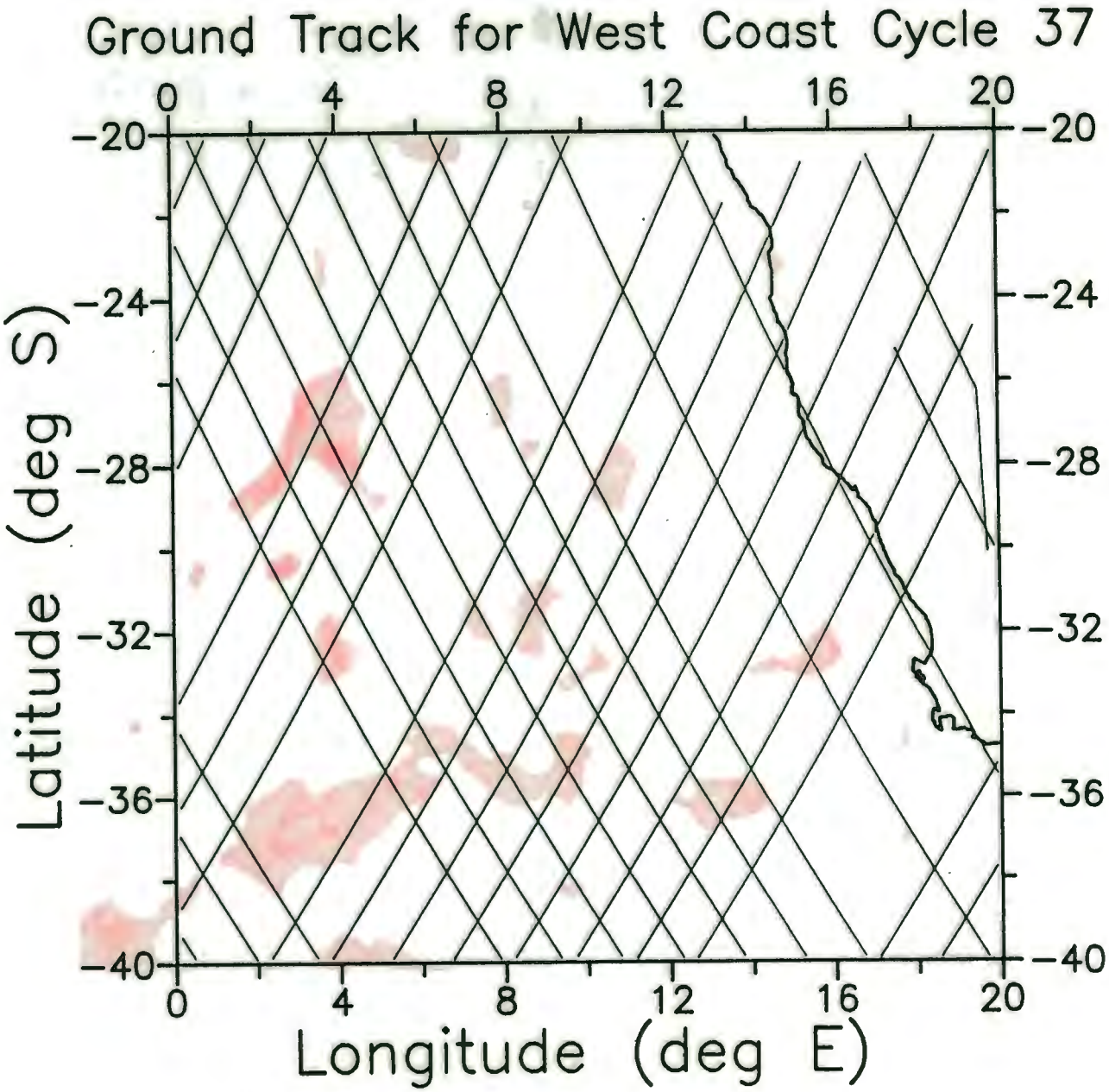
Ground Track for West Coast Cycle 37
0
4
8
12
16
20
-20
-24
-28
-32
-36
-40
Latitude (deg S)
Longitude (deg E)

Fig.19a

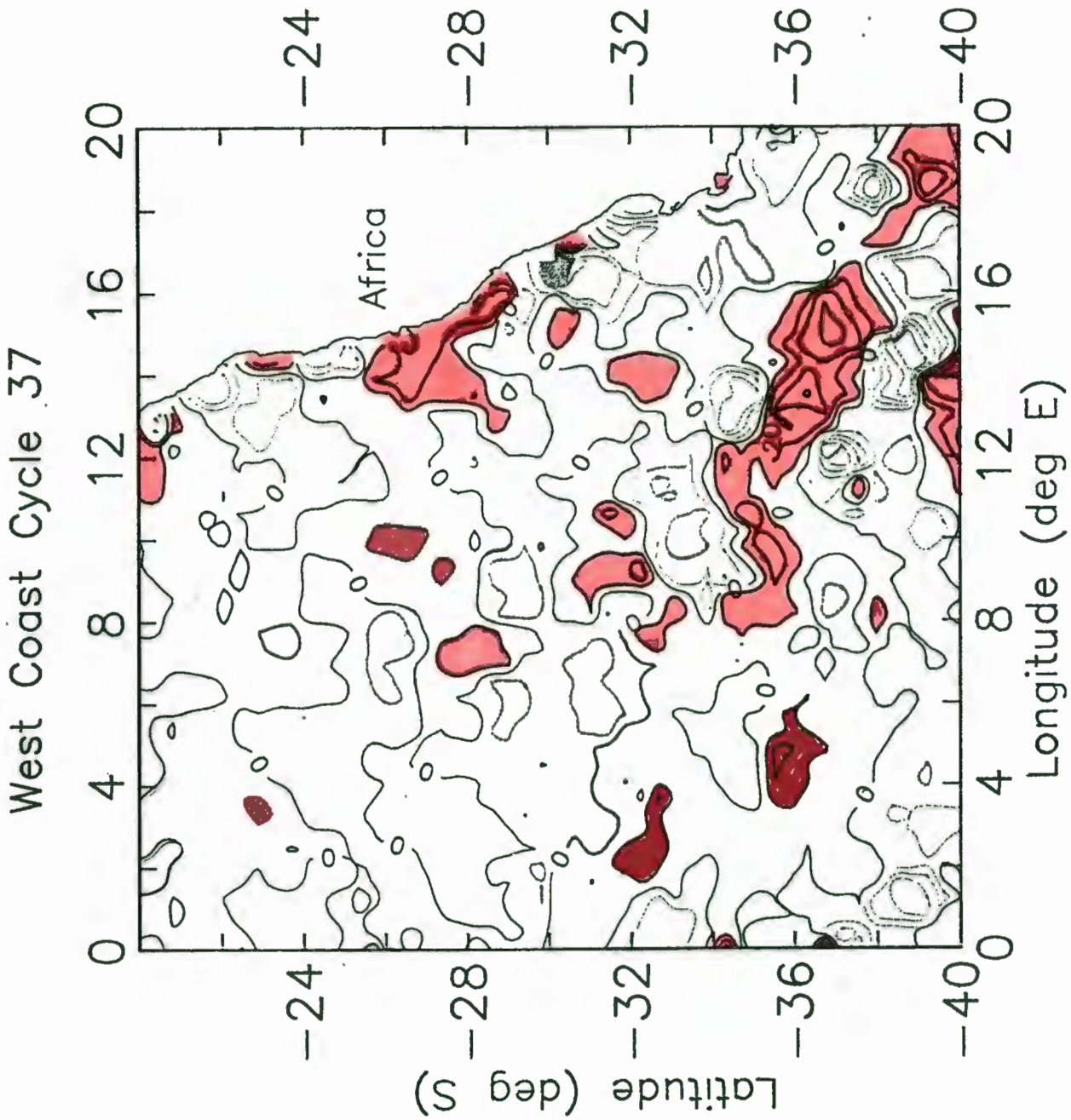
West Coast Cycle 37
Africa
Latitude (deg S)
Longitude (deg E)
0
4
8
12
16
20
-24
-28
-32
-36
-40

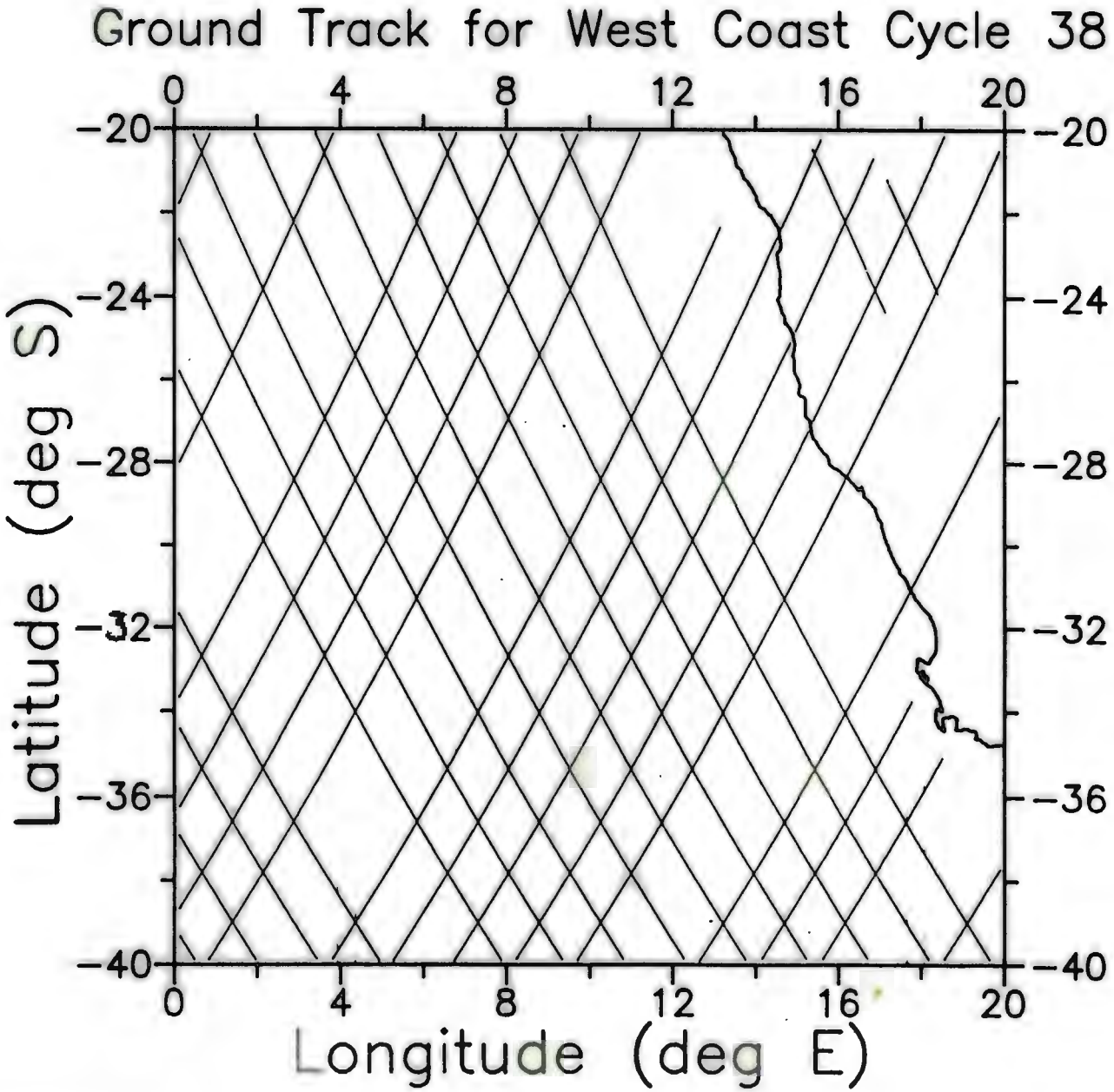
Ground Track for West Coast Cycle 38
0
4
8
12
16
20
-20
-24
-28
-32
-36
-40
Latitude (deg S)
Longitude (deg E)

Fig.19b

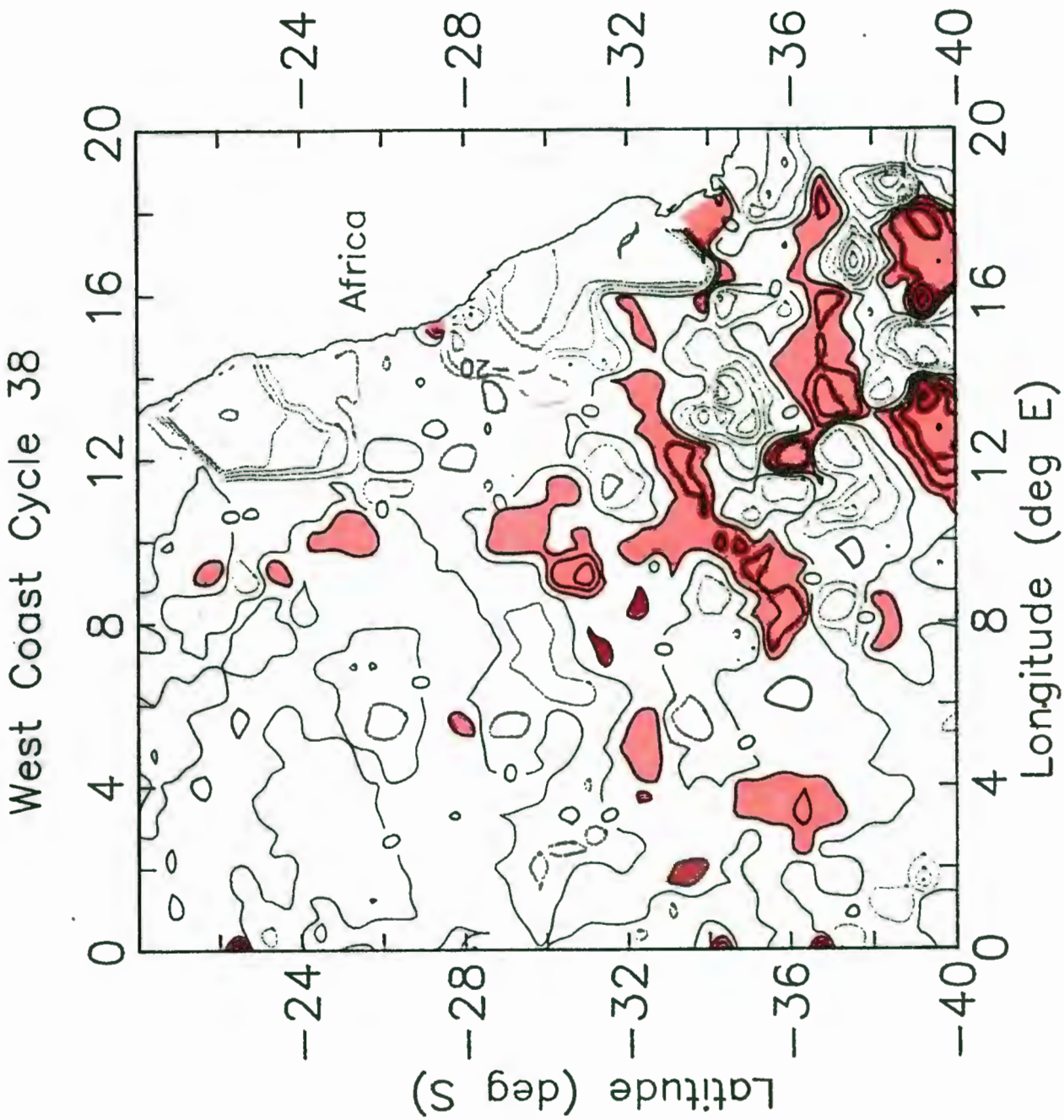
West Coast Cycle 38
Africa
20
Latitude (deg S)
Longitude (deg E)
0
4
8
12
16
20
−24
−28
−32
−36
−40

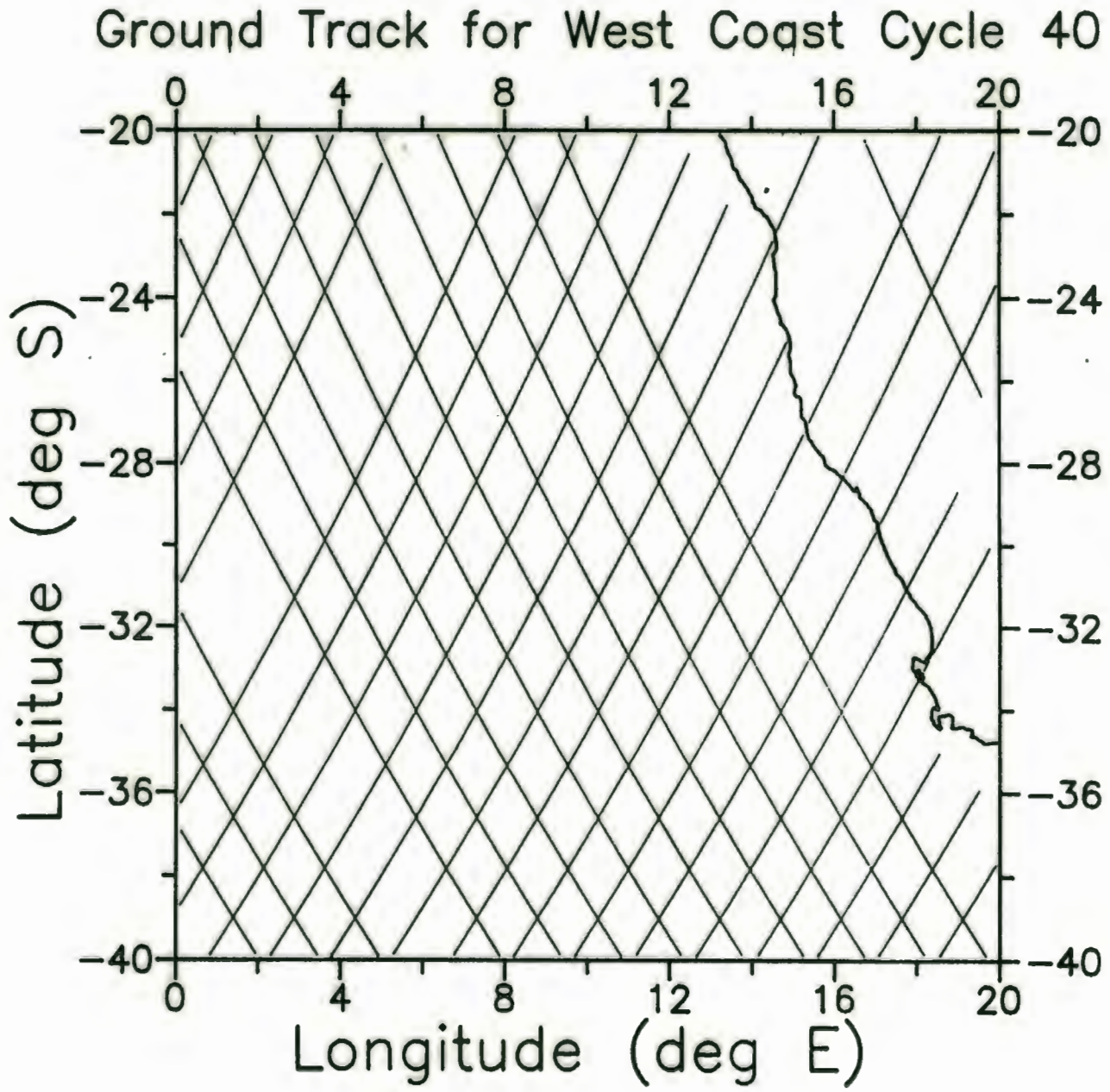
Ground Track for West Coast Cycle 40
0
4
8
12
16
20
-20
-24
-28
-32
-36
-40
Latitude (deg S)
Longitude (deg E)

Fig.19c

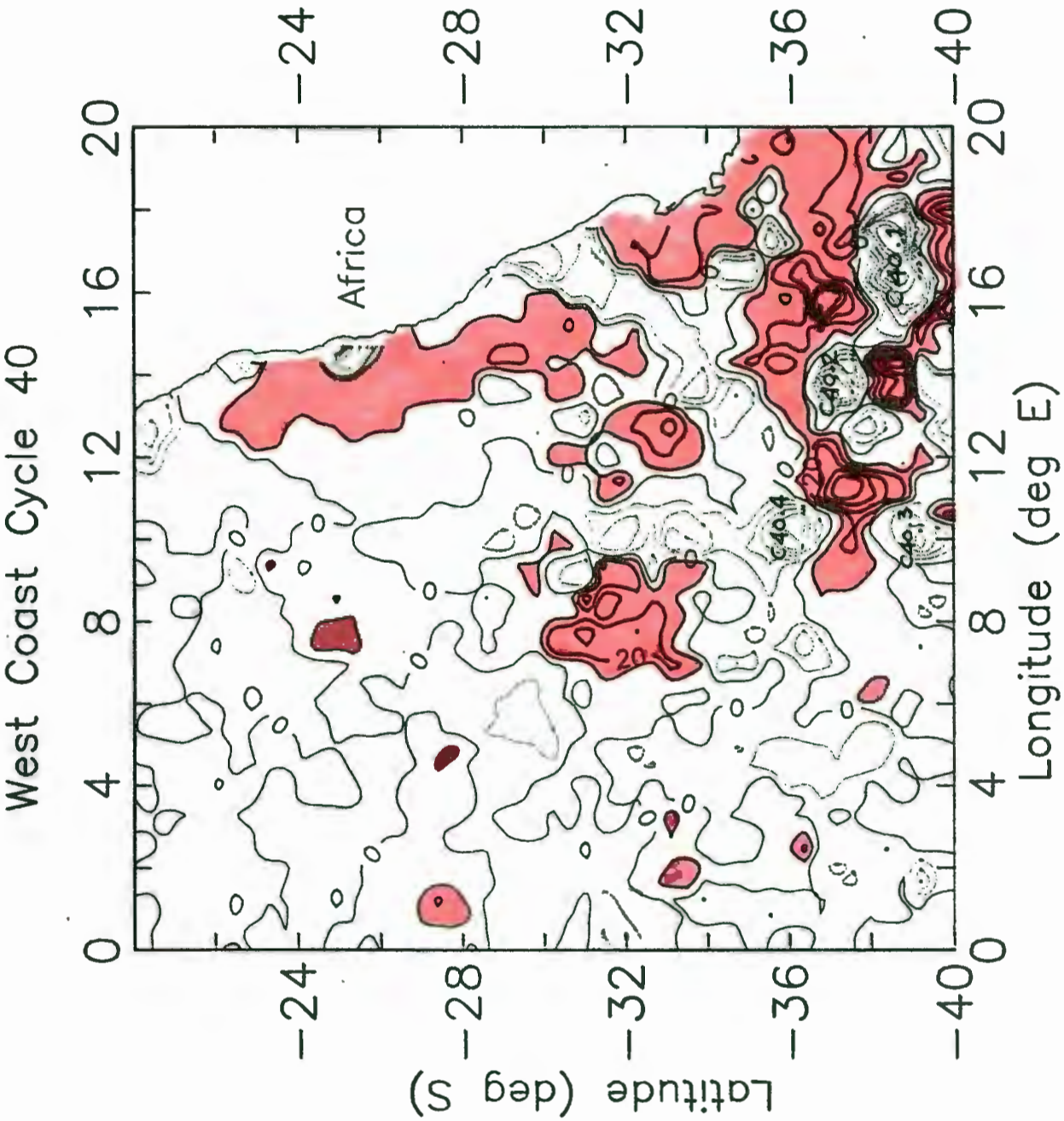
West Coast Cycle 40
Africa
20
C40.1
C40.2
C40.3
C40.4
Latitude (deg S)
Longitude (deg E)
0
4
8
12
16
20
-24
-28
-32
-36
-40

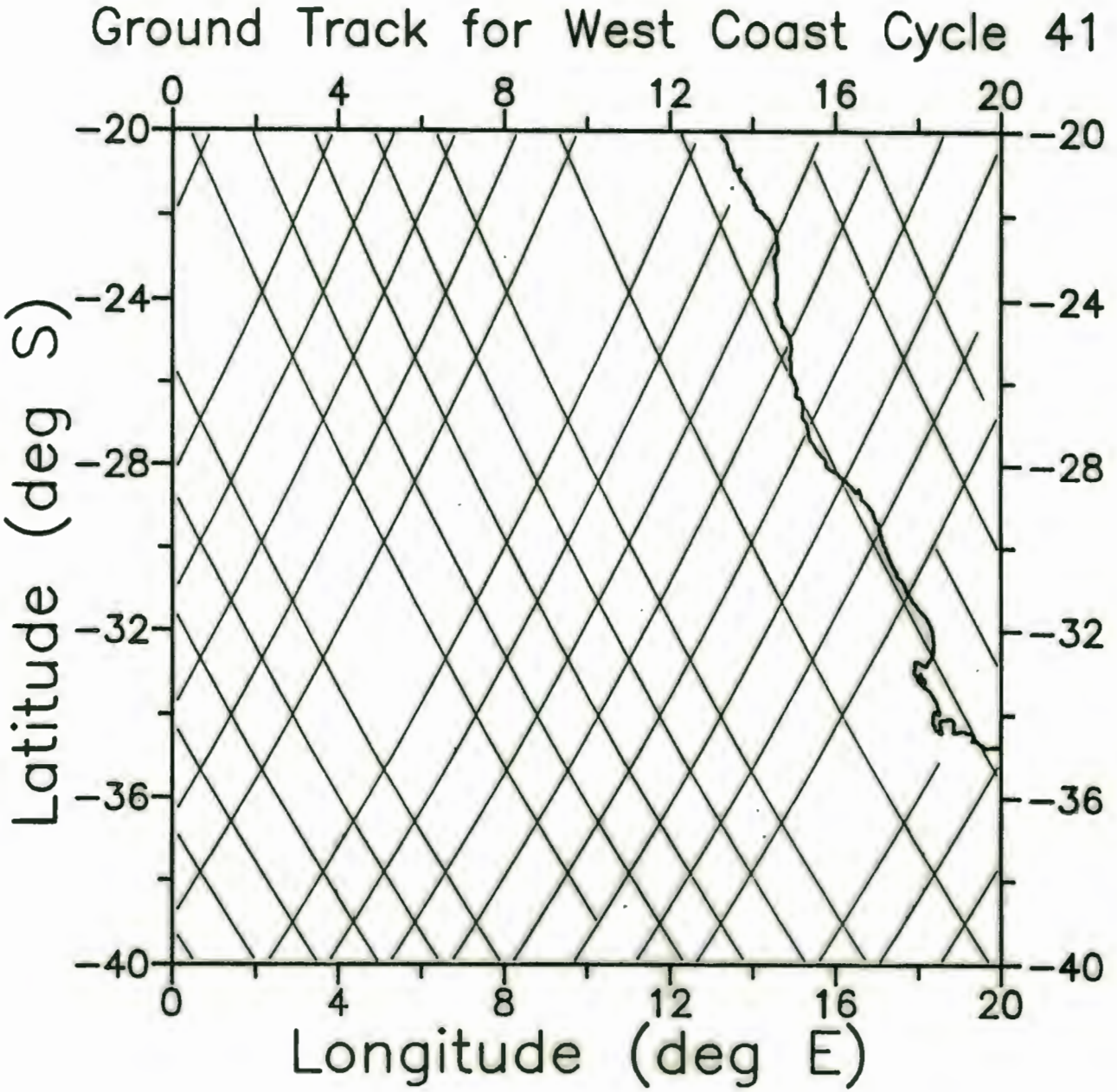
Ground Track for West Coast Cycle 41
0
4
8
12
16
20
-20
-24
-28
-32
-36
-40
Latitude (deg S)
Longitude (deg E)

Fig.19d

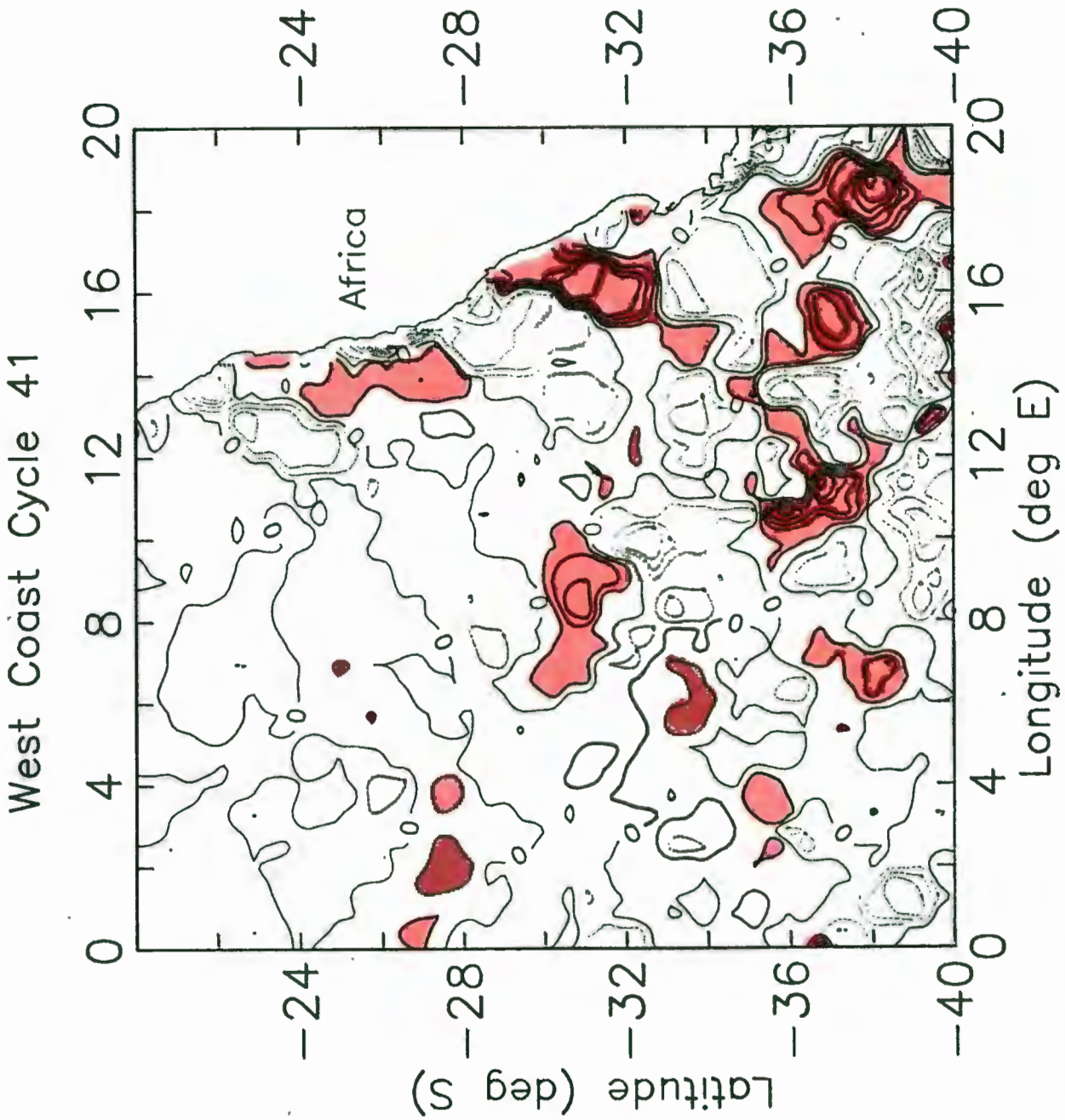
West Coast Cycle 41
Africa
Latitude (deg S)
Longitude (deg E)
−24
−28
−32
−36
−40
0
4
8
12
16
20

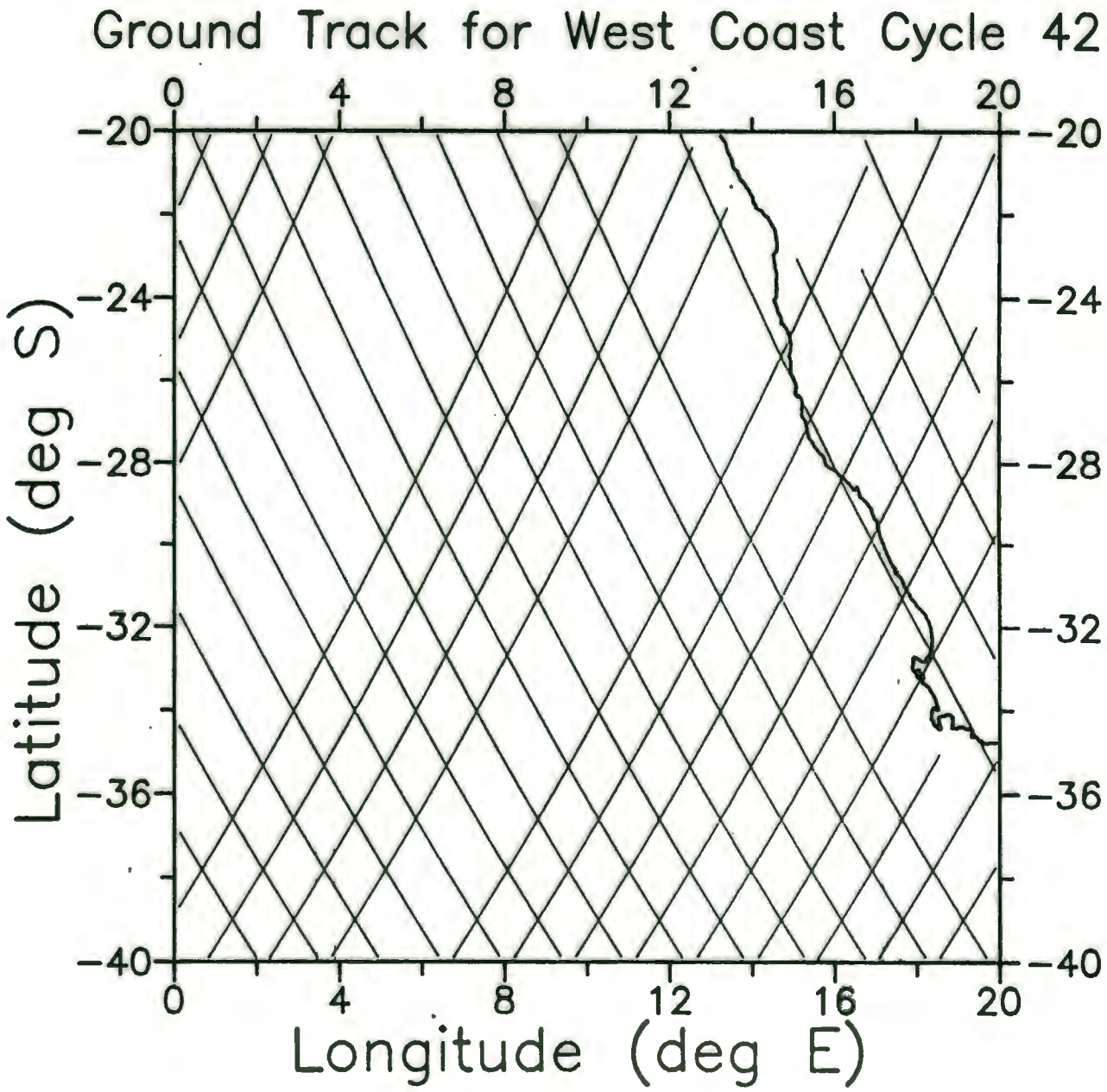
Ground Track for West Coast Cycle 42
0
4
8
12
16
20
-20
-24
-28
-32
-36
-40
Latitude (deg S)
Longitude (deg E)

Fig.19e

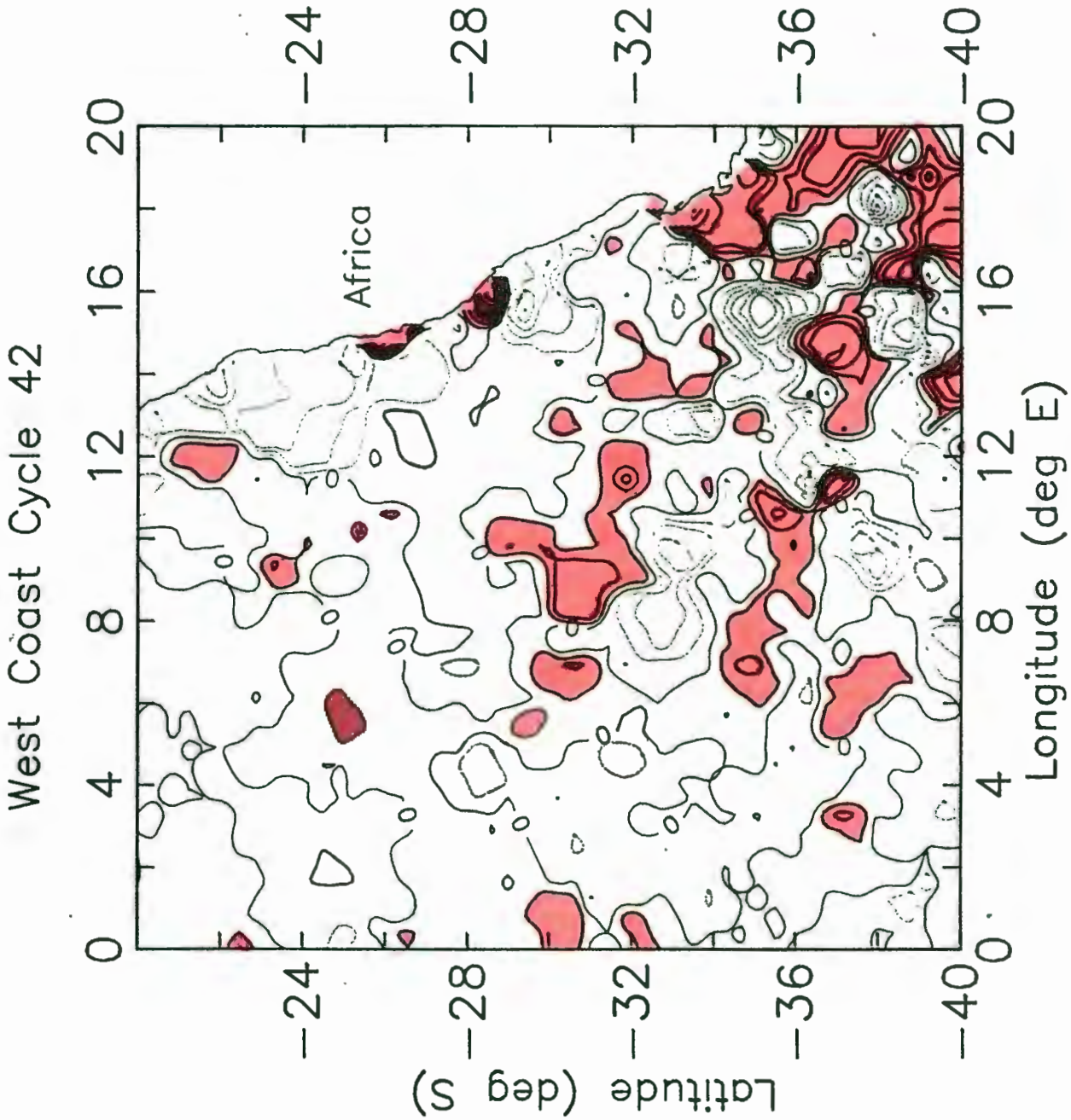
West Coast Cycle 42
Africa
Latitude (deg S)
Longitude (deg E)
-24
-28
-32
-36
-40
0
4
8
12
16
20

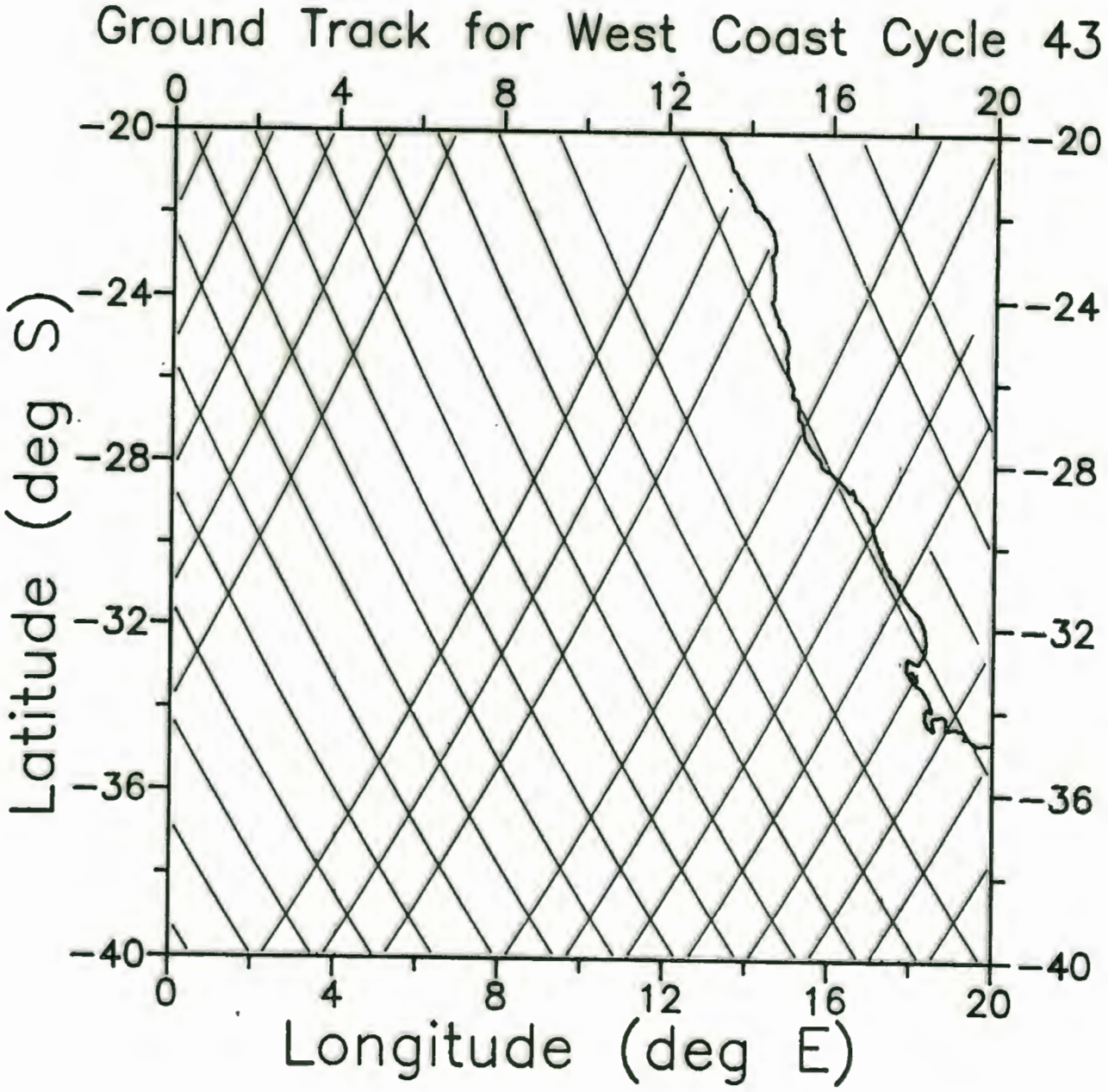
Ground Track for West Coast Cycle 43
0
4
8
12
16
20
-20
-24
-28
-32
-36
-40
Latitude (deg S)
Longitude (deg E)

Fig.19f

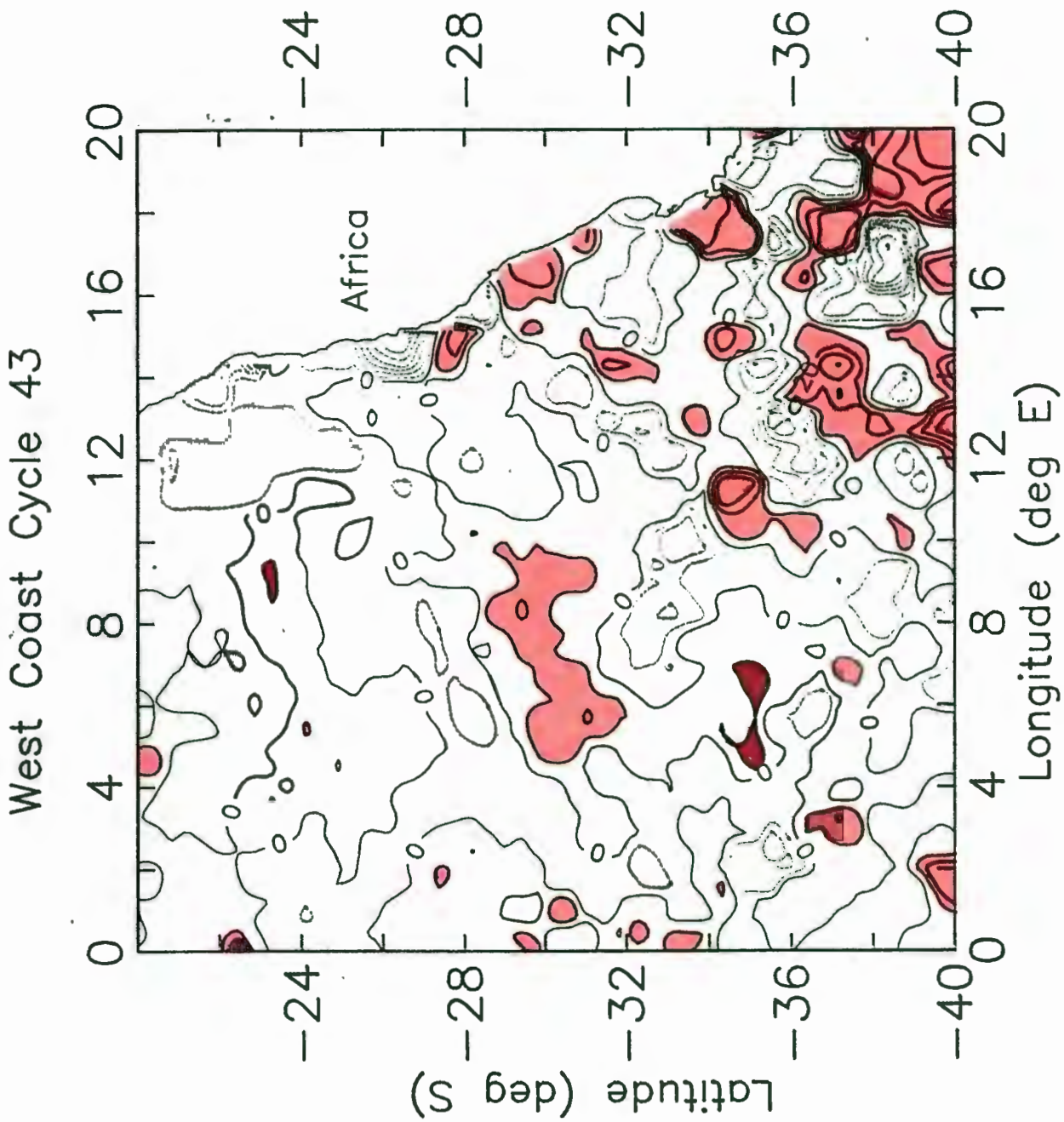
West Coast Cycle 43
Africa
Latitude (deg S)
Longitude (deg E)
0
4
8
12
16
20
−24
−28
−32
−36
−40

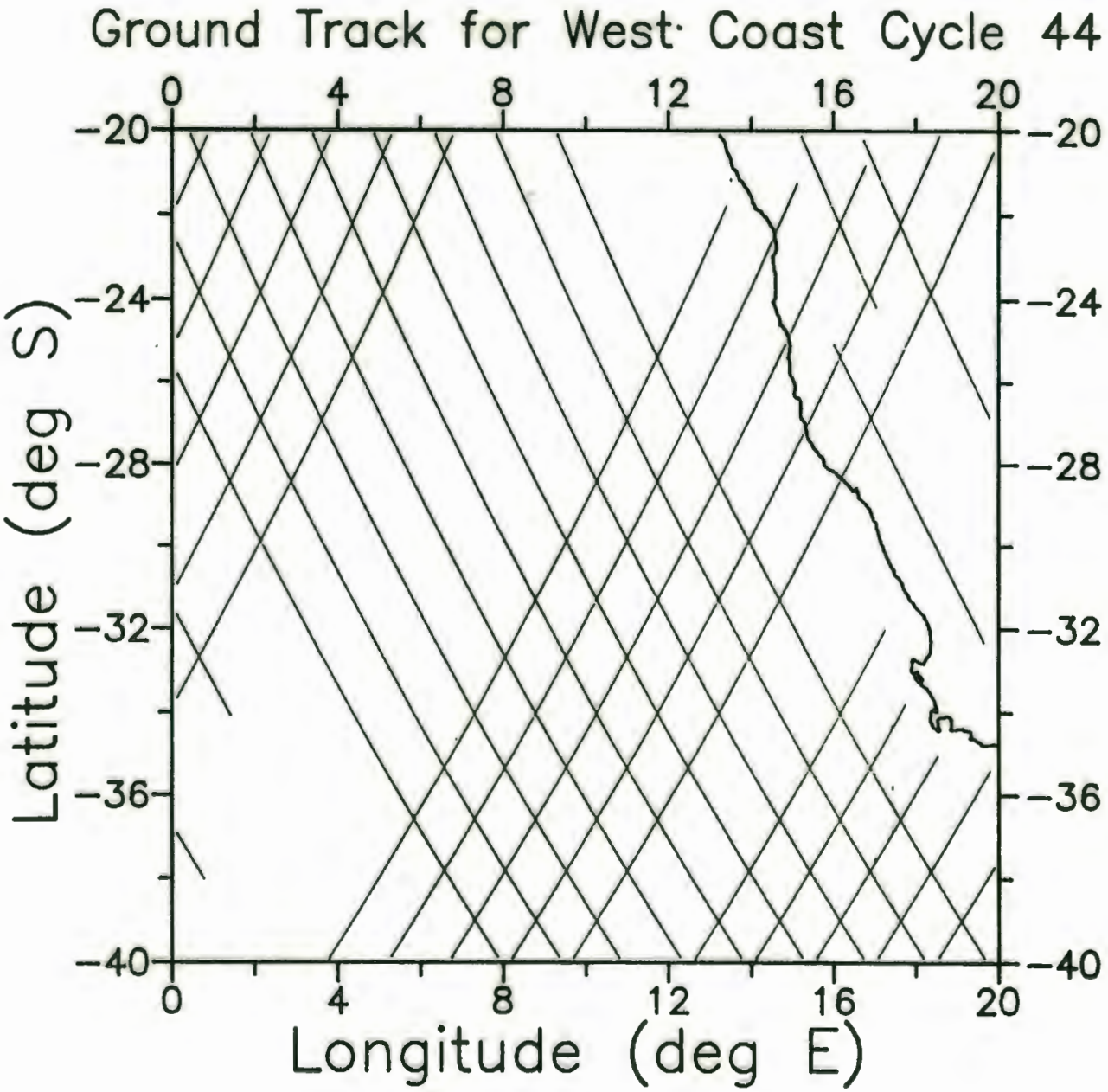
Ground Track for West Coast Cycle 44
0
4
8
12
16
20
-20
-24
-28
-32
-36
-40
Latitude (deg S)
Longitude (deg E)

Fig.19g

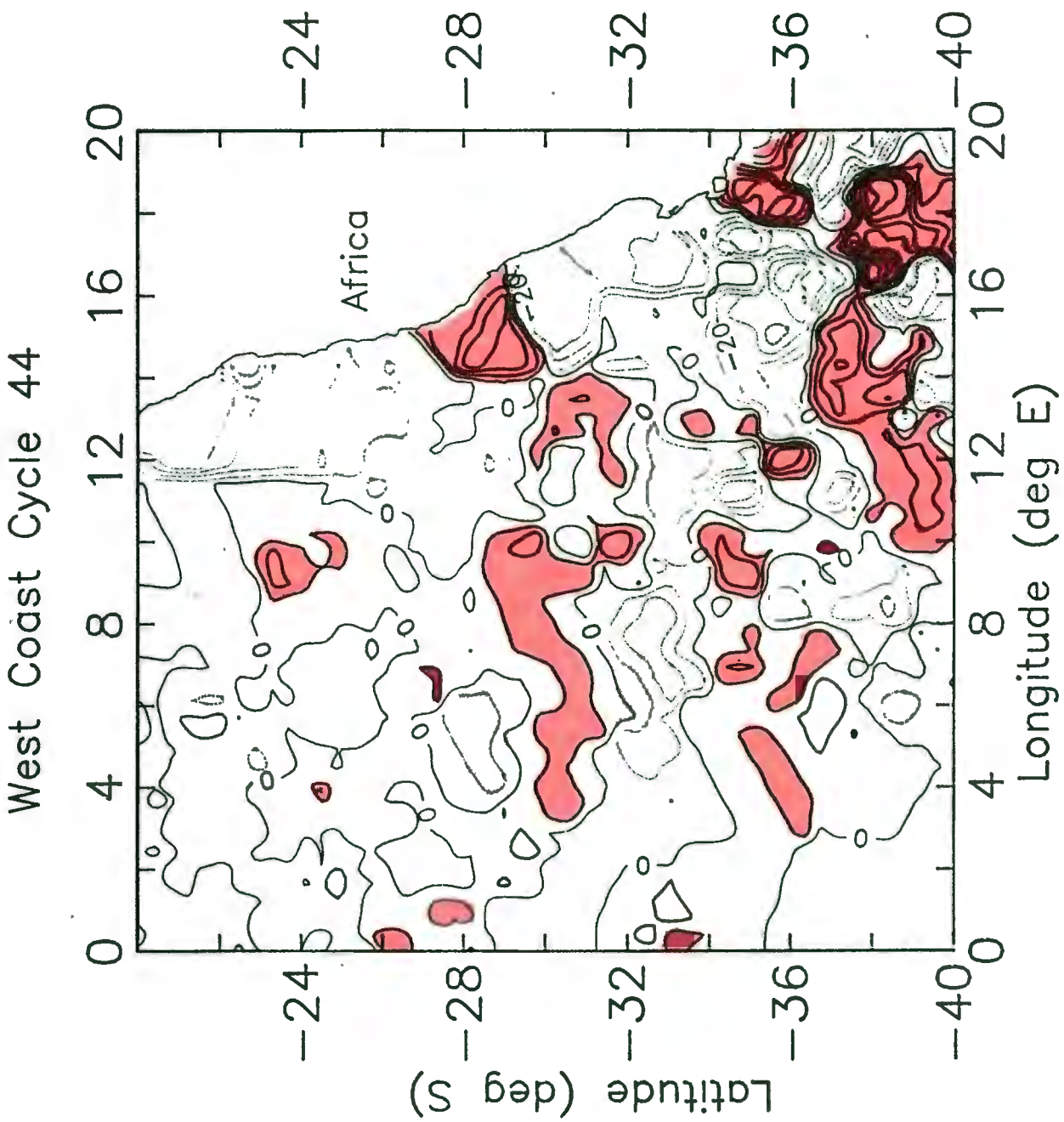
West Coast Cycle 44
Africa
−20
−20
Latitude (deg S)
Longitude (deg E)
0
4
8
12
16
20
−24
−28
−32
−36
−40

Ground Track for West Coast Cycle 46
Latitude (deg S)
Longitude (deg E)
0
-20
-40
-60
-80
-100
-120
-140
-160
-180
4
8
12
16
20

Fig.19h

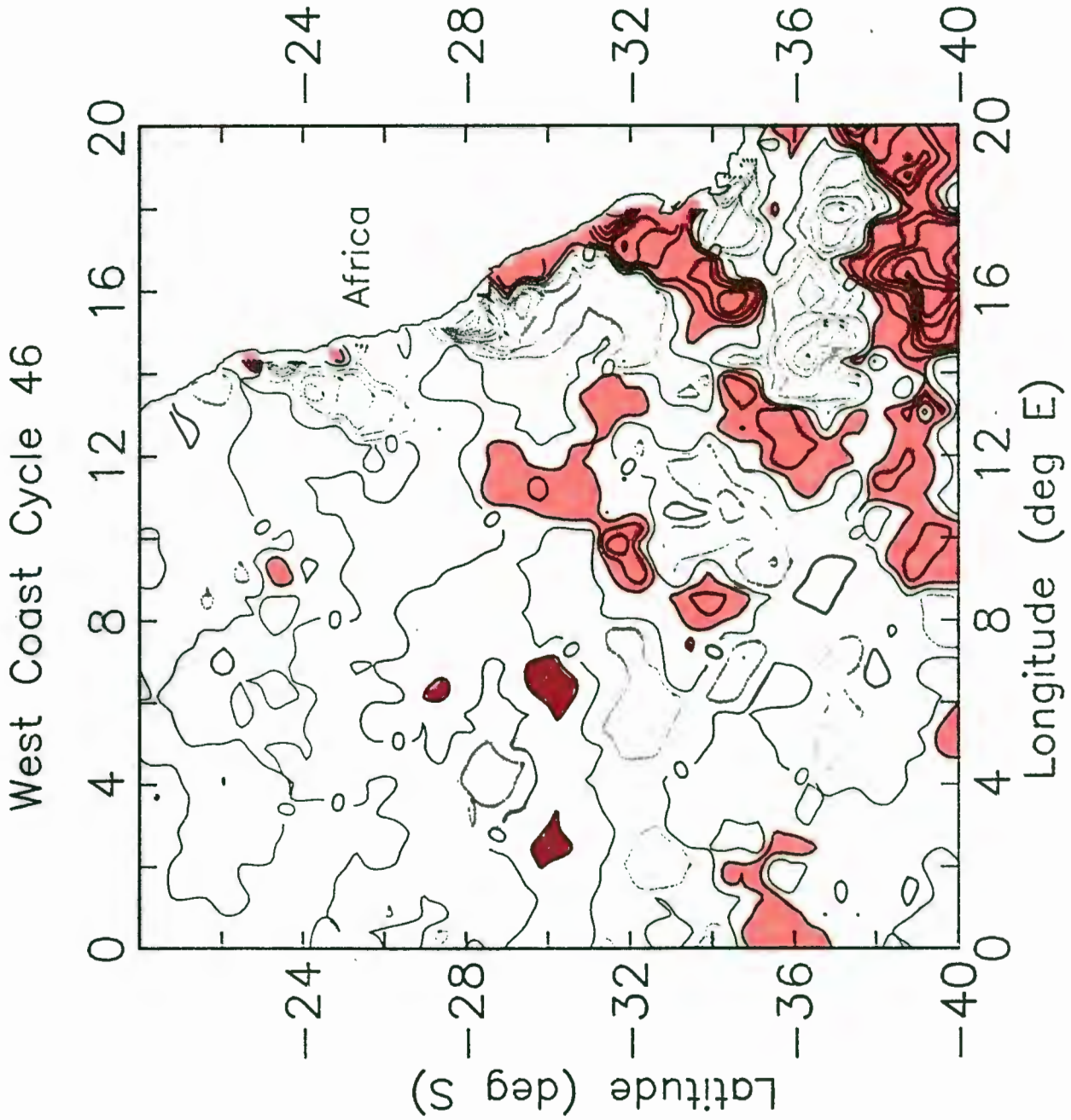
West Coast Cycle 46
Africa
Latitude (deg S)
Longitude (deg E)
0
4
8
12
16
20
−24
−28
−32
−36
−40

Fig.19h

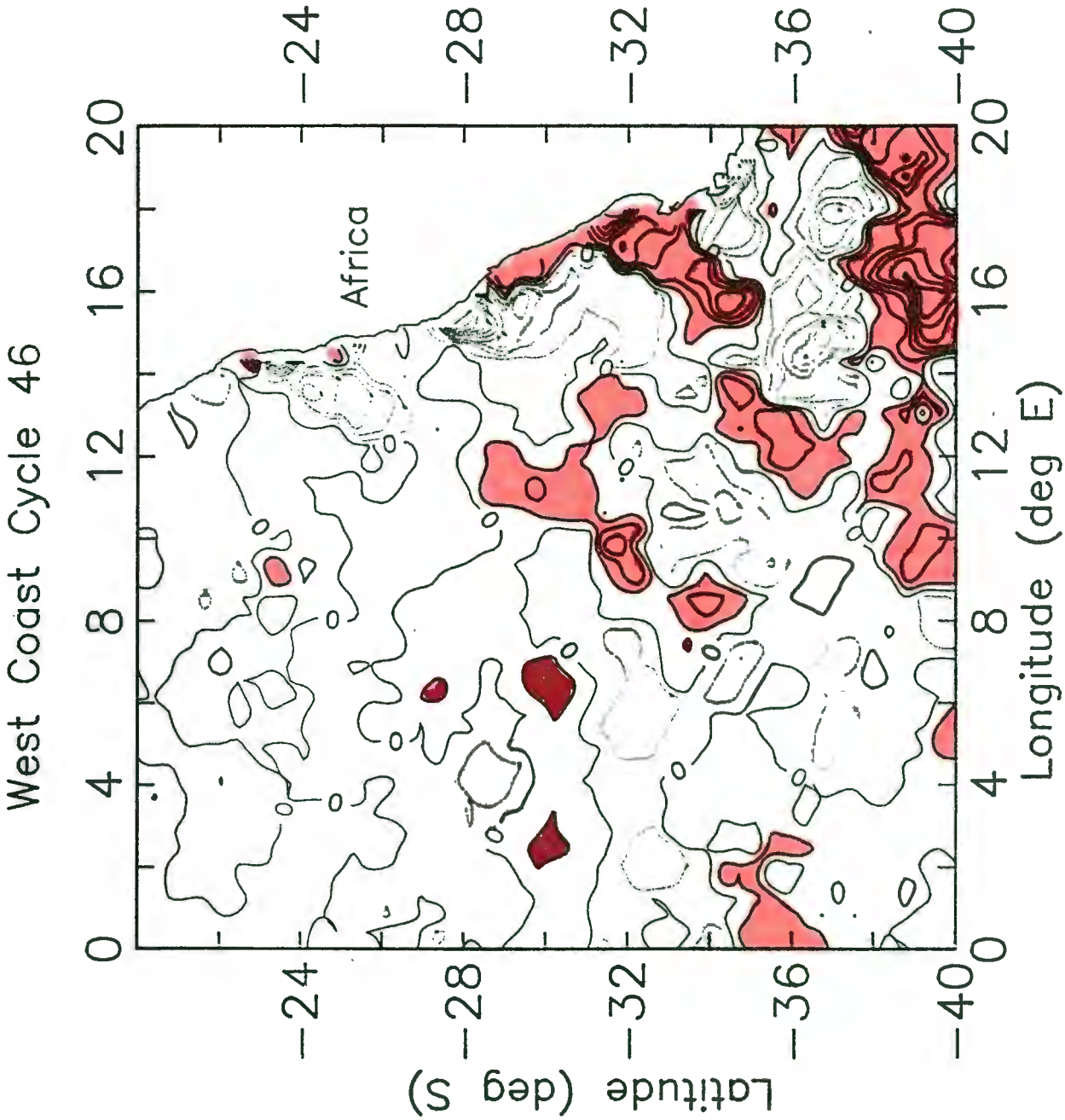
West Coast Cycle 46
Africa
Latitude (deg S)
Longitude (deg E)
0
4
8
12
16
20
-24
-28
-32
-36
-40

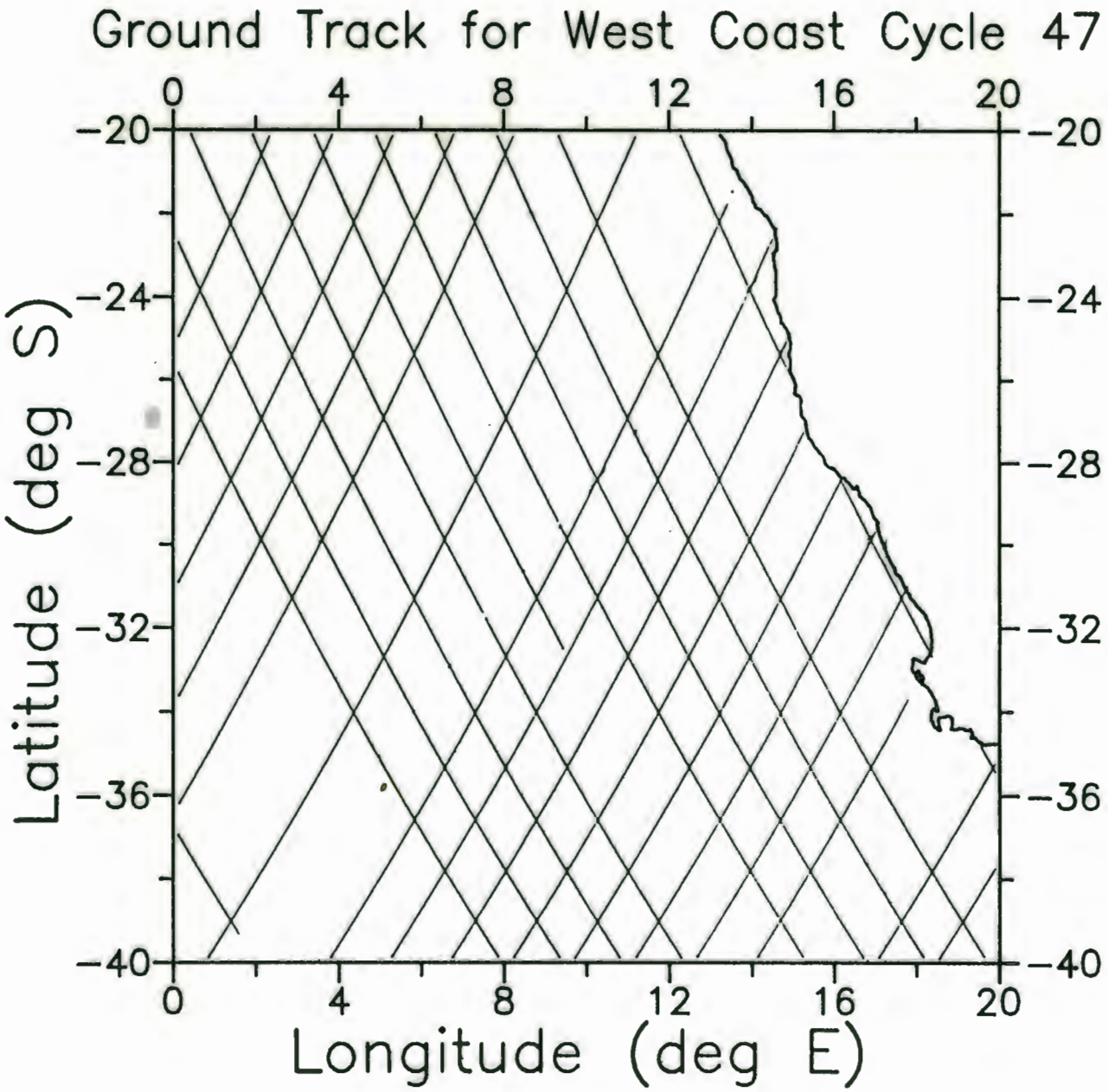
Ground Track for West Coast Cycle 47
0
4
8
12
16
20
-20
-24
-28
-32
-36
-40
Latitude (deg S)
Longitude (deg E)

Fig.19i

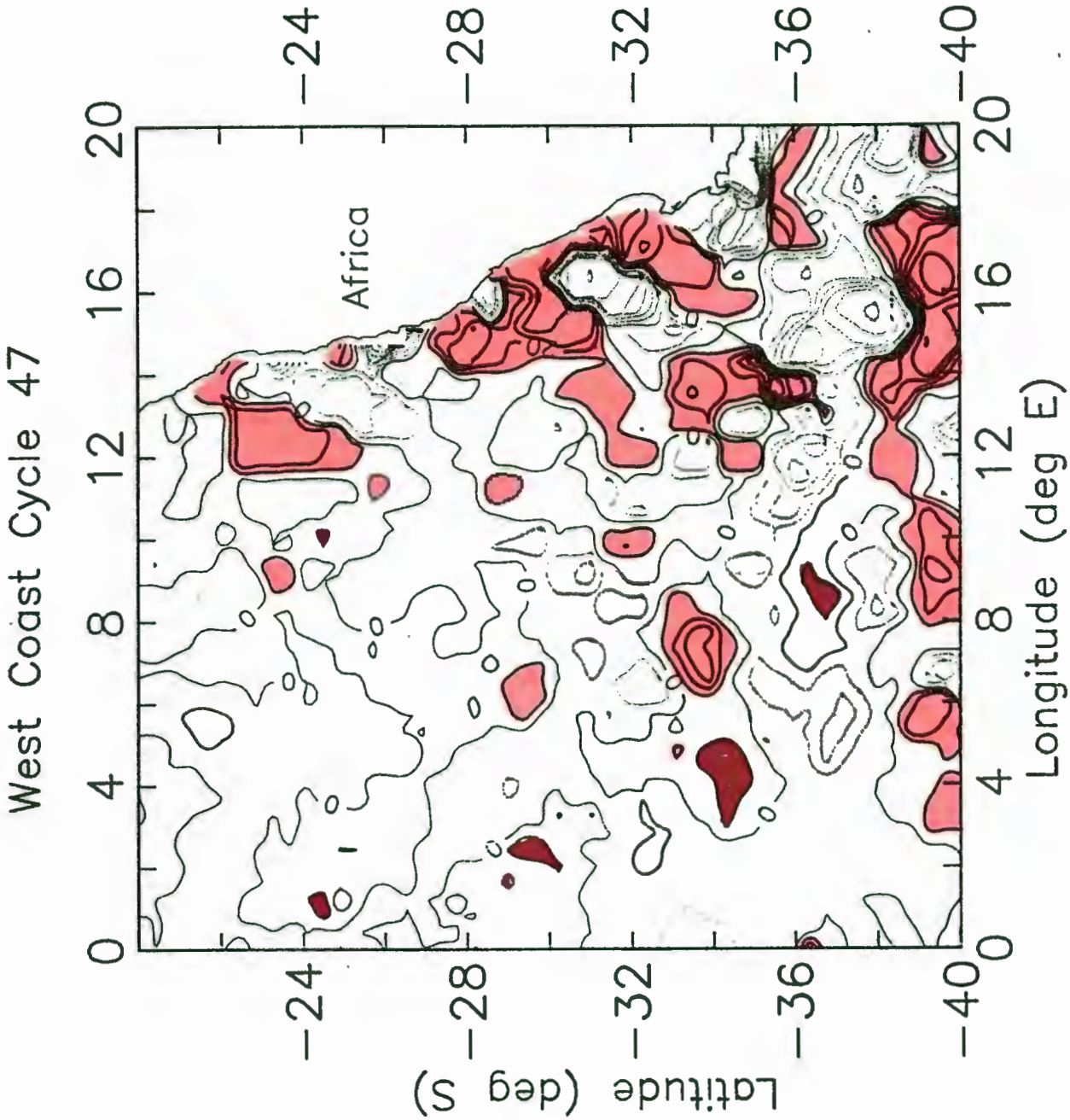
West Coast Cycle 47
Africa
Latitude (deg S)
Longitude (deg E)
−24
−28
−32
−36
−40
0
4
8
12
16
20

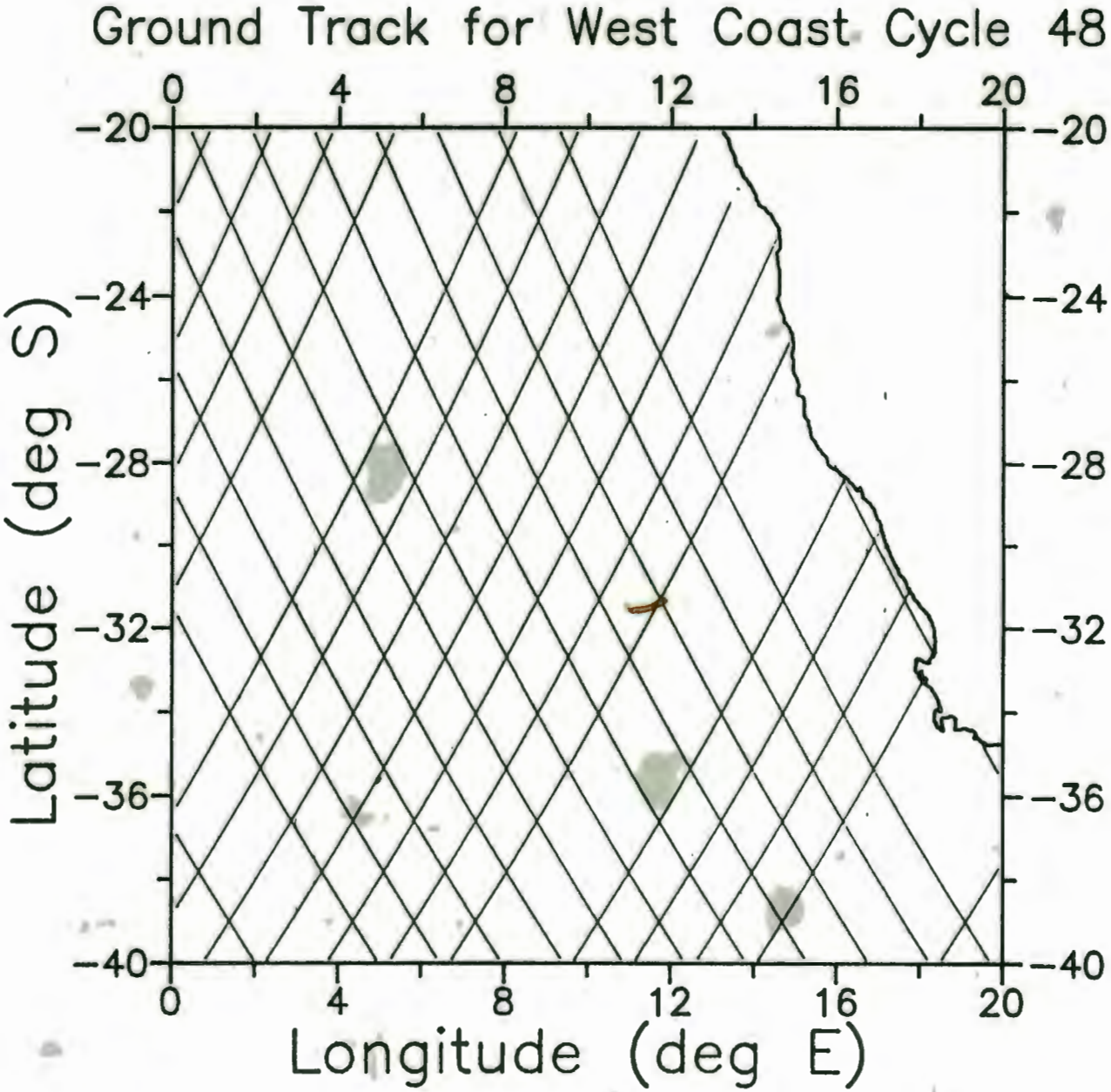
Ground Track for West Coast Cycle 48
0
4
8
12
16
20
-20
-24
-28
-32
-36
-40
Latitude (deg S)
Longitude (deg E)

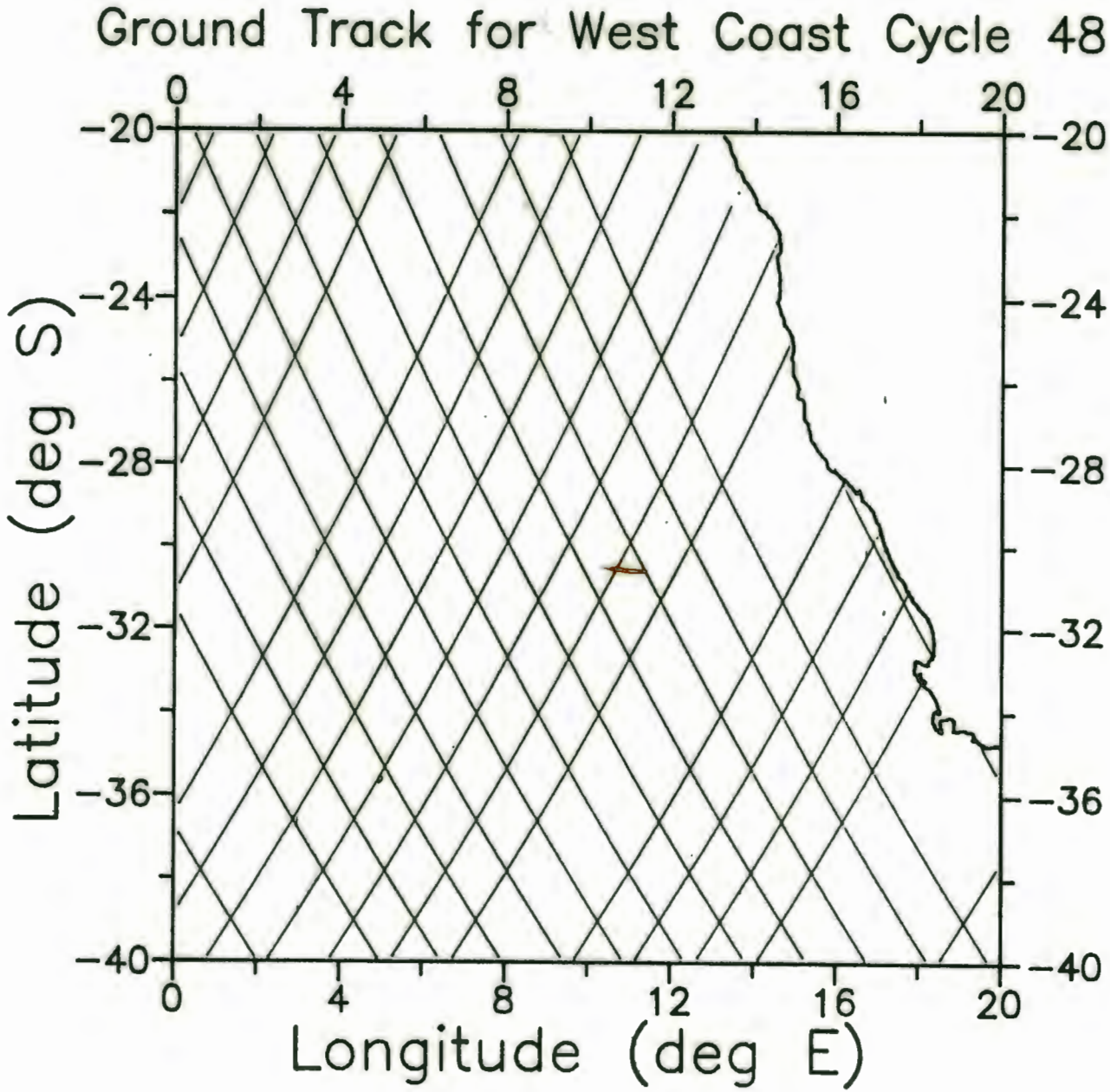
Ground Track for West Coast Cycle 48
0
4
8
12
16
20
-20
-24
-28
-32
-36
-40
Latitude (deg S)
Longitude (deg E)

Fig.19j

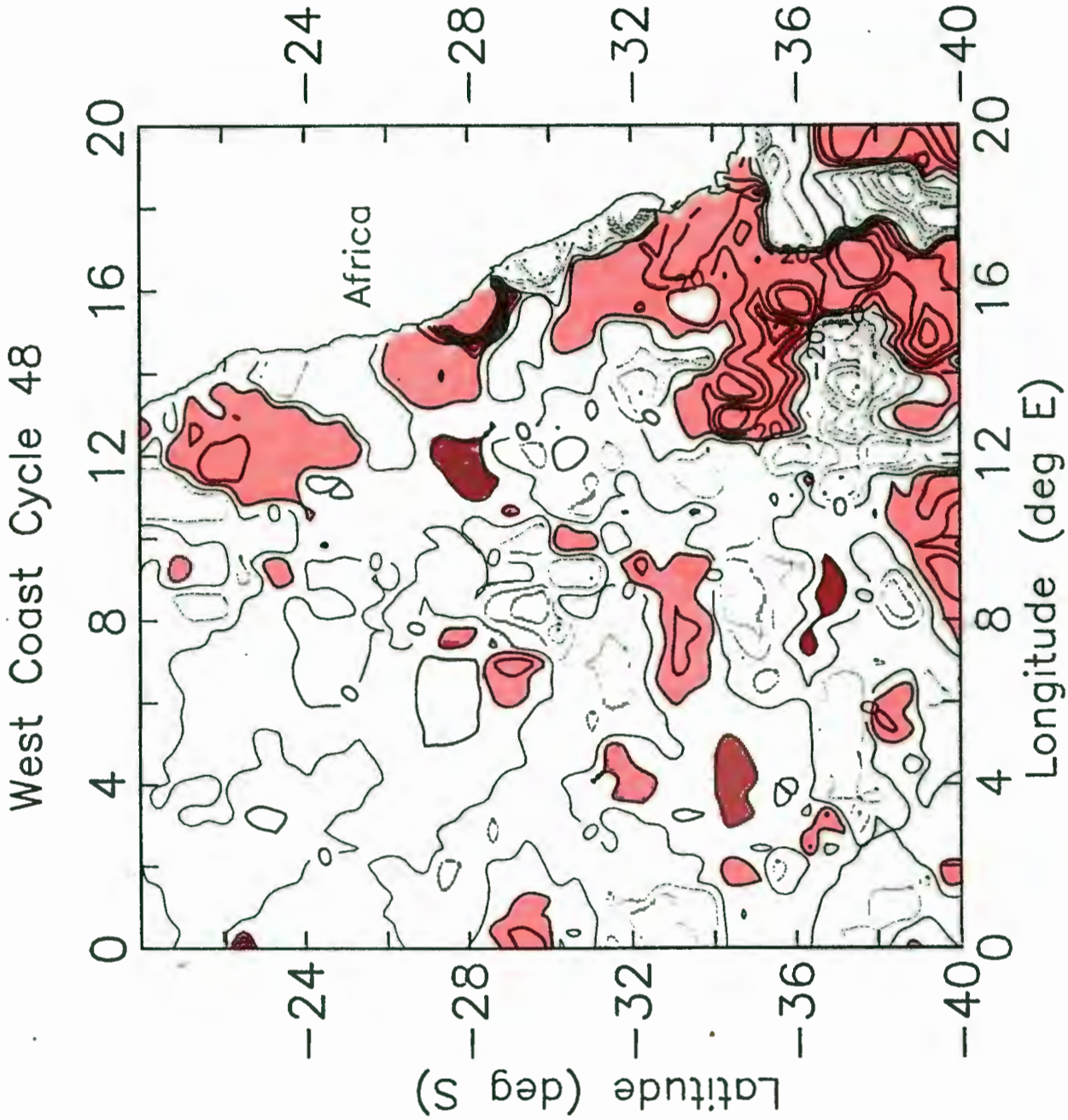
West Coast Cycle 48
Africa
Latitude (deg S)
Longitude (deg E)
-24
-28
-32
-36
-40
0
4
8
12
16
20
20
-20

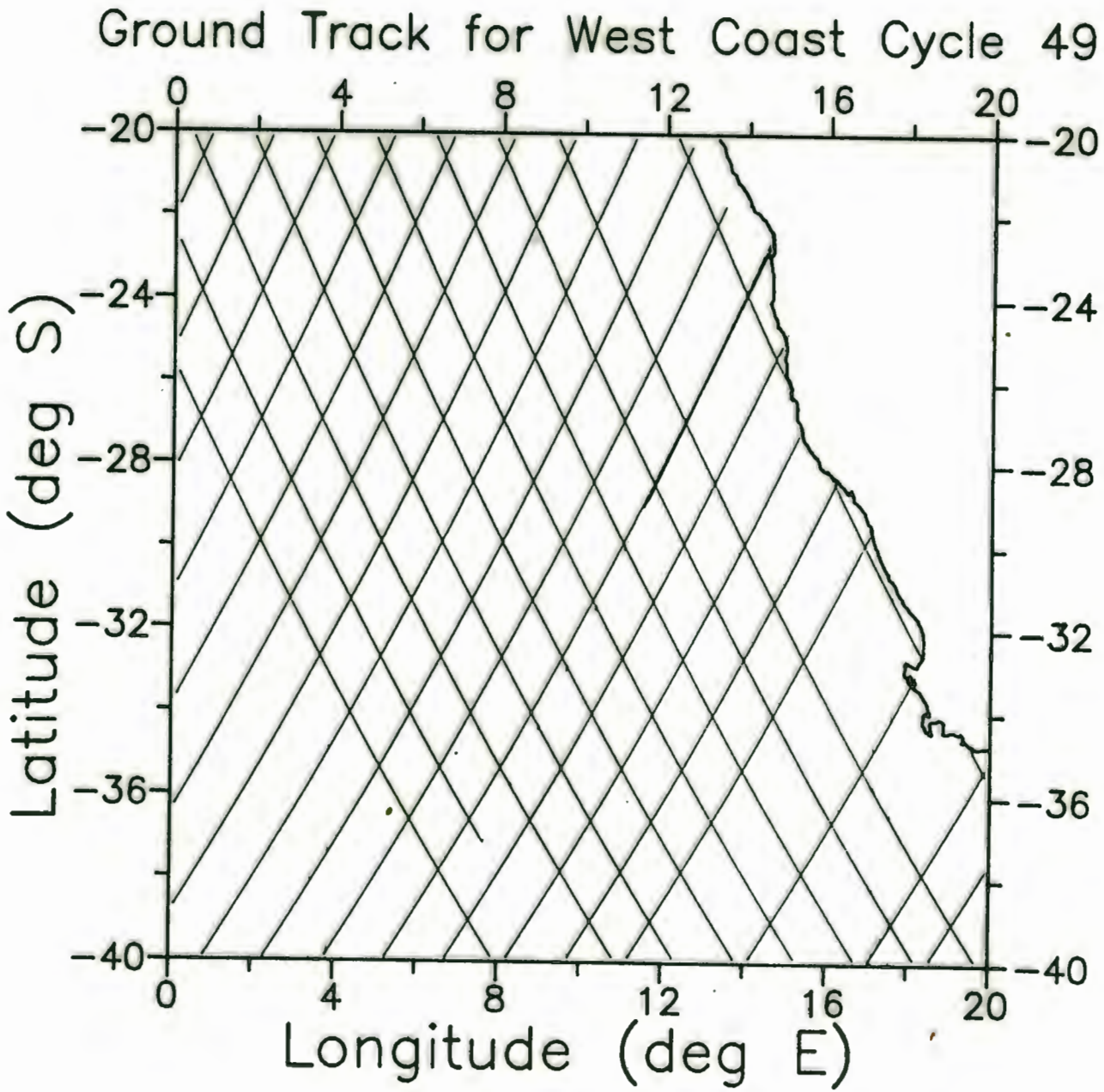
Ground Track for West Coast Cycle 49
0
4
8
12
16
20
-20
-24
-28
-32
-36
-40
Latitude (deg S)
Longitude (deg E)

Fig.19k

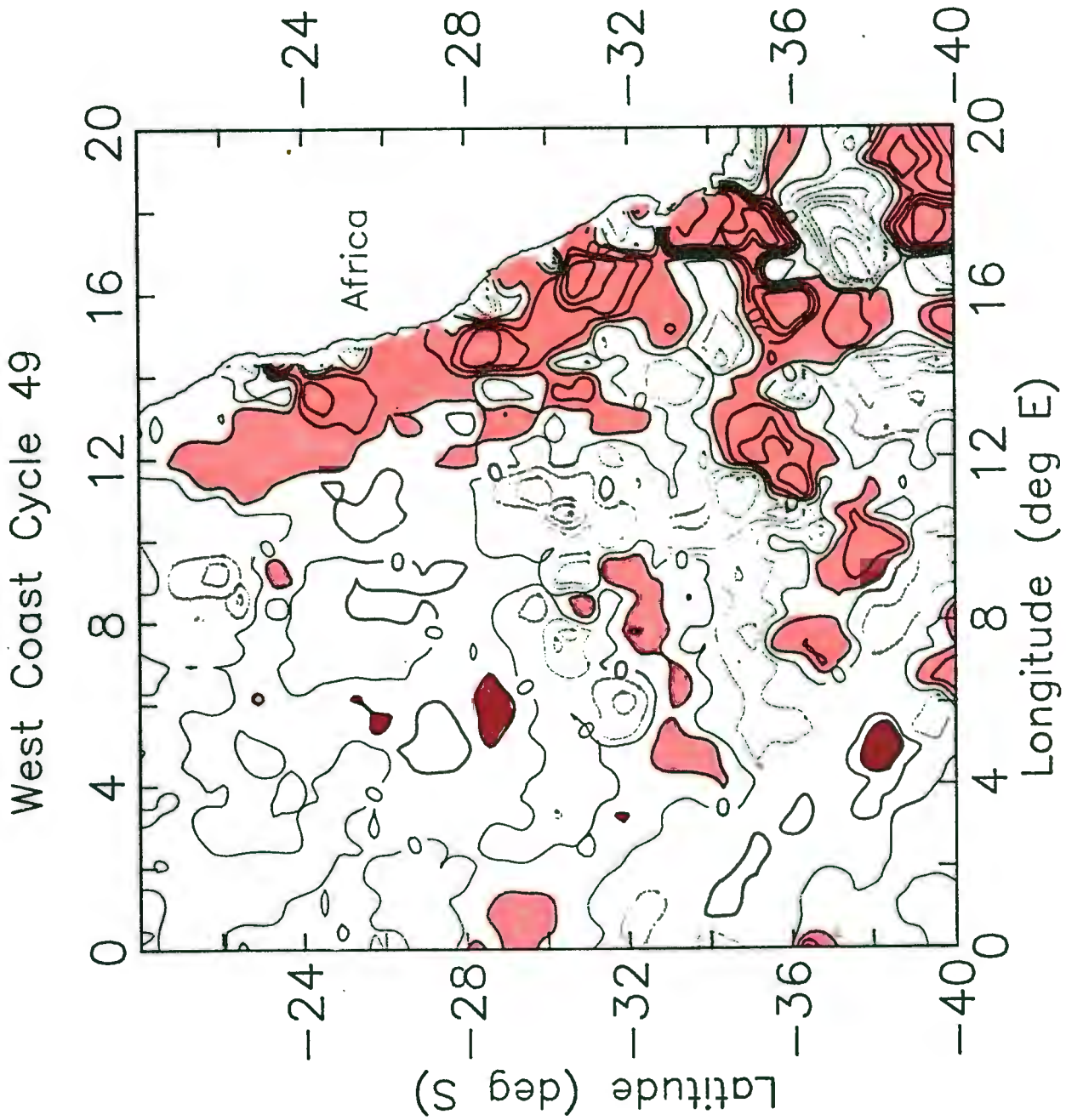
West Coast Cycle 49
Africa
Latitude (deg S)
Longitude (deg E)
-24
-28
-32
-36
-40
0
4
8
12
16
20

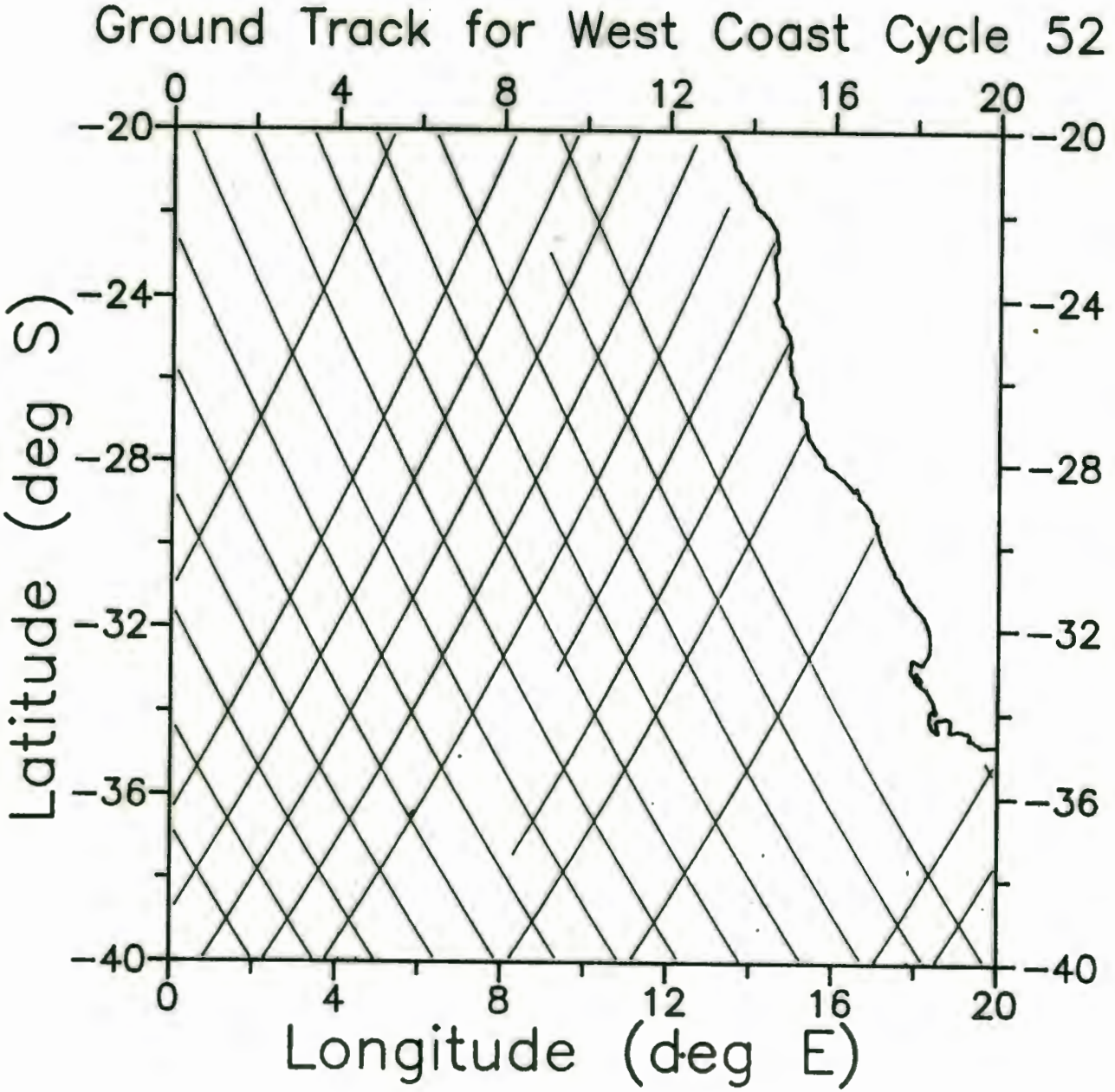
Ground Track for West Coast Cycle 52
0
4
8
12
16
20
-20
-24
-28
-32
-36
-40
Latitude (deg S)
Longitude (deg E)

Fig.19l

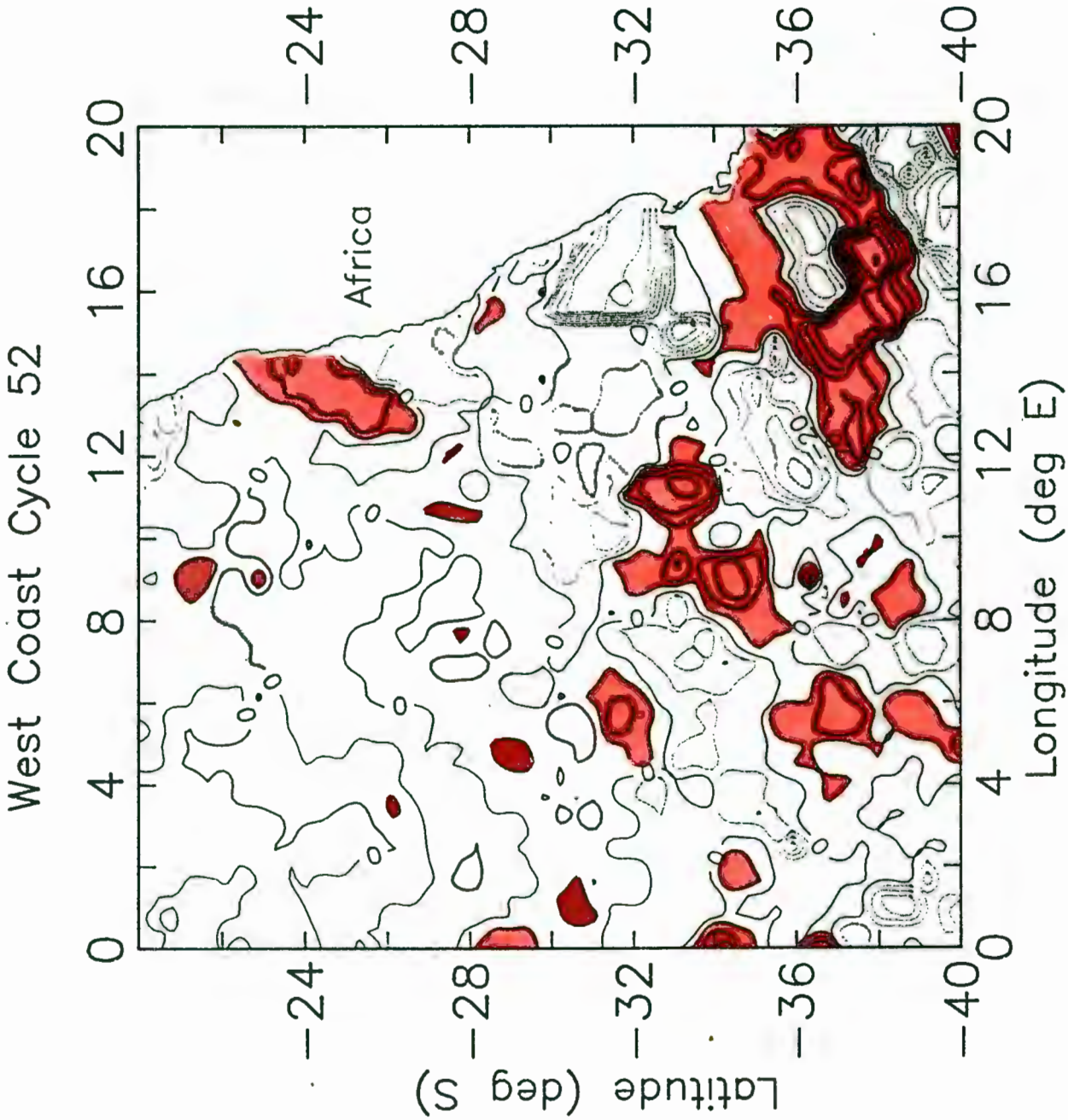
West Coast Cycle 52
Africa
Latitude (deg S)
Longitude (deg E)
0
4
8
12
16
20
−24
−28
−32
−36
−40

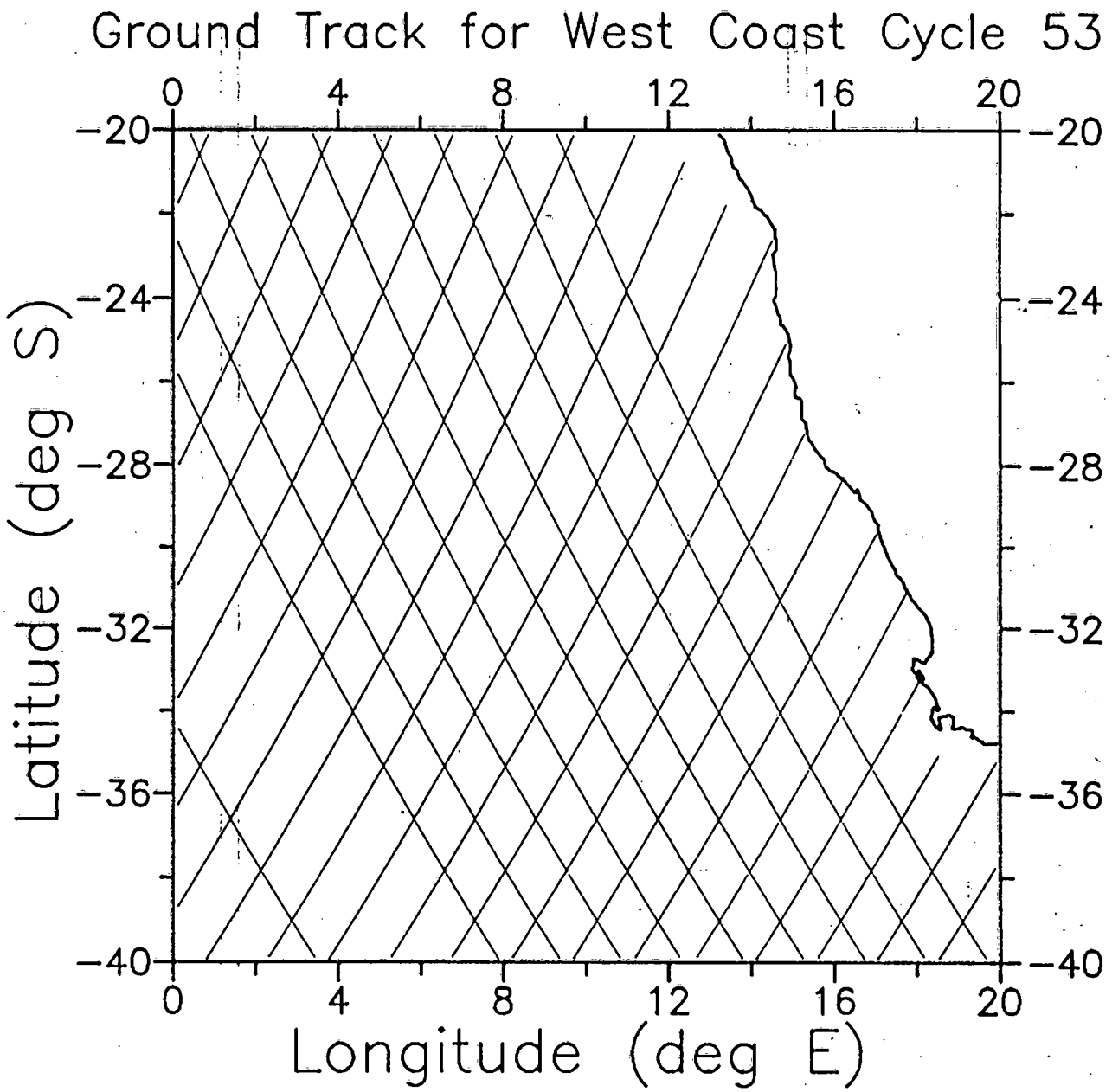
Ground Track for West Coast Cycle 53
0
4
8
12
16
20
-20
-24
-28
-32
-36
-40
Latitude (deg S)
Longitude (deg E)

Fig.19m

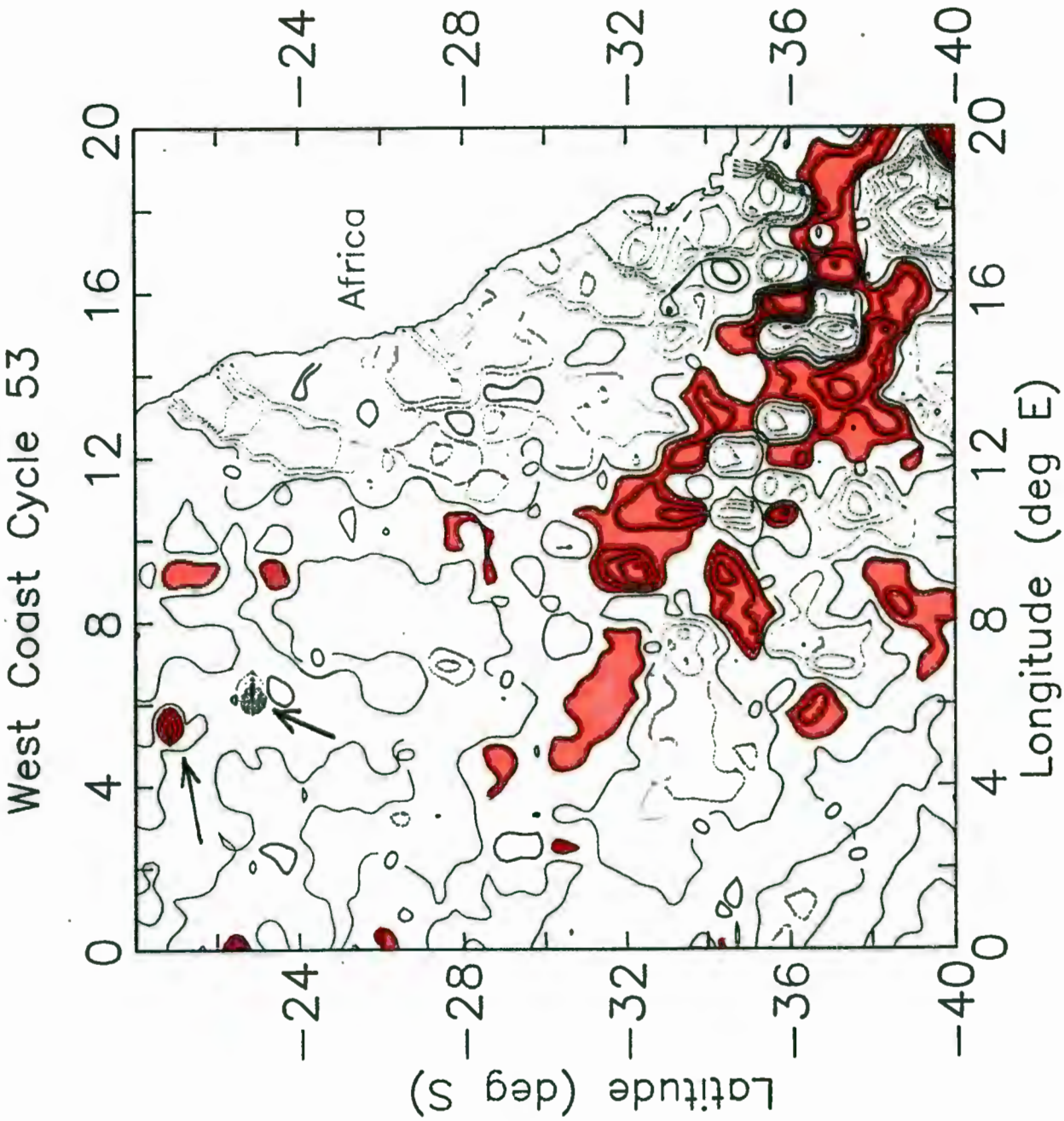
West Coast Cycle 53
Africa
Latitude (deg S)
Longitude (deg E)
-24
-28
-32
-36
-40
0
4
8
12
16
20

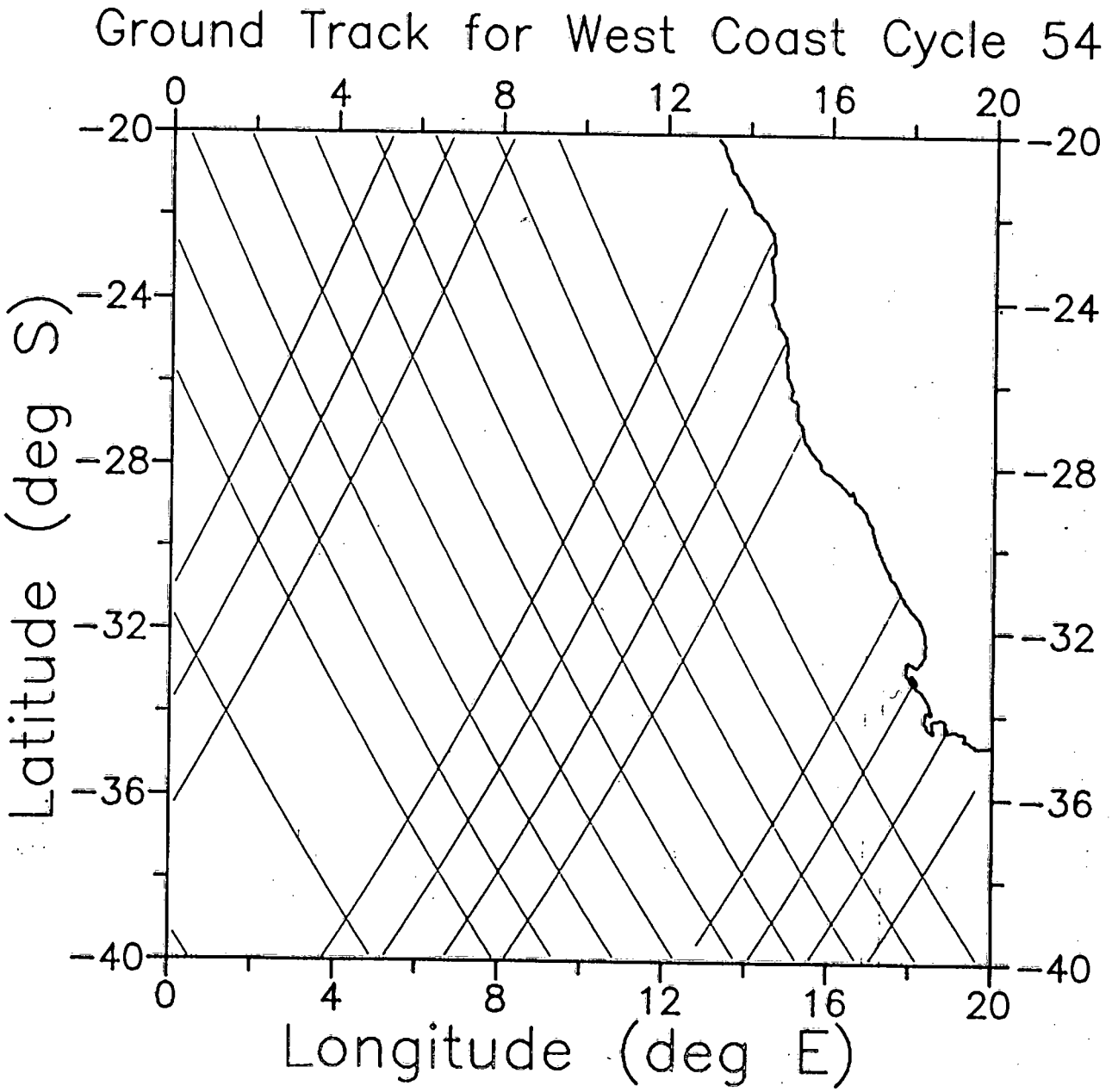
Ground Track for West Coast Cycle 54
0
4
8
12
16
20
-20
-24
-28
-32
-36
-40
Latitude (deg S)
Longitude (deg E)

Fig.19n

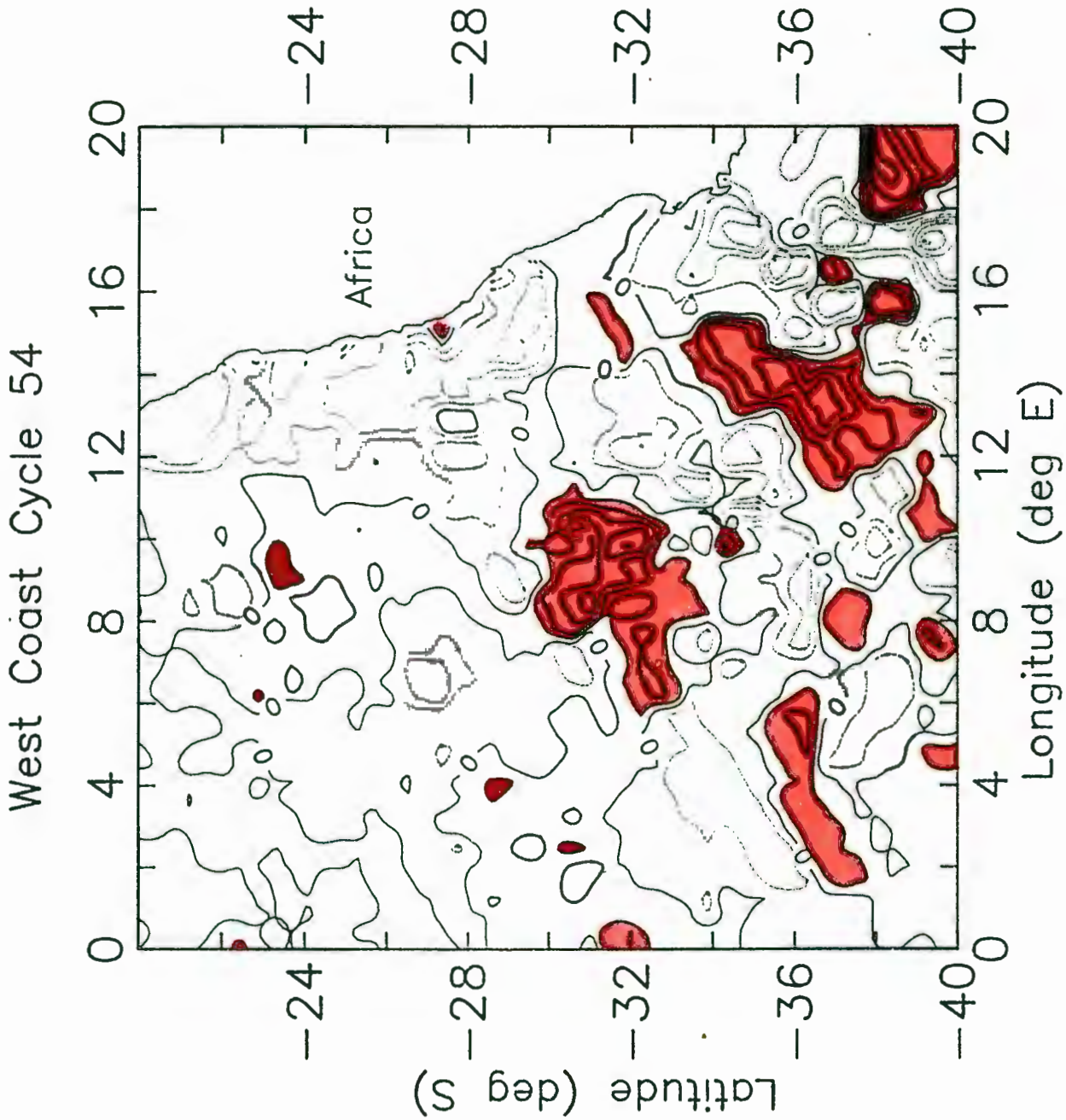
West Coast Cycle 54
Africa
Latitude (deg S)
Longitude (deg E)
-24
-28
-32
-36
-40
0
4
8
12
16
20

Table 7. Locations of possible Agulhas rings identified from the GEOSAT altimeter data for cycle 40

Ring number	Position of centre	Approximate maximum diameter (km) of 20 cm contour	Maximum elevation (cm) relative to zero
A40.1	37°S, 15.5°E	270	60
A40.2	38.5°S, 14°E	170	60
A40.3	37.5°S, 11.5°E	250	50
A40.4	33°S, 12.5°E	140	30
A40.5	31°S,7.5°E	310	30

Table 8. Locations of possible Agulhas rings identified from the GEOSAT altimeter data for cycle 53

Ring number	Position of centre	Approximate diameter (km)	Maximum elevation (cm)
A53.1	37°S, 16.5°E	110	40
A53.2	36°S, 15.5°E	140	40
A53.3	32°S, 9°E	170	50
A53.4	33°S, 10.5°E	240	30
A53.5	35°S, 9°E	270	30
A53.6	37.5°S, 11.5°E	>400	40

4.2.2 Contours of the "snapshot" SST

Residual sea surface heights at 7 day intervals were interpolated following the procedures described in Chapter 3. These values were gridded and contoured as previously described. Snapshots for the period 14 February 1989 to 14 April 1989 are shown in Figures 20(a) to 20(i).

Since it is possible for the features being investigated to move a half diameter within 17 days, it was anticipated that the reduced time distortion provided by the snapshots would help in the identification and tracking of features (Van Ballegooyen *et al. in prep.*).

Positive topographic features are identifiable as possible Agulhas rings, but the identification of the same feature in subsequent snapshots is difficult. A subjective interpretation of the snapshots identified a persistent topographic elevation in the region of the Agulhas retroflection south west of Cape Town at about 35°S, 13°E. This feature is spatially consistent over several weeks until a feature of markedly greater elevation than the background seems to bud off early in March (see Fig.21) and propagate northwestwards. Its path roughly follows the nominal ground track of ascending pass A158 through to a position centered approximately at 33°S, 10.5°E by the time of the final snapshot of 14 April 1989.

Although later altimeter data were not available for synoptic comparison with the hydrographic data, some corroboration was evident. The location of the ring centre on 6 April (see Fig. 21 - from hydrographic data in Duncombe Rae *et al.* 1992) agrees well with the altimeter-defined feature for 14 April (Fig. 21). Simple measurements taken from the plots show the ring to have travelled about 400 km in a northwestward direction between 14 February and 14 April. This equates to an approximate translation rate of about 7 $cm \cdot s^{-1}$ which is within the range given in the literature (e.g. Olson and Evans 1986, Gordon and Haxby 1990).

Interpretation of the SST contours for the snapshots is difficult, partly due to the spatial smearing which results (Duncombe Rae *et al.* 1992b). It should be simpler to identify features and follow their progress along individual passes.

Figure 20. Maps showing the residual sea surface heights interpolated at 7 day intervals to give "snapshots" of the sea surface topography. Snapshots covering the period 14 February 1989 to 14 April 1989 are shown in Figures 20a to 20i respectively..

Fig. 20a

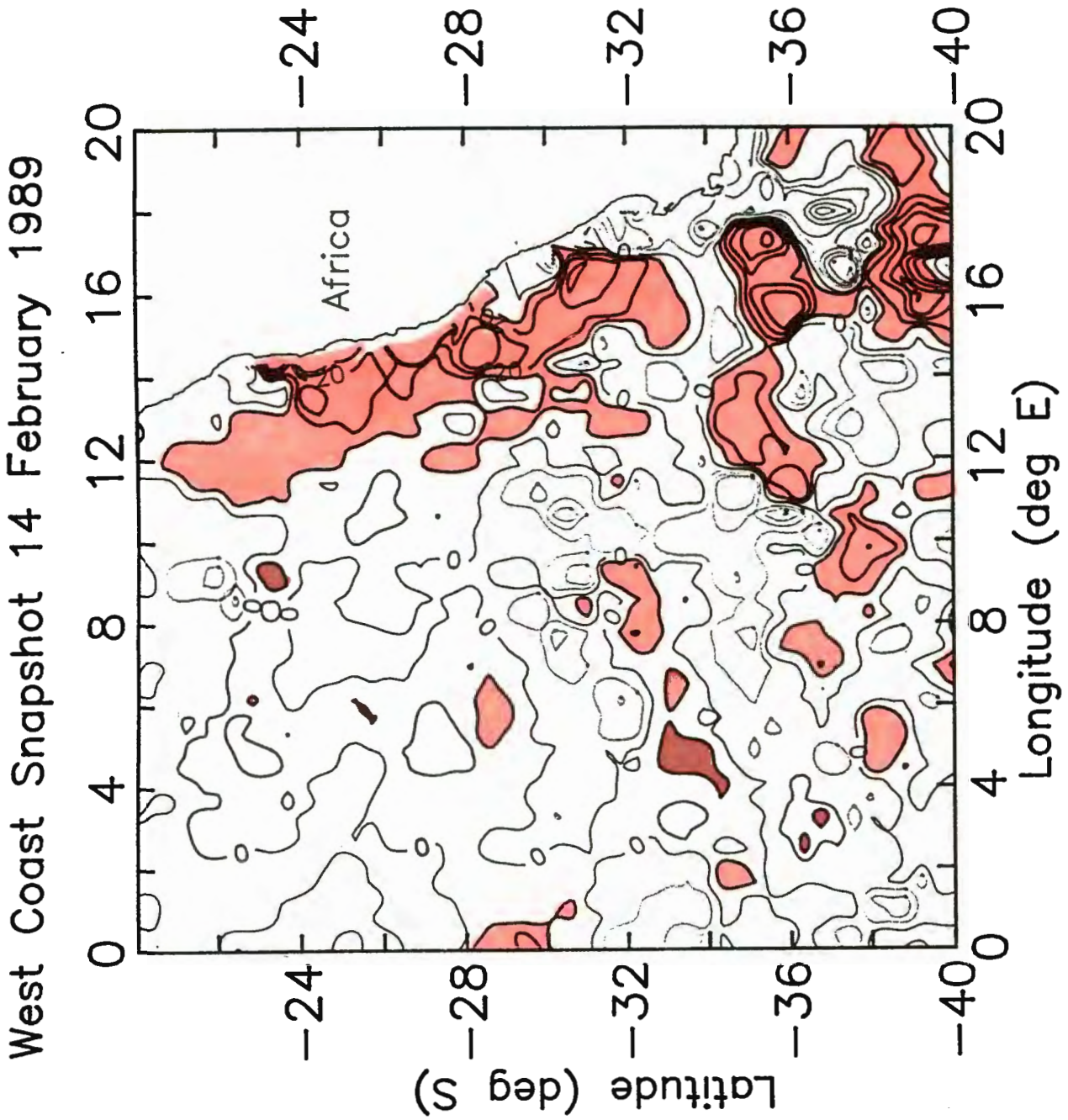
West Coast Snapshot 14 February 1989
Africa
Latitude (deg S)
Longitude (deg E)
-24
-28
-32
-36
-40
0
4
8
12
16
20

Fig. 20c

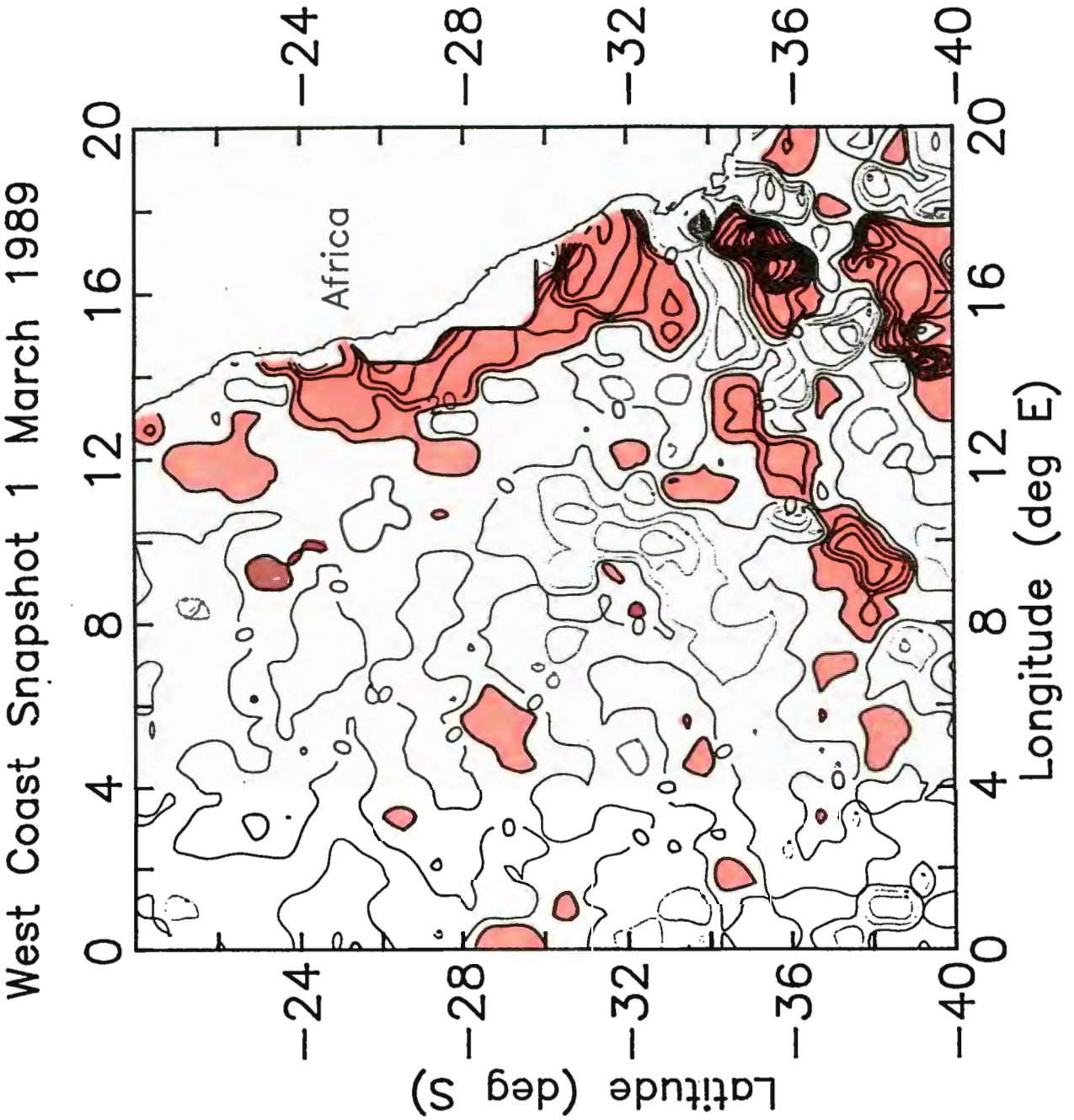
West Coast Snapshot 1 March 1989
Africa
Latitude (deg S)
Longitude (deg E)
0
4
8
12
16
20
-24
-28
-32
-36
-40

Fig. 20d

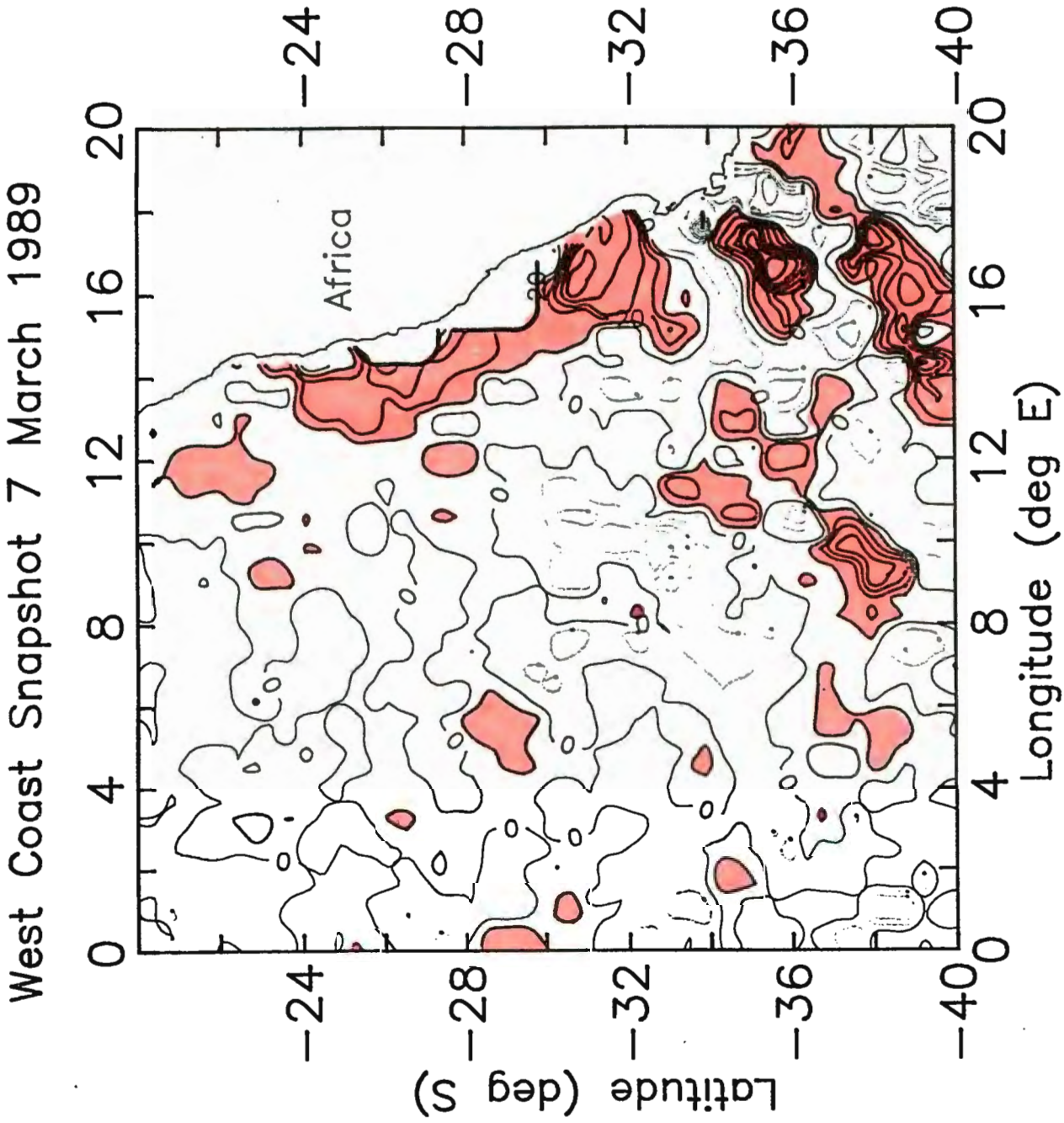
West Coast Snapshot 7 March 1989
Africa
Latitude (deg S)
Longitude (deg E)
0
4
8
12
16
20
−24
−28
−32
−36
−40

Fig. 20e

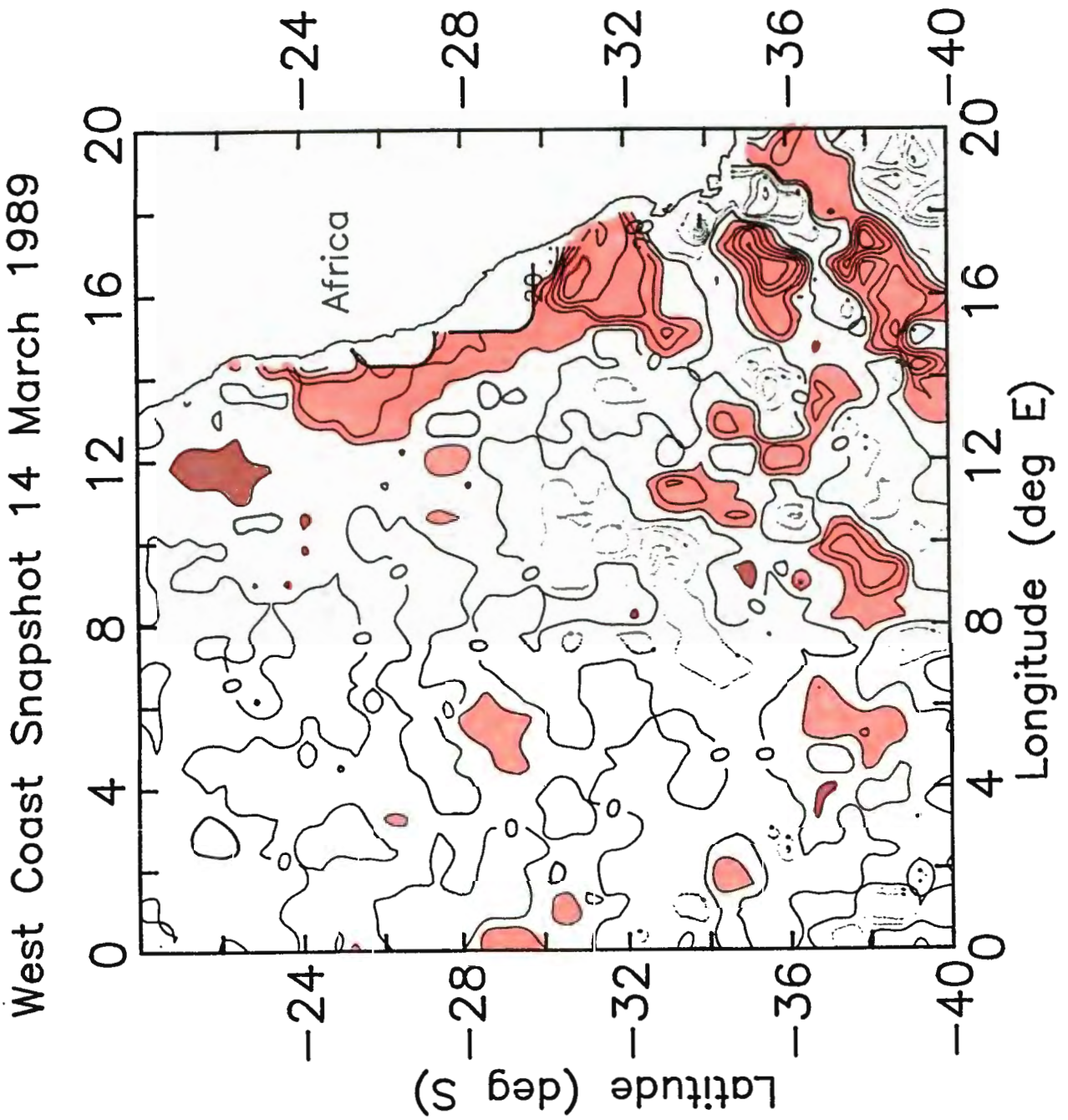
West Coast Snapshot 14 March 1989
Africa
Latitude (deg S)
Longitude (deg E)
0
4
8
12
16
20
-24
-28
-32
-36
-40

Fig. 20f

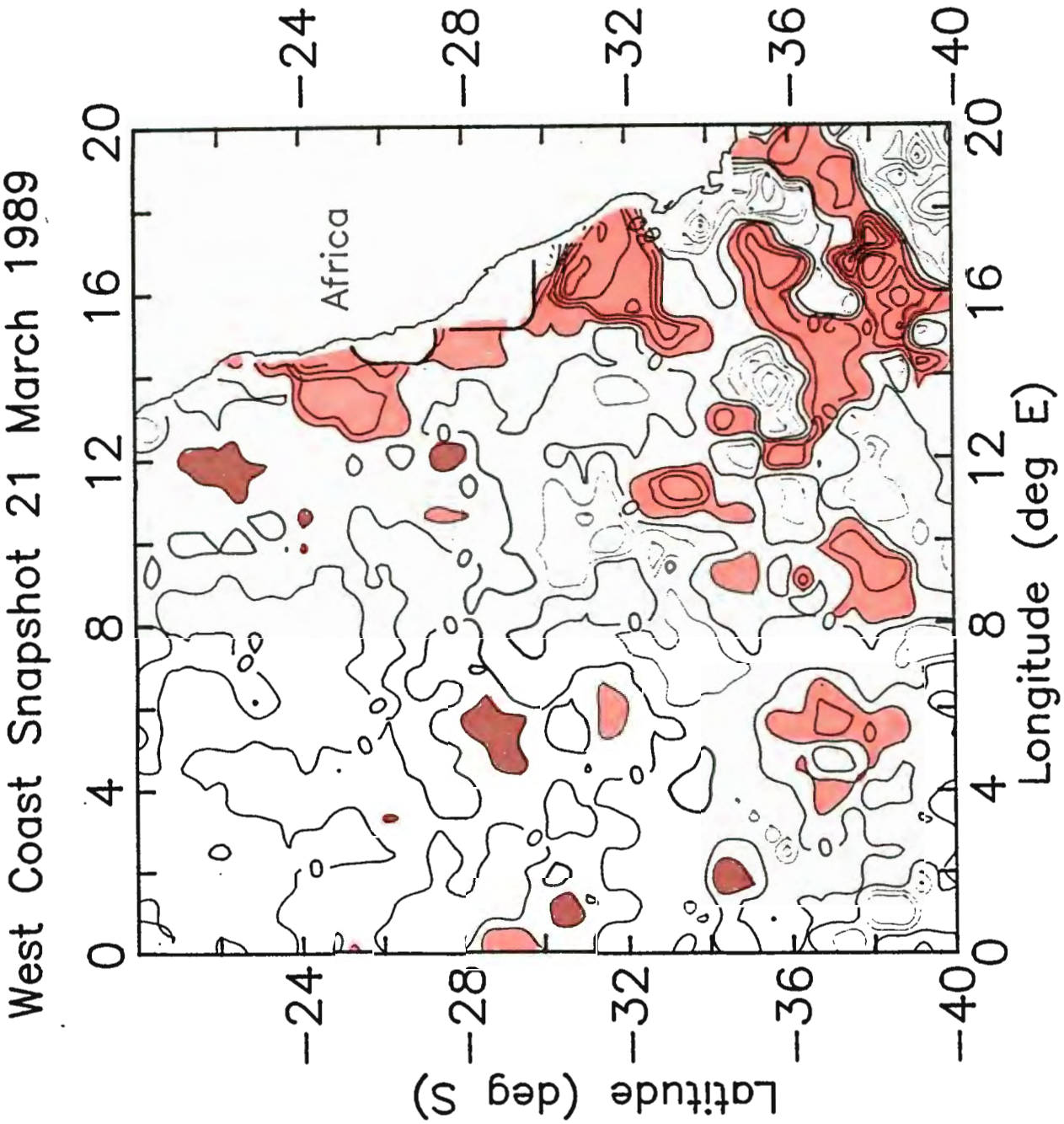
West Coast Snapshot 21 March 1989
Africa
Latitude (deg S)
Longitude (deg E)
0
4
8
12
16
20
-24
-28
-32
-36
-40

Fig. 20g

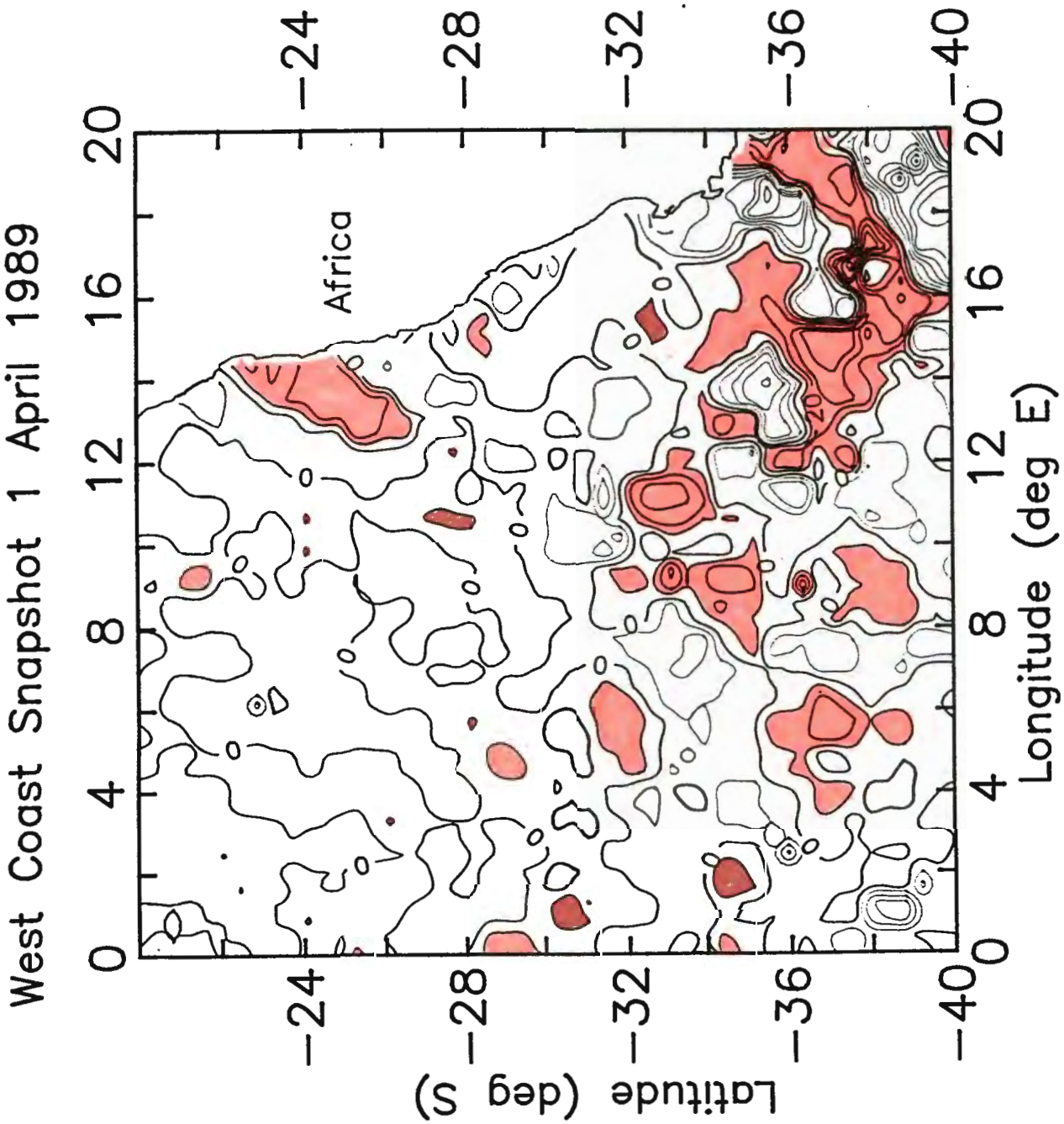
West Coast Snapshot 1 April 1989
Africa
Latitude (deg S)
Longitude (deg E)
0
4
8
12
16
20
−24
−28
−32
−36
−40
20

Fig. 20h

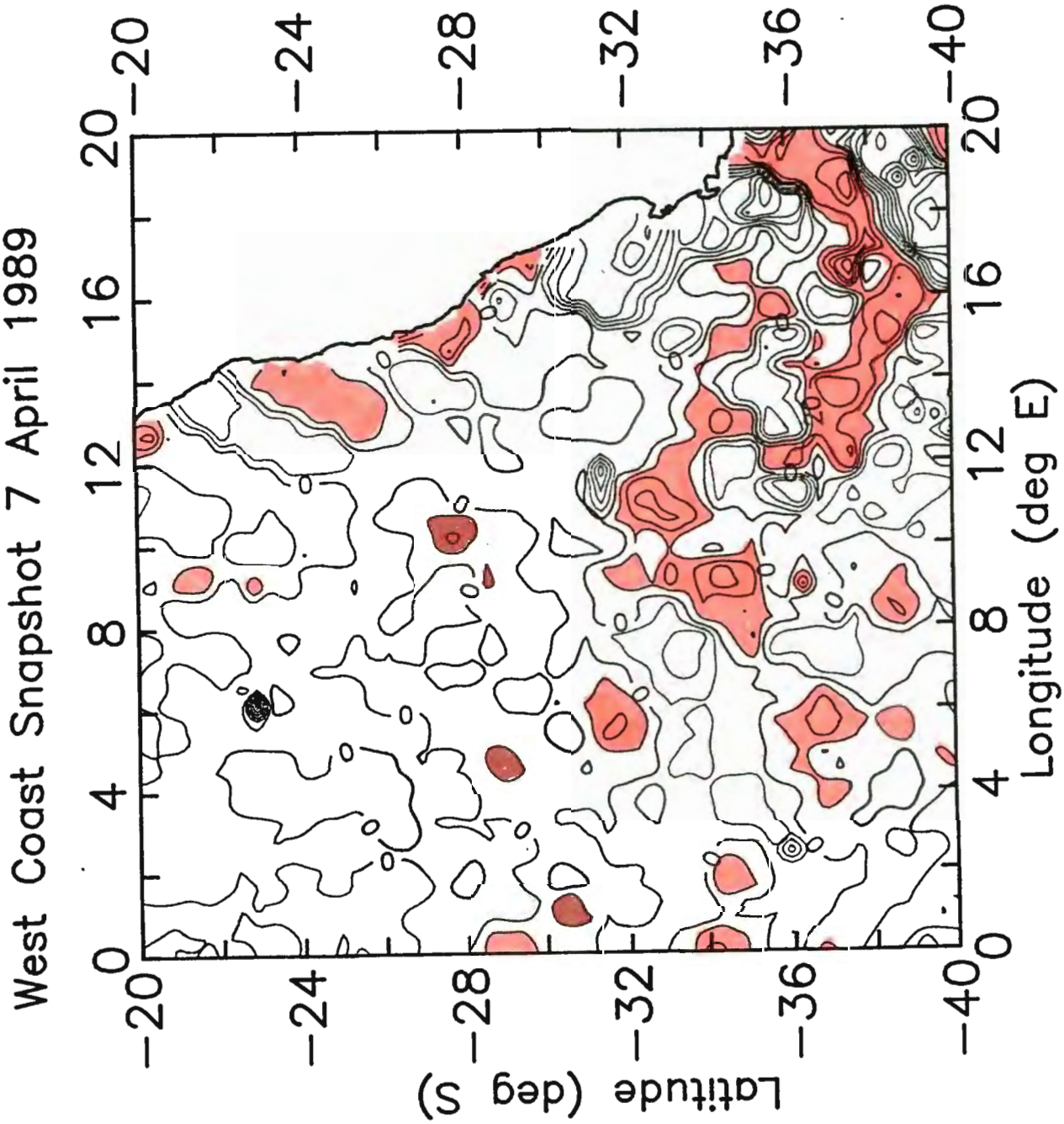
West Coast Snapshot 7 April 1989
Latitude (deg S)
Longitude (deg E)
−20
−24
−28
−32
−36
−40
0
4
8
12
16
20

Fig. 20i

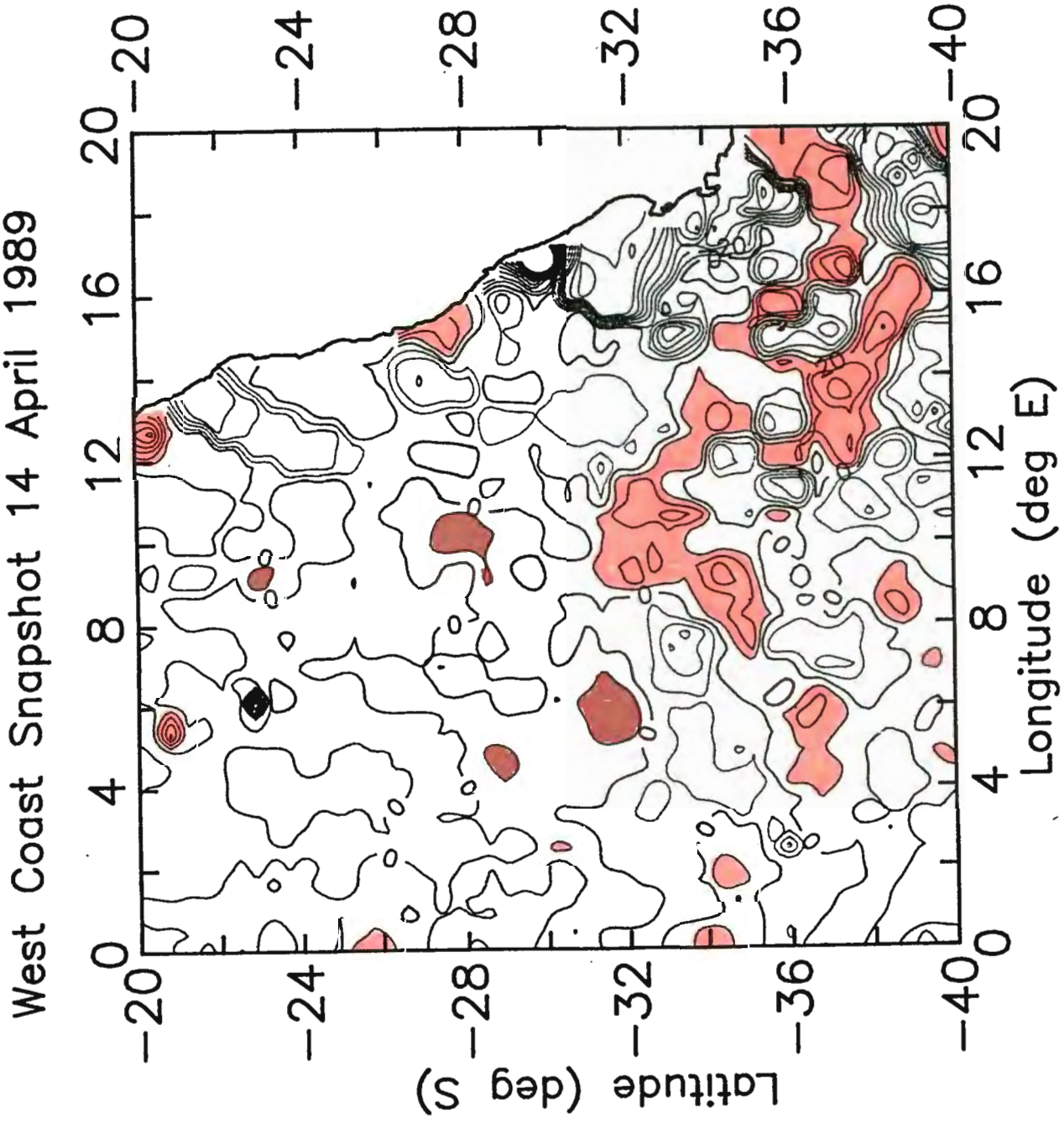
West Coast Snapshot 14 April 1989
Latitude (deg S)
Longitude (deg E)
−20
−24
−28
−32
−36
−40
0
4
8
12
16
20

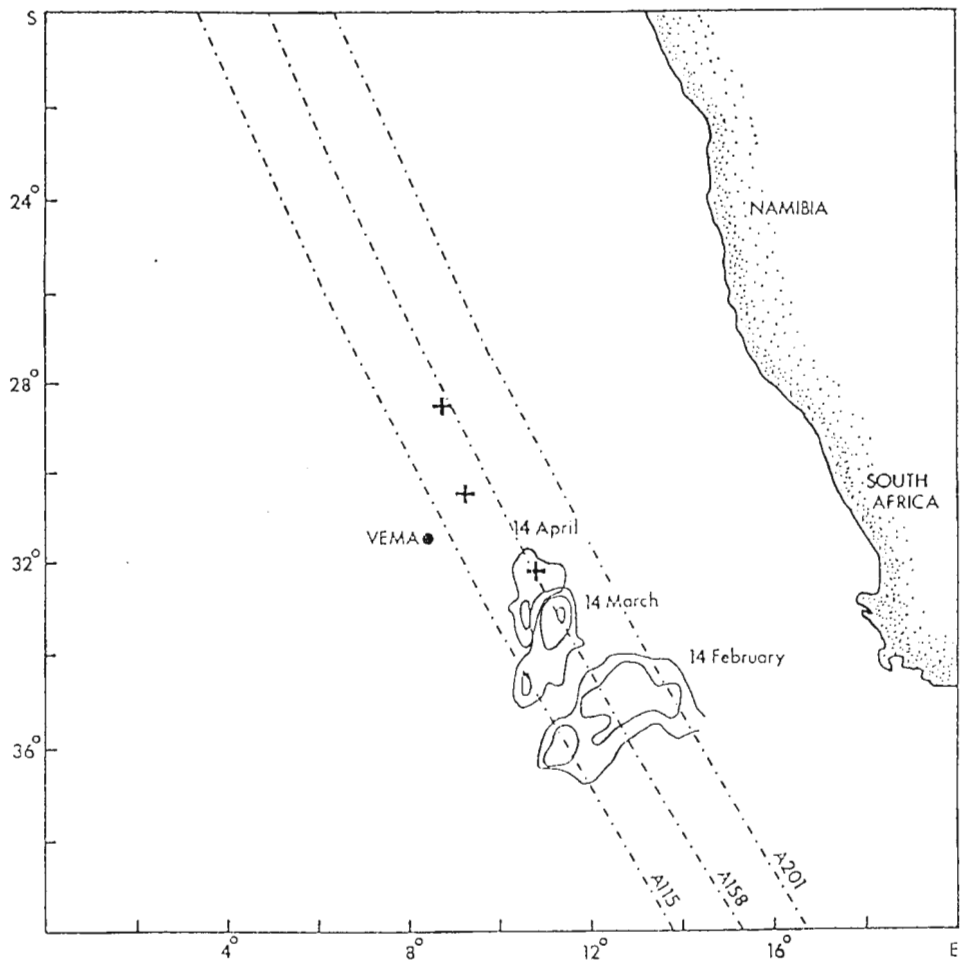

Figure 21. Composite of snapshot sea elevations from mid-February to mid-April. Contours less than 20 cm and elevations away from the features of interest have been omitted. The ascending satellite ground tracks over the area (A115, A158, A201) are marked. The approximate positions of the ring centre on 6 April and 20 May 1989 determined by hydrography and on 15 June 1989 by NOAA infrared imagery are indicated by crosses (from Duncombe Rae *et al.* 1992b).

4.2.3 The along-track profiles of SST

The along-track sea height profiles were plotted for the ascending pass A158 along which the Vema ring appeared to have travelled after early March 1989. Figure 22 shows the profiles between 40°S and 24°S for cycles 52, 53 and 54, representing the period 24 March to 27 April 1989. No data were available for cycles 50 and 51 or later than cycle 54.

A region of topographic elevation greater than 30 cm (relative to the zero background) exists between 36°S and 38°S which may signify a westward intrusion of the Agulhas retroflection loop to about 14°E into the south east Atlantic (altimetry will only show the variable component relative to the mean over the one year of data analysed here). Its diameter of about 250 km is somewhat less than the "reasonably constant" retroflection loop diameter of 342 ± 66 km given by Lutjeharms and Van Ballegooyen (1988). This may be as a result of the pass crossing the westward edge of the loop and not its complete diameter. However, since the SST and diameters of the retroflection and rings are comparable, it is difficult to distinguish between them from a single pass. Inspection of neighbouring passes did not afford a clear decision.

The feature assumed to be an anticyclonic Agulhas ring is evident centered at about 33°S. Assuming the background topography to be represented by the zero line, the ring

shows topographic elevations of some 30 cm and a N-S diameter of 200 to 300 km which is in general agreement with the hydrographic observations and accepted ring dimensions (180 km with respect to the 10° C isotherm - Duncombe Rae 1991, Duncombe Rae *et al.* 1992b). The dashed line in Figure 22 indicates the ring's equatorward movement along track A158. Its displacement of some 200 km over the 34 days from cycle 52 to cycle 54 suggests a translation rate of 5.9 $km \cdot day^{-1}$ or 6.8 $cm \cdot s^{-1}$ which again compares favourably with the 6.4 $cm \cdot s^{-1}$ derived from the XBT sections (Duncombe Rae *et al.* op. cit.) and falls within the range reported (Duncombe Rae op. cit.).

Pass A158 lies approximately along the same ground track as the line BB' sampled hydrographically by the RS *Benguela* (see Fig. 16). The along-track profiles were graphically subsampled at approximately 30 nautical mile intervals in order to calculate sea surface slopes from which geostrophic velocities could be computed for comparison with those which were calculated from the CTD stations. Table 9 gives the topographic values extracted from the profiles at 0.5° latitude intervals (approximately 65 km due to the 108° tilt of the orbit) along track. Using equation 12 we can compute the cross-track components of the surface geostrophic velocities within the ring and these are also given in Table 9.

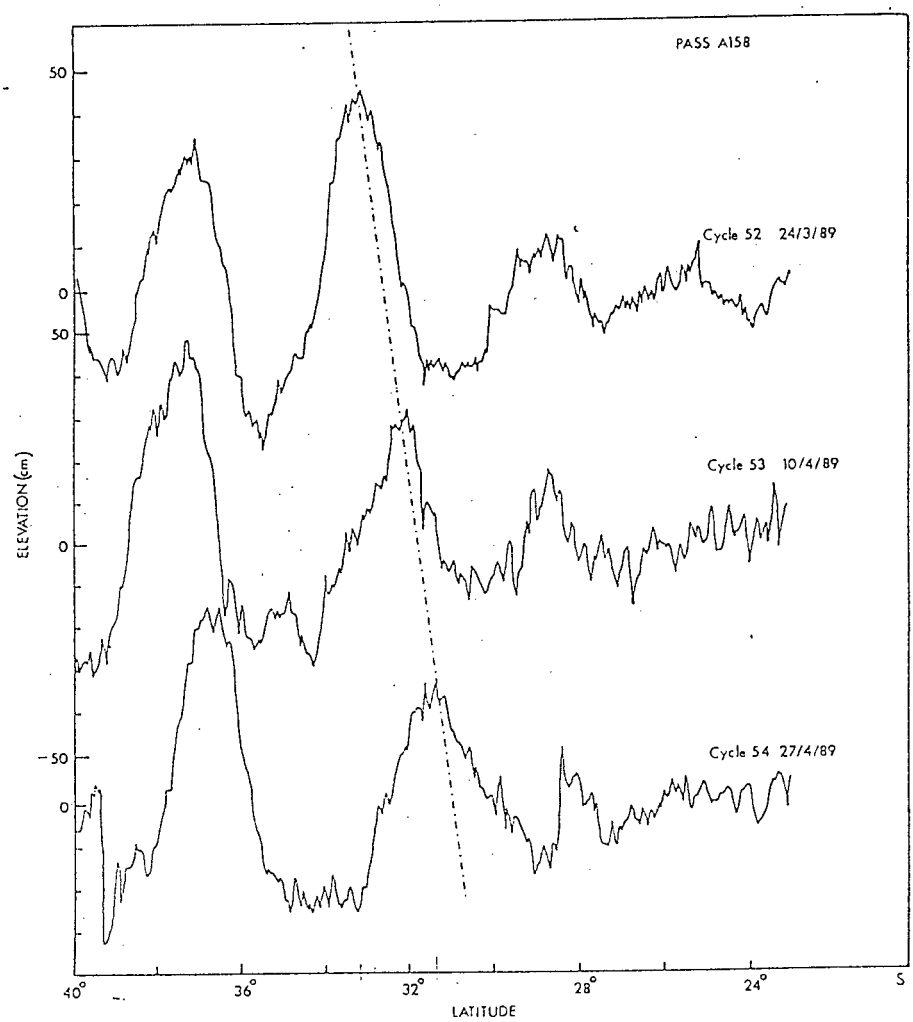

Figure 22. Along-track elevations from three successive cycles (52, 53, 54) along pass A158 in March and April 1989. The progress of the elevation corresponding to the ring is indicated by the dashed line. (from Duncombe Rae *et al.* 1992b)

Table 9. Sea surface elevations, slopes and cross-track surface geostrophic speeds from GEOSAT altimeter data for cycles 52, 53 and 54

Position °S	Height difference (cm)	Slope $*10^{-5}$	Velocity ($cm \cdot s^{-1}$)
cycle 52			
34			
33.5	32	0.49	70
33	4	0.06	9
32.5	-17	-0.26	-38
32	-28	-0.43	-64
cycle 53			
33.5			
33	7	0.11	13
32.5	13	0.20	25
32	10	0.15	19
31.5	-20	-0.31	-39
31	-17	-0.26	-34
cycle 54			
32.5			
32	16	0.24	37
31.5	8	0.12	19
31	-8	-0.12	-19
30.5	-7	-0.11	-17
30	-9	-0.14	-22

The anticyclonic sense of flow within the ring is indicated. Cross-track velocities at the southern edge of the ring are approximately toward the NE (positive in Table 9), while those at the northern edge are toward the SW (negative in Table 9).

The maximum velocities are encountered toward the outer edges of the ring and are highest at 70 $cm \cdot s^{-1}$ (southern edge) and -64 $cm \cdot s^{-1}$ (northern) for cycle 52 with characteristic values of about 30 $cm \cdot s^{-1}$. These velocities compare well with those computed from the hydrographic data and from feature-tracking on satellite infrared imagery (Duncombe Rae *et al.* 1992b). Figure 23 shows, for comparison, the geostrophic velocities calculated from the hydrographic data on line BB′ during May and those from the altimeter data for cycle 53 (April).

These estimates were refined by the calculation of geostrophic velocities from the "instantaneous" surface slopes for the individual along-track residual height pairs (not shown). These velocities exhibited a great deal of variability in the along-track direction as may be expected from the relative noisiness of the signals shown in Figure 22. Calculating the slopes from the second order differenced data according to:

$$slope_i = (y_{x(i+1)} - y_{x(i-1)})/(x_{(i+1)} - x_{(i-1)}) \qquad (13)$$

provided some smoothing of the velocity profile (not

shown), but still passed much of the noise.

The residual sea heights were then smoothed with a 70 km running median filter (used by Didden and Schott 1992) in order to remove the outlying values. The smoothed altimeter sea surface topography profiles were then subsampled at 0.5^{o} latitude intervals for spatial resolution comparable to the hydrographic station data. An example of these values for cycle 53 is shown in Figure 24.

The general features observable are similar, but quite large differences in velocities may result from the various methods. It would appear that the profiles should first be smoothed before subsampling at suitable intervals for the computation of surface slopes and geostrophic velocities (note that Didden and Schott (1992) used a 70 km running median filter on the residual heights and then subsampled every 20 km).

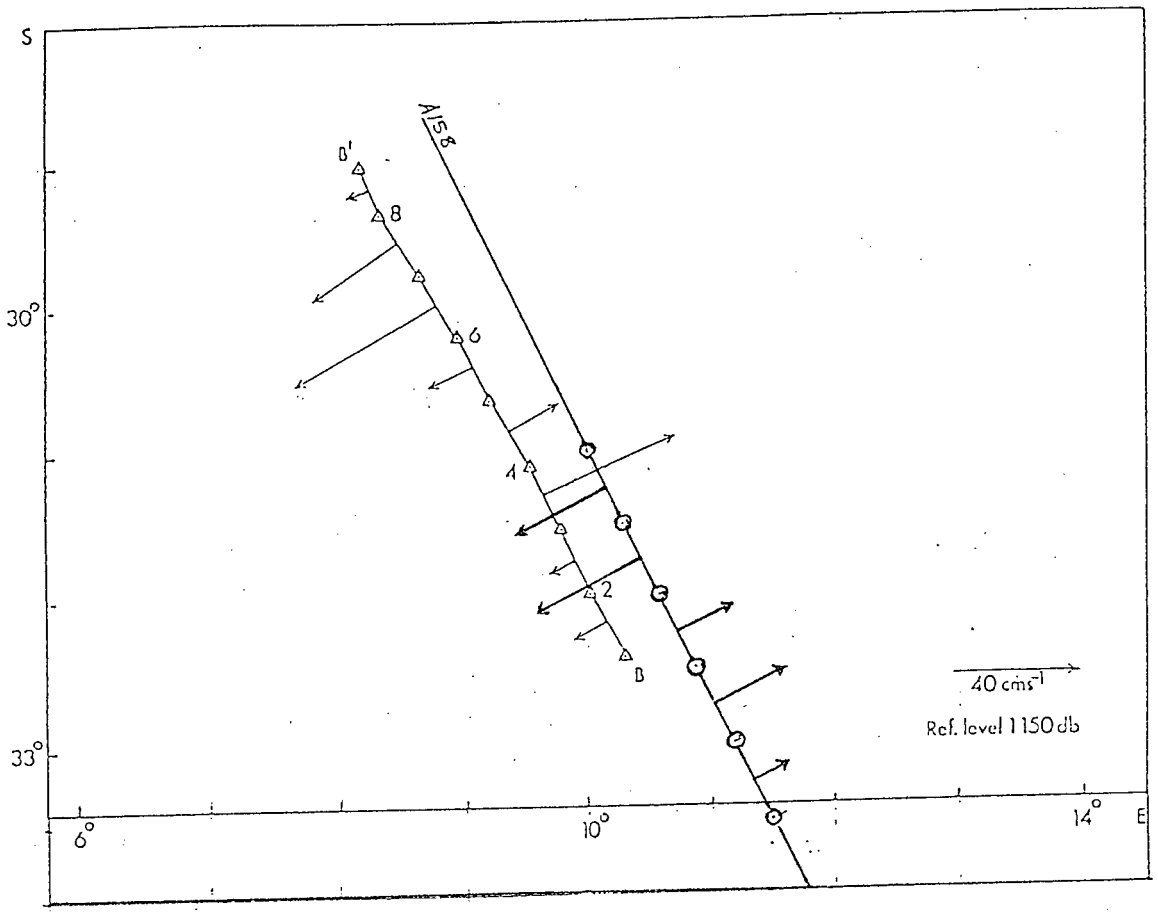

Figure 23. Surface geostrophic velocities for the Vema ring computed from hydrographic data referenced to 1150 db (line BB' : May 1989 (from Duncombe Rae *et al.* 1992b)) and from GEOSAT altimeter data (pass A158 : 10 April 1989). Triangles indicate the positions of hydrographic stations and circles the positions where altimeter data were the altimeter height profiles were subsampled.

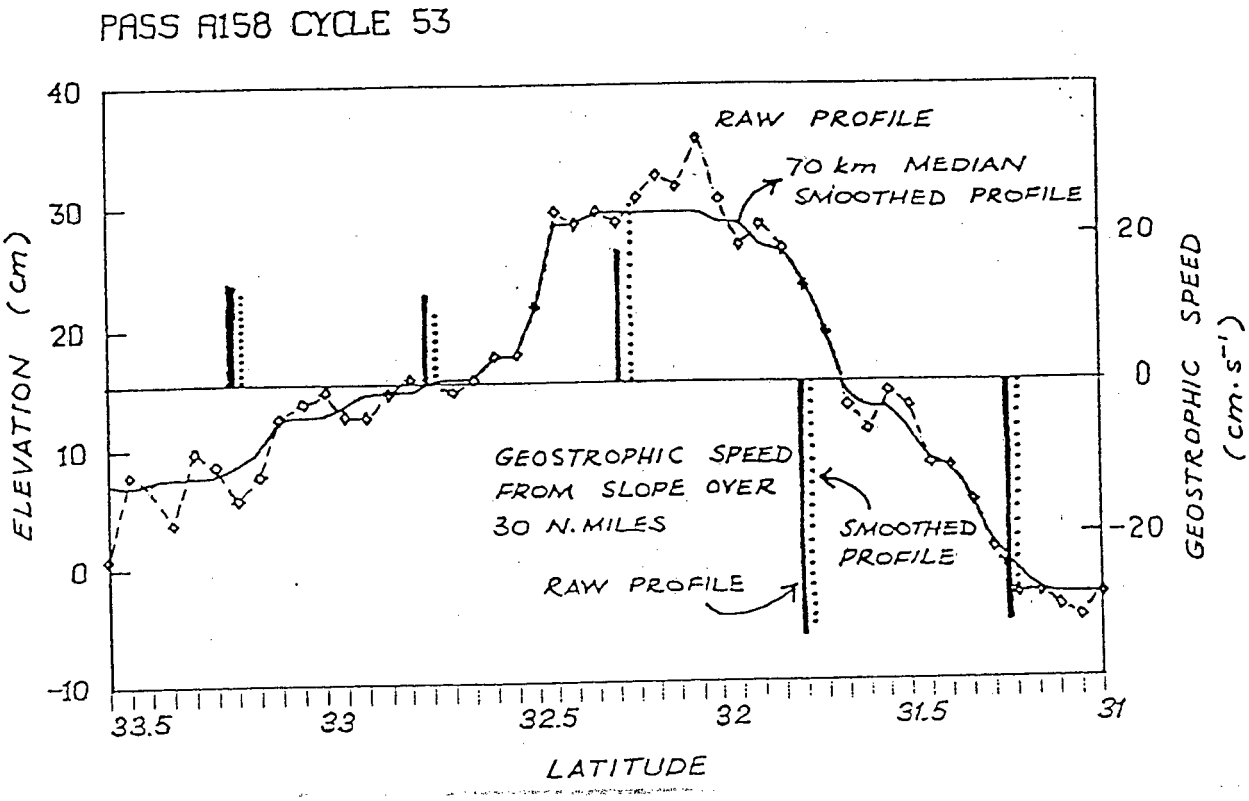

Figure 24. Raw altimeter height profile along pass A158 and the smoothed profile after filtering with a 70 km running median filter. Cross-track surface geostrophic speeds for data subsampled at approximately 30 nautical mile spacing are shown for the raw and smoothed profiles for comparison.

CHAPTER 5

CONCLUSIONS

Previous authors have shown that GEOSAT altimeter data are capable of resolving Agulhas rings and indicating their progress through the southeast Atlantic (Fu and Zlotnicki 1989, Gordon and Haxby 1990, Wakker *et al.* 1990b, Feron *et al.* 1992, Van Ballegooyen *et al. in prep.*). The analysis of the GEOSAT altimeter data for July 1988 to May 1989 presented in this thesis again confirms this facility, but also serves to indicate some limitations on the method which are worth noting.

The contours of the sea surface topography for each 17 day repeat cycle or weekly "snapshot" indicate that a population of anticyclonic (and cyclonic) ring-like features was present within the southeast Atlantic near the Agulhas retroflection region. The horizontal and vertical form of these features was consistent with that reported by other authors for Agulhas rings in the region. The positive identification of any particular feature in subsequent repeat cycles was, however, difficult. Van Ballegooyen *et al.* (*in prep.*) report that rings may interact and move somewhat erratically while close to their separation from the retroflection which itself behaves erratically (Lutjeharms and Van Ballegooyen 1988). This may mean that the geoid approximation synthesised over only one year of altimeter data for this analysis failed to adequately smooth the prevalent mesoscale features and so failed to unambiguously indicate rings. In

In support of this conclusion, Feron *et al.* (1992) stated that although the altimetric "detection of Agulhas rings in the relatively quiet South Atlantic gyre is rather straightforward, the shedding process itself is rather difficult to extract from the altimeter measurements" and that a "straightforward interpretation of the sea level maps in the retroflection area is extremely difficult". These authors concluded this was a result of the meandering of the Agulhas Current in the retroflection region which introduced artificial ring-like features into the sea surface height departures from the mean sea surface.

Another problem possibly responsible for the difficulty experienced in tracking rings was that of the decline in quality and quantity of the altimeter measurements as GEOSAT reached the end of its life, resulting in frequent data dropouts on two or more passes in the area of interest. This obviously impacted on what could be revealed by the sea surface topography maps and may also have affected the synthesised mean sea surface.

Knowing, from hydrographic measurements, the location of the Vema ring in April and May of 1989, it was possible to backtrack the path of a topographic elevation which was assumed to be the same ring. Confirmation of the characteristics of this feature were made from the along-track sea surface topography profile from ascending pass A158, along whose ground track the ring seemed to propagate between February and April 1989. The altimeter data showed that the ring progressed toward the NW at an average rate

of 6.8 $cm \cdot s^{-1}$ which agrees well with the hydrographically derived rate of 6.4 $cm \cdot s^{-1}$ for this particular ring (Duncombe Rae *et al.* 1992b) and data found for other rings (Olson and Evans 1986, Gordon and Haxby 1990, Van Ballegooyen *et al. in prep.*).

Sea surface slopes computed from the along-track sea surface topographic profiles provided cross-track surface geostrophic velocities of up to 25 $cm \cdot s^{-1}$ toward the NE at the southern rim and up to 39 $cm \cdot s^{-1}$ toward the SW at the northern rim of the ring. Comparison of the altimeter-derived velocities and velocity structure of the ring with those from the hydrography for the Vema ring shows good agreement in both direction and speed, although the altimeter-detected ring was located farther south. This served to confirm the altimeter-detected feature as being an Agulhas ring. A high degree of small spatial scale variability (between consecutive 1-second along-track values which represent a spacing of about 7 km) in the sea surface slopes was present and taken to be spurious. The 1-second measurements were then smoothed by the application of a 70 km running median filter as reported by Didden and Schott (1992). The resulting smoothed sea surface height residuals were again subsampled at approximately 30 nautical mile (55 km) intervals in order to provide the same horizontal spatial resolution as achieved by the hydrographic station spacing. Surface geostrophic velocities computed from these smoothed values still provided results consistent with the hydrographic description of the Vema ring. Since no altimeter data were available for direct synoptic comparison with the hydrography it was not possible to use the altimeter data to

investigate aspects of the decay of the ring over time.

It has been shown that the GEOSAT altimeter data provided a valuable tool for the study of the mesoscale variability of the southeastern Atlantic Ocean region. It is anticipated that the improved measurement accuracy of the TOPEX/POSEIDON altimeter will allow the full development of the altimetric methods for the further investigation and monitoring of Agulhas ring shedding and propagation features. The TOPEX/POSEIDON satellite has an exact repeat orbit period of 10 days which provides an improved temporal resolution over the 17 days of GEOSAT. It is unfortunate, however, that the more frequent repeat cycle has the inverse effect on the spatial resolution. The ground track separation of TOPEX/POSEIDON is some 300 km at mid-latitudes which will make it difficult to spatially resolve Agulhas rings. The usefulness of the sea surface topography maps from TOPEX/POSEIDON will therefore be limited in terms of the detection of Agulhas rings unless a ring happens to propagate along the path of a ground track of the altimeter.

REFERENCE LIST

BANG, N. D. 1970a - Dynamic interpretations of a detailed surface temperature chart of the Agulhas Current retroflexion and fragmentation area. *S. Afr. geogrl J.* **52**: 67-76.

BANG, N. D. 1970b - Major eddies and frontal structures in the Agulhas current retroflexion area in March, 1969. In *Proceedings of the Symposium on Oceanography in South Africa 1970.* [Pretoria;] Council for Scientific and Industrial Research: 16 pp.

BLAHA, J. and B. LUNDE 1992 - Calibrating altimetry to geopotential anomaly and isotherm depths in the western North Atlantic. *J. geophys. Res.* **97(C5)**: 7465-7477.

BROECKER, W.S. 1987 - The biggest chill. *Nat. Hist. Mag.* **97**: 74-82.

BROECKER, W.S. 1991 - The Great Ocean Conveyor. *Oceanography* **4(2)**: 79-89.

BOUDRA, D. B. and E. P. CHASSIGNET 1988 - Dynamics of Agulhas retroflection and ring formation in a numerical model. 1. The vorticity balance. *J. phys. Oceanogr.* **18**(2): 280-303.

BOUDRA, D. B. and W. P. M. DE RUIJTER 1986 - The wind-driven

circulation of the South Atlantic-Indian Ocean. 2. Experiments using a multi-layer numerical model. *Deep-Sea Res.* 33(4A): 447-482.

BRUNDRIT, G.B. and L.V. SHANNON 1989 - Cape storms and the Agulhas Current: a glimpse of the future. *S. Afr. J. Sci.* 85: 619-620.

BRENNER, A.C., KOBLINSKY, C.J. and B.D. BECKLEY 1990 - A preliminary estimate of geoid-induced variations in repeat orbit satellite altimeter observations. *J. geophys. Res.* 95(C3): 3033-3040.

CALMAN, J. 1987 - Introduction to sea-surface topography from satellite altimetry. *Johns Hopkins APL TECHNICAL DIGEST* 8(2): 206-211.

CHASSIGNET, E. P. and D. B. BOUDRA 1988 - Dynamics of Agulhas retroflection and ring formation in a numerical model. 2. Energetics and ring formation. *J. phys. Oceanogr.* 18(2): 304-319.

CHASSIGNET, E.P., OLSON, D.B. and D.B. BOUDRA 1990 - Motion and evolution of oceanoc rings in a numerical model and in observations. *J. geophys. Res.* 95(C12): 22121-22140.

CHELTON, D. B., SCHLAX, M. G., WITTER, D. L. and J. G. RICHMAN 1990 - GEOSAT altimeter observations of the surface

circulation of the Southern Ocean. *J. geophys. Res.* **95(C10)**: 17877-903.

CHENEY, R. E., MILLER, L.L., DOUGLAS, B. C. and R. W. AGREEN 1987 - Monitoring Equatorial Pacific sea level with GEOSAT. *Johns Hopkins APL TECHNICAL DIGEST* **8(2)**: 245-250.

CHENEY, R. E., DOUGLAS, B. C. and L. MILLER 1989 - Evaluation of GEOSAT altimeter data with application to Tropical Pacific sea level variability. *J. geophys. Res.* **94(C4)**: 4737-4747.

COLTON, M. T. and R. R. P. CHASE 1983 - Interaction of the Antarctic Circumpolar Current with bottom topography: an investigation using satellite altimetry. *J. geophys. Res.* **88**(C3): 1825-1843.

CRAWFORD, R. J. M., SHANNON, L. V. and D. E. POLLOCK 1987 - The Benguela ecosystem. 4. The major fish and invertebrate resources. In *Oceanography and Marine Biology. An Annual Review* 25. Barnes, M. (Ed.). Aberdeen; University Press: 353-505.

DARBYSHIRE, J. 1972 - The effect of bottom topography on the Agulhas Current. *Pure appl. Geophys.* **101**: 208-220.

DE RUIJTER, W. [P. M.] 1982 - Asymptotic analysis of the Agulhas and Brazil Current systems. *J. phys. Oceanogr.* **12**: 361-373.

DE RUIJTER, W. P. M. and D. B. BOUDRA 1985 - The wind-driven circulation in the South Atlantic-Indian Ocean. 1. Numerical experiments in a one-layer model. *Deep-Sea Res.* **32**(5): 557-574.

DIDDEN, N. and F. SCHOTT 1992 - Seasonal variations in the western tropical Atlantic: surface circulation from GEOSAT altimetry and WOCE model results. *J. geophys. Res.* **97(C3)**: 3529-3542.

DIETRICH, G. 1935 - Aufbau und Dynamik des südlichen Agulhas-stromgebietes. *Veröff. Inst. Meeresk. Univ. Berl. (Neue Folge) A. Geogr-natwiss.* **27**: 79 pp.

DOUGLAS, B. C. and R. W. AGREEN 1983 - The sea state correction for GEOS 3 and SEASAT satellite altimeter data. *J. geophys. Res.* **88(C3)**: 1655-1661.

DOUGLAS, B.C. and R.E. CHENEY 1990 - GEOSAT: Beginning a new era in satellite oceanography. *J. geophys. Res.* **95**: 2833-2836.

DOUGLAS, B.C., McADOO, D.C. and R.E. CHENEY 1987 - Oceanographic and geophysical applications of satellite altimetry. *Reviews of Geophysics* **25(5)**: 875-880.

DUNCAN, C. P. 1968 - An eddy in the subtropical convergence southwest of South Africa. *J. geophys. Res.* **73**(2): 531-534.

DUNCAN, C. P. 1970 - The Agulhas Current. Ph.D. thesis, University of Hawaii: 76 pp.

DUNCOMBE RAE, C. M. 1991 - Agulhas retroflection rings in the South Atlantic Ocean: an overview. *S. Afr. J. mar. Sci.* 11: 327-344.

DUNCOMBE RAE, C. M., SHANNON, L. V. and F. A. SHILLINGTON 1989 - An Agulhas ring in the South Atlantic ocean. *S. Afr. J. Sci.* 85: 747-748.

DUNCOMBE RAE, C.M., BOYD, A.J. and R.J.M. CRAWFORD 1992a - 'Predation' of anchovy by an Agulhas ring : a possible contributory cause of the very poor yearclass of 1989. In *Benguela Trophic Functioning*. Payne, A.I.L., Brink, K.H., Mann, K.H. and R. Hilborn (Eds). *S. Afr. J. mar. Sci.* 12: 167-173.

DUNCOMBE RAE, C.M., SHILLINGTON, F.A., AGENBAG, J.J., TAUNTON-CLARK, J. and M.L. GRÜNDLINGH 1992b - An Agulhas ring in the South Atlantic Ocean and its interaction with the Benguela upwelling frontal system. *Deep-Sea Res.* (in press).

FERON, R.C.V., DE RUIJTER, W.P.M. and D. OSKAM 1992 - Ring shedding in the Agulhas Current system. *J. geophys. Res.* 97(C6): 9467-9477.

FORRISTALL, G.Z., SCHAUDT, K.J. and J. CALMAN 1990 - Verification of GEOSAT altimetry for operational use in the Gulf of Mexico. *J.geophys.Res.* **95(C3)**: 2985-2989.

FRAIN, W.E., BARBAGALLO, M.H. and R.J. HARVEY 1987 - The design and operation of GEOSAT. *Johns Hopkins APL TECHNICAL DIGEST* **8(2)**: 184-189.

FRAM Group 1991 - An eddy-resolving model of the southern ocean. *Eos Trans. AGU* **72(169)**: 174-175.

FU, L-L. and R. GLAZMAN 1991 - The effect of the degree of wave development on the sea state bias in radar altimetry measurement. *J. geophys. Res.* **96(C1)**: 829-834.

FU, L-L. and V. ZLOTNICKI 1989 - Observing oceanic mesoscale eddies from Geosat altimetry: preliminary results. *Geophys. Res. Letts* **16**: 457-460.

FU, L-L., CHELTON, D.B. and V. ZLOTNICKI 1988 - Satellite altimetry: observing variability from space. *Oceanography* **1(2)**: 4-11.

FU, L-L., LIU, T.W. and M.R.ABOTT 1990 - Satellite remote sensing of the ocean. In *The Sea: Ocean Engineering Science* **9**:1193-1236.

GILL, A. E. and E. H. SCHUMANN 1979 - Topographically induced

changes in the structure of an inertial coastal jet : application to the Agulhas Current. *J. phys. Oceanogr.* **9**(5): 975-991.

GOLDEN SOFTWARE, INC. 1989,1990 - SURFER Version 4 reference manual. Golden, Colorado, U.S.A. *Golden Software, Inc.* 300 pp. plus appendices.

GORDON, A. L. 1985 - Indian-Atlantic transfer of thermocline water at the Agulhas retroflection. *Science, N.Y.* **227**(4690): 1030-1033.

GORDON, A. L. 1986 - Interocean exchange of thermocline water. *J. geophys. Res.* **91**(C4): 5037-5046.

GORDON, A. L. and W. F. HAXBY 1990 - Agulhas eddies invade the South Atlantic: evidence from Geosat altimeter and shipboard Conductivity-Temperature-Depth survey. *J. geophys. Res.* **95**(C3): 3117-3125.

GORDON, A. L., LUTJEHARMS, J. R. E. and M. L. GRÜNDLINGH 1987a - Stratification and circulation at the Agulhas retroflection. *Deep-Sea Res.* **34**(4A): 565-599.

GORDON, A. L., LUTJEHARMS, J. R. E. and M. L. GRÜNDLINGH 1987b - Select hydrographic sections from the Agulhas research cruises of the research vessels Knorr and Meiring Naudé - 1983. *Tech. Rep. Lamont-Doherty geol. Observatory* LDGO-87-

1: 28 pp.

GORDON, A.L., WEISS, R.F. SMETHIE, W.M. and M.J. WARNER 1992 - Thermocline and intermediate water communication between the South Atlantic and Indian Oceans. *J. geophys. Res.* **97(C5)**: 7223-7240.

GOSCHEN, W. S. and E. H. SCHUMANN 1990 - Agulhas Current variability and inshore structures off the Cape Province, South Africa. *J. geophys. Res.* 95(C1): 667-678.

GRÜNDLINGH, M. L. 1977 - Drift observations from Nimbus VI satellite-tracked buoys in the southwestern Indian Ocean. *Deep-Sea Res.* 24(10): 903-913.

GRÜNDLINGH, M. L. 1978 - Drift of a satellite-tracked buoy in the southern Agulhas Current and Agulhas Return Current. *Deep-Sea Res.* 25: 1209-1224.

GRÜNDLINGH, M. L. 1979 - Observation of a large meander in the Agulhas Current. *J. geophys. Res.* 84(C7): 3776-3778.

GRÜNDLINGH, M. L. 1980 - On the volume transport of the Agulhas Current. *Deep-Sea Res.* 27(7A): 557-563.

GRÜNDLINGH, M. L. 1983a - On the course of the Agulhas Current. *S. Afr. geogrl J.* 65(1): 49-57.

GRÜNDLINGH, M. L. 1983b - Eddies in the southern Indian Ocean and Agulhas Current. In *Eddies in Marine Science*. Robinson, A. R. (Ed.). Berlin; Springer: 245-264.

GRÜNDLINGH, M. L. 1988 - Altimetry in the southwest Indian Ocean. *S. Afr. J. Sci.* **84**: 568-573.

GRÜNDLINGH, M. L. and J. R. E. LUTJEHARMS 1979 - Large-scale flow patterns of the Agulhas Current system. *S. Afr. J. Sci.* **75**(6): 269-270.

HARRIS, T. F. W. 1970 - Features of the surface currents in the south west Indian Ocean. In *Papers Presented to the SANCOR Symposium, Oceanography in South Africa - 1970, Durban*. **C3**: 12 pp.

HARRIS, T. F. W. and N. D. BANG 1974 - Topographic Rossby waves in the Agulhas Current. *S. Afr. J. Sci.* **70**(7): 212-214.

HARRIS, T. F. W. and D. VAN FOREEST 1977 - The Agulhas Current system. Processing and interpretation of some existing physical data. Unpublished Report, Department of Oceanography, University of Cape Town: 38 pp.

HARRIS, T. F. W. and D. VAN FOREEST 1978 - The Agulhas Current in March 1969. *Deep-Sea Res.* **25**: 549-561.

HARRIS, T. F. W., LEGECKIS, R. and D. VAN FORE[E]ST 1978 -

Satellite infra-red images in the Agulhas Current system. *Deep-Sea Res.* **25**(6): 543-548.

HAYNE, G.S. and D.W. HANCOCK 1990 - Corrections for the effects of significant wave height and attitude on GEOSAT radar altimeter measurements. *J. geophys. Res.* **95**: 2837-2842.

HOLLAND, W. R. 1978 - The role of mesoscale eddies in the general circulation of the ocean - numerical experiments using a wind-driven quasigeostrophic model. *J. phys. Oceanogr.* **8**: 363-392.

HOLLAND, W. R., ZLOTNICKI, V. and L-L. FU 1991 - Modelled time-dependent flow in the Agulhas retroflection region as deduced from altimeter data assimilation. *S. Afr. J. mar. Sci.* **10**: 407-427.

JENSEN, J. J. and F. R. WOOLDRIDGE 1987 - The Navy GEOSAT mission: an introduction. *Johns Hopkins APL TECHNICAL DIGEST* **8(2)**: 169.

JONES, S.C., TOSSMAN, B.E. and L.M. DUBOIS 1987 - The GEOSAT ground station. *Johns Hopkins APL TECHNICAL DIGEST* **8(2)**: 190-196.

LEBEN, R.R., BORN, G.H., THOMPSON, J.D. and C.A. FOX 1990 - Mean sea surface and variability of the Gulf of Mexico using GEOSAT altimetry data. *J. geophys. Res.* **95(C3)**: 3025-3032.

LEGECKIS, R. and A. L. GORDON 1982 - Satellite observations of the Brazil and Falkland currents - 1975 to 1976 and 1978. *Deep-Sea Res.* 29(3A): 375-401.

LEWIS, L. 1990a - Satellite altimetry data system report: the NOAA GEOSAT programs. *CSIR Report EMA-I 8934* 32pp.

LEWIS, L. 1990b - Satellite altimetry data system (SADS) Part 1: the design of SADS. *CSIR Report EMA-I* 15pp.

LEWIS, L. 1990c - Satellite altimetry data system (SADS) Part 2: programmer's reference manual. *CSIR Report EMA-T 8905/02* 40pp plus unpaginated program listings.

LEWIS, L. and U. v St ANGE 1990 - Satellite altimetry data system (SADS) Part 3: user's manual. *CSIR Report EMA-T 8905/3* 20pp plus unpaginated diagrams.

LUTJEHARMS, J. R. E. 1981a - Spatial scales and intensities of circulation in the ocean areas adjacent to South Africa. *Deep-Sea Res.* 28(11A): 1289-1302.

LUTJEHARMS, J. R. E. 1981b - Features of the southern Agulhas Current circulation from satellite remote sensing. *S. Afr. J. Sci.* 77(5): 231-236.

LUTJEHARMS, J. R. E. 1988a - Remote sensing corroboration of retroflection of the East Madagascar Current. *Deep-Sea Res.*

35(12): 2045-2050.

LUTJEHARMS, J. R. E. 1988b - Examples of extreme circulation events at the Agulhas retroflection. *S. Afr. J. Sci.* **84**: 584-586.

LUTJEHARMS, J. R. E. and A. L. GORDON 1987 - Shedding of an Agulhas Ring observed at sea. *Nature, Lond.* **325**(7000): 138-140.

LUTJEHARMS, J. R. E. and H. R. ROBERTS 1988 - The Natal pulse: an extreme transient on the Agulhas Current. *J. geophys. Res.* **93**(C1): 631-645.

LUTJEHARMS, J. R. E. and H. R. VALENTINE 1988 - Evidence for persistent Agulhas rings south-west of Cape Town. *S. Afr. J. Sci.* **84**(9): 781-783.

LUTJEHARMS, J. R. E. and R. C. VAN BALLEGOOYEN 1984 - Topographic control in the Agulhas Current system. *Deep-Sea Res.* **31**(11): 1321-1337.

LUTJEHARMS, J. R. E. and R. C. VAN BALLEGOOYEN 1988a - The retro-flection of the Agulhas Current. *J. phys. Oceanogr.* **18**(11): 1570-1583.

LUTJEHARMS, J. R. E. and R. C. VAN BALLEGOOYEN 1988b - Anomalous upstream retroflection in the Agulhas Current. *Science, N.Y.* **240**: 1770-1772.

LUTJEHARMS, J. R. E., CATZEL, R. and H. R. VALENTINE 1989 - Eddies and other boundary phenomena of the Agulhas Current. *Continent. Shelf Res.* 9(7): 597-616.

LUTJEHARMS, J. R. E., SHILLINGTON, F. A. and C. M. DUNCOMBE RAE 1991 - Observations of extreme upwelling filaments in the Southeast Atlantic Ocean. *Science, N.Y.* **253**(5021): 774-776.

MacARTHUR, J.L, MARTH, P.C.(Jr.) and J.G. WALL 1987 - The GEOSAT radar altimeter. *Johns Hopkins APL TECHNICAL DIGEST* **8(2)**: 176-181.

McCARTNEY, M. S. and M. E. WOODGATE-JONES 1991 - A deep-reaching anticyclonic eddy in the subtropical gyre of the eastern South Atlantic. *Deep-Sea Res.* **38**(Suppl.1): S411-S443.

McCONATHY, D. R. and C. C. KILGUS 1987 - The Navy Geosat mission: an overview. *Johns Hopkins APL tech. Dig.* 8:170-175.

MEY, R. D., WALKER, N. D. and M. R. JURY 1990 - Surface heat fluxes and marine boundary layer modification in the Agulhas retroflection region. *J. geophys. Res.* **95**(C9): 15997-16015.

MONALDO, F. 1990 - Path length variations caused by atmospheric water vapo[u]r and their effects on the measurement of mesoscale ocean circulation features by a radar altimeter.

J. geophys. Res. 95(C3): 2923-2932.

NEREM, R.S., TAPLEY, B.D. and C.K. SHUM 1990 - Determination of the ocean circulation using GEOSAT altimetry. *J. geophys. Res.* 95(C3): 3163-3179.

NEUMANN, G. and W. J. PIERSON 1966 - *Principles of Physical Oceanography*. Englewood Cliffs, New Jersey; Prentice-Hall: 545 pp.

NIILER, P.P. and A. R. ROBINSON 1967 - The theory of free inertial jets. II. A numerical experiment for the path of the Gulf Stream. *Tellus* 19: 601-618.

NILSSON, C. S. and G. R. CRESSWELL 1981 - The formation and evolution of East Australian Current warm-core eddies. *Prog. Oceanogr.* 9: 133-183.

OLSON, D. B. and R. H. EVANS 1986 - Rings of the Agulhas Current. *Deep-Sea Res.* 33(1A): 27-42.

OU, H. W. and W. P. M. DE RUIJTER 1986 - Separation of an inertial boundary current from a curved coastline. *J. phys. Oceanogr.* 16: 280-28

PATTERSON, S. L. 1985 - Surface circulation and kinetic energy distributions in the southern hemisphere oceans from FGGE drifting buoys. *J. phys. Oceanogr.* 15: 865-884.

PEARCE, A. F. 1977 - The shelf circulation off the east coast of South Africa. *Prof. Res. Ser. S. Afr. Coun. scient. ind. Res. (NRIO)* 1: 220 pp.

PEARCE, A. F. 1977 - Some features of the upper 500 m of the Agulhas Current. *J. mar. Res.* 35(4): 731-753.

PEARCE, A. F. and M. L. GRÜNDLINGH 1982 - Is there a seasonal variation in the Agulhas Current? *J. mar. Res.* **40**(1): 177-184.

PIOLA, A. R. and A. L. GORDON 1986 - On oceanic heat and freshwater fluxes at 30°S. *J. phys. Oceanogr.* **16**(12): 2184-2190.

POND, S. and G. L. PICKARD 1978 - *Introductory Dynamic Oceanography*. Oxford; Pergamon: 241 pp.

RAY, R.D., KOBLINSKY, C.J. and B.D. BECKLEY 1991 - On the effectiveness of GEOSAT altimeter corrections. *Int. J. Rem. Sens.* **12(9)**: 1979-1984.

ROBINSON A. R. and P. P. NIILER 1967 - The theory of free inertial jets. I. Path and structure. *Tellus* **19**: 269-288.

SAILOR, R.V. AND A.R. LeSCHACK 1987 - Preliminary determination of the GEOSAT radar altimeter noise spectrum. *Johns Hopkins*

APL TECHNICAL DIGEST **8(2)**: 182-183.

SEMTNER, A.J. Jr. and R.M. CHERVIN 1992 - Ocean general circulation from a global eddy-resolving model. *J. geophys. Res.* **97(C4)**: 5493-5550.

SHANNON, L. V. 1985 - The Benguela ecosystem. 1. Evolution of the Benguela, physical features and processes. In *Oceanography and Marine Biology. An Annual Review* 23. Barnes, M. (Ed.). Aberdeen; University Press: 105-182.

SHANNON, L. V., AGENBAG, J. J., WALKER, N. D. and J. R. E. LUTJEHARMS 1990 - A major perturbation in the Agulhas retroflection area in 1986. *Deep-Sea Res.* 37(3): 493-512.

SHANNON, L. V., POLLOCK, D. E., CHAPMAN, P. and A. A. ROBERTSON 1989 - South-East Atlantic expedition of R.S. *Africana*, April 1989: some preliminary results. *S. Afr. J. Sci.* **85**(10): 665-669.

SHUM, C.K., WERNER, R.A., SANDWELL, D.T., ZHANG, B.H., NEREM, R.S. and B.D. TAPLEY 1990 - Variations of global mesoscale eddy energy observed from GEOSAT. *J. geophys. Res.* **95(C10)**: 17865-17876.

SMITH, S.L. III, WEST, G.B. and C.W. MALYEVAC 1987 - Determination of ocean geodetic data from GEOSAT. *Johns*

Hopkins APL TECHNICAL DIGEST **8(2)**: 197-200.

STRAMMA, L. 1989 - The Brazil Current transport south of 23°S. *Deep-Sea Res.* **36(4A)**: 639-646.

TOURNADRE, J. 1990 - Sampling of oceanic rings by satellite radar altimeter. *J. geophys. Res.* **95(C1)**: 693-697.

VAN BALLEGOOYEN, R.C., GRÜNDLINGH, M.L. and J.R.E. LUTJEHARMS (1993) - On the fluxes of heat and salt from the southwest Indian Ocean into the southeast Atlantic Ocean: a case study. (In prep.).

VERONIS, G. 1973 - Model of world ocean circulation: I. Wind-driven, two-layer. *J. mar. Res.* 31: 228-288.

WAKKER, K.F., ZANDBERGEN, R.C.A., VAN GELDORP, G.H.M. and B.A.C. AMBROSIUS 1988 - From satellite altimetry to ocean topography. A survey of data processing techniques.*Int.J. Rem. Sens.* **9**: 1797-1818.

WAKKER, K.F., NAEJE, M.C., SCHARROO, R. and B.A.C. AMBROSIUS 1990(a) - Extraction of mesoscale ocean currents information from GEOSAT altimeter data. *Proceedings of the Space and Sea Colloquium*, Paris, 24-26 September, ESA SP-312, pp 221-226.

WAKKER, K.F., ZANDBERGEN, R.C.A., NAEJE, M.C. and B.A.C.

AMBROSIUS 1990(b) - GEOSAT altimeter data analysis for the oceans around South Africa. *J. geophys. Res.* **95(C3)**: 2991-3006.

WALKER, N. D. 1989 - Sea surface temperature-rainfall relationships and associated ocean-atmosphere coupling mechanisms in the southern Africa region. *Res. Rep. Coun. scient. ind. Res. S. Afr.* **683**: 173 pp.

WALKER, N. D. 1990 - Links between South African summer rainfall and temperature variability of the Agulhas and Benguela Current systems. *J. geophys. Res.* **95**(C3): 3297-3319.

WALKER, N. D. and J. A. LINDESAY 1989 - Preliminary observations of oceanic influences on the February-March 1988 floods in central South Africa. *S. Afr. J. Sci.* **85**(3): 164-169.

WALKER, N. D. and R. D. MEY 1988 - Ocean/atmosphere heat fluxes within the Agulhas Retroflection region. *J. geophys. Res.* **93**(C12): 15473-15483.

WELLS, N. 1986 - *The atmosphere and ocean - a physical introduction*. London; Taylor & Francis: 347 pp.

Deep-Sea Research, Vol. 39, No. 11/12, pp. 2009–2027, 1992.
Printed in Great Britain.

0198–0149/92 $5.00 + 0.00
Pergamon Press Ltd

An Agulhas ring in the South Atlantic Ocean and its interaction with the Benguela upwelling frontal system

C. M. DUNCOMBE RAE,*† F. A. SHILLINGTON,† J. J. AGENBAG,*†
J. TAUNTON-CLARK*† and M. L. GRÜNDLINGH‡

(*Received* 20 *May* 1991; *in revised form* 6 *January* 1992; *accepted* 14 *January* 1992)

Abstract—An Agulhas ring was detected using XBT probes on a cruise between Cape Town and Vema Seamount in the south-east Atlantic Ocean in April 1989. CTD and nutrient data, collected on a second cruise in May 1989, GEOSAT altimeter data for February–April 1989 and cloud-free NOAA-11 satellite imagery from June 1989 were used to characterize the ring. The ring was elliptical (330 km E–W and 165 km N–S, relative to the 16°C isotherm at 200 m depth), evident to at least 1200 m, and centred on 30.5°S, 9.2°E in May, about 700 km west of the Orange River. Its drift velocity was 6.4 ± 1 cm s^{-1} to the NW. Maximum anticyclonic geostrophic surface currents near its edge were 55 cm s^{-1} relative to 1150 db. The available potential energy was estimated to be 38.8×10^{15} J and the kinetic energy 2.3×10^{15} J using a two layer model of the ring. A cool filament extending 450 km offshore from the Benguela upwelling front was identified in the hydrography and the NOAA-11 imagery. Entrainment velocities (maximum of 75 cm s^{-1}) of mature upwelled water from the Benguela frontal region were inferred from feature tracking.

INTRODUCTION

RESEARCH into the behaviour of the Agulhas Current at its retroflection point south of Africa (e.g. BANG, 1970; HARRIS and VAN FOREEST, 1978; BENNETT, 1988) has highlighted the need to understand the volume flux and characteristics of the flow of Indian Ocean water into the South Atlantic Ocean. GORDON (1985, 1986) has demonstrated that warm, salty thermocline water must round the Cape of Good Hope in order to balance the production of cold, salty North Atlantic Deep Water which then spreads into the world's deep ocean basins. The manner in which this transport takes place is of great interest and it has been assumed by many workers that the shedding of rings at the Agulhas retroflection will assist the transport of the warm thermocline water around Africa. Ocean modelling (e.g. BOUDRA and CHASSIGNET, 1988; CHASSIGNET and BOUDRA, 1988) has increased our understanding of the mechanism of ring formation at the retroflection.

There have been few observations of the formation of warm Agulhas rings at or near the retroflection region (e.g. LUTJEHARMS and GORDON, 1987), and the best evidence to date of the possible large number of anticyclonic rings that can be present in the South Atlantic Ocean at any one time is to be found from the GEOSAT satellite altimetry data for

*Sea Fisheries Research Institute, Private Bag X2, Roggebaai 8012, South Africa.
†Department of Oceanography, University of Cape Town, Rondebosch 7700, South Africa.
‡CSIR, P.O. Box 320, Stellenbosch 7600, South Africa.

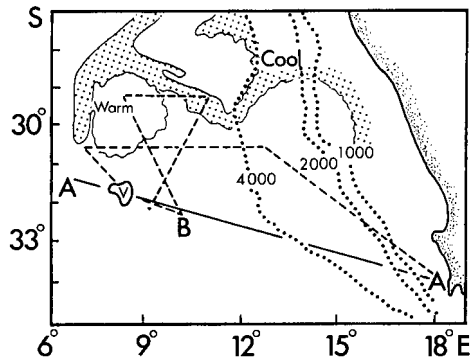

Fig. 1. Cruise track of F.R.S. *Africana* (line A...A) April 1989 and R.S. *Benguela* (dashed A..V..B) May 1989 in the South Atlantic. V indicates Vema Seamount. Bottom contours (dotted lines) in metres, surface temperatures from NOAA-11 imagery for 15 June 1989.

November 1986–November 1987 (GORDON and HAXBY, 1990). Their study suggests a production rate of about five rings per year, accumulating a mean volume flux of 15×10^6 $m^3\ s^{-1}$ of Indian Ocean water into the Atlantic Ocean.

Ship-borne observations based on CTD, drifter and satellite data of Agulhas rings near the Agulhas retroflection and in the South Atlantic Ocean have been discussed by OLSON and EVANS (1986), GORDON *et al.* (1987a), LUTJEHARMS and GORDON (1987), LUTJEHARMS (1987), LUTJEHARMS and VAN BALLEGOOYEN (1988), GORDON and HAXBY (1990), and MCCARTNEY and WOODGATE-JONES (1991). SHANNON *et al.* (1990) discussed a major intrusion of Agulhas water into the South Atlantic during 1986 and 1987, and suggested that their NOAA satellite data confirmed the initiation of an Agulhas ring observed later by GORDON and HAXBY (1990). DUNCOMBE RAE *et al.* (1989) presented two expendable bathythermograph (XBT) derived temperature sections of an Agulhas ring in the South Atlantic Ocean and discussed the resulting northward heat transport. It is the intention of this paper to explore the hydrography, dynamics and nutrient data of this latter Agulhas ring and to show that it is possible for Agulhas rings to interact significantly with the Benguela frontal system.

DATA AND METHODS

(a) *Hydrographic measurements*

During voyage 071 of F.R.S. *Africana* (SHANNON *et al.*, 1989), vertical temperature sections were obtained from XBTs launched at approximately 40 km intervals between Cape Town (34°S, 18°E) and Vema Seamount (31°40′S, 8°20′E) in April 1989 (Fig. 1: A...A), and on this leg an Agulhas ring was discovered. A specially designed follow-up cruise on the R.S. *Benguela* was undertaken in May 1989 to make a more detailed CTD and nutrient survey of this feature. (Fig. 1: A..V..B). The ring was found on the first E–W exploratory XBT transect. Two detailed CTD sections were then made at 30 nautical mile (55.5 km) intervals SE–NW and NE–SW through the ring. A Mark III Neil Brown CTD was deployed at a descent rate of 1 m s^{-1}, with a data value stored once per metre, down to a nominal depth of 1200 m. Nutrient samples were taken at depths of 0, 50, 100, 200, 250,

300, 500, 750, 1000 and 1200 m on the up-cast. The nutrient samples were frozen and later analysed ashore (MOSTERT, 1983) for nitrate, silicate and phosphate.

(b) *NOAA imagery*

NOAA-11 AVHRR infrared imagery was available for the period January–July 1989. Cloud-free images showing the ring were available for 24 and 30 April as well as 15 and 16 June 1989. The pair of images, approximately 24 h apart, for 15 and 16 June was transformed to Mercator projection using an ARIES II image processing system and software developed for this purpose by the Sea Fisheries Research Institute (SFRI). The surface circulation pattern was then constructed by manual tracking of small-scale thermal features (AGENBAG and SHANNON, 1988).

(c) *GEOSAT altimetry*

GEOSAT altimeter data were available from November 1986 to April 1989, but it was decided that the data of cycles 37–54 would provide a suitable representation of the geoid for the period prior to the cruises, from 29 December 1988 to 27 April 1989. Complete data were not available for cycles 39, 45, 50 or 51.

The data were processed using software developed by the CSIR at Stellenbosch (LEWIS 1990a, b; LEWIS and ST. ANGE, 1990). The 1 s along-track averages of sea surface height from the geophysical data records (GDR) received from the National Oceanic and Atmospheric Administration (NOAA, U.S.A.) were corrected for tidal and atmospheric effects using values supplied with the GDRs. Spurious data were edited following rejection criteria similar to those employed by WAKKER *et al.* (1990b).

A collinear analysing technique was employed in which the mean sea surface elevation profile for a track or pass (repeated every 17 days) was computed. This mean profile approximates to the marine geoid. The approximate geoid was subtracted from the individual passes, leaving residual height profiles that contain details of the mesoscale ocean circulation with which we are concerned.

Using all the passes within a complete 17 day cycle of the satellite to create a surface profile of the sea surface elevation yields a temporally aliased picture. To minimize this temporal smearing, a reduced grid consisting of the passes in a 7 day period was used to create "snapshot" pictures of the sea surface height. Whilst rendering a better temporal representation these snapshots rely on a reduced data set so only a qualitative indication of the features present can be obtained.

RESULTS

(a) *Hydrography*

1. *Horizontal sections.* The temperature field at 200 m (Fig. 2) from the *Benguela* cruise data in May 1989 indicates that at this time the ring was highly elliptical, with the 16°C isotherm giving a major axis diameter of 330 km and a minor axis diameter of 165 km (a ratio of about 2:1). The geostrophic velocity of the surface with respect to a level-of-no-motion of 1150 db (Fig. 3), calculated from the CTD station data, shows the highest speeds between Stas 6 and 7 (to the SW at 55 cm s^{-1}) and Stas 3 and 4 (to the NE at

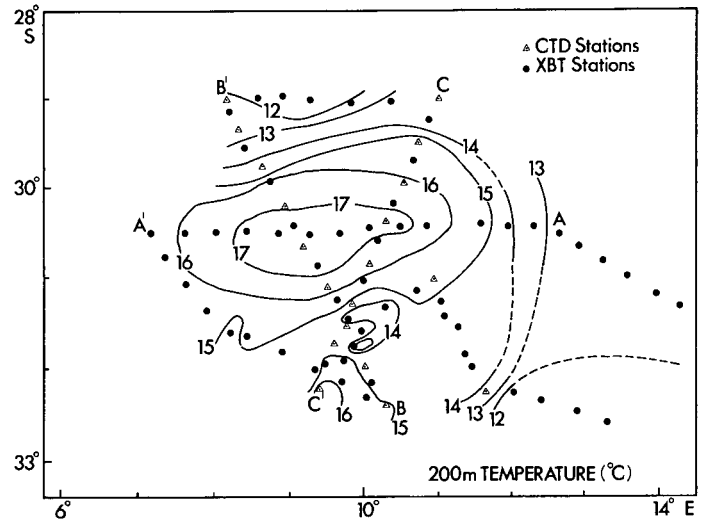

Fig. 2. Temperatures at 200 m depth contoured from XBT and CTD data for the May 1989 *Benguela* cruise. Solid circles are XBT drops and triangles indicate CTD casts. The E–W XBT line is from A to A′, the S–N CTD and XBT line is from B to B′, and the N–S CTD and XBT line is from C to C′.

46 cm s^{-1}). The anticyclonic nature of the circulation was also confirmed by ship's drift obtained from SATNAV fixes while on station (wind speeds were less than 5 m s^{-1} throughout the cruise).

2. *Vertical profiles.*

(i) *F.R.S.* Africana *data—April* 1989. It is clear from the vertical bathythermograph section obtained in April 1989 between Cape Town (CT) and Vema Seamount (V) (Fig. 4) that the ring had little surface expression. The upper 100 m layer was well-mixed with a temperature of 21°C at the ring's centre. A horizontal diameter of the ring at this stage can be determined from the section to be 240 km, while the 6°C isotherm was depressed by 320 m at the centre of the ring. Referenced to a level surface at 500 m, the temperature difference between water at the centre of the ring and at the edge was 5°C.

(ii) *R.S.* Benguela *data—May* 1989. Three vertical temperature sections were made through the ring in May 1989. It is evident from the E–W XBT section (Fig. 5a) that the western edge of the ring had not been reached, as the isotherms were still rising towards the surface. To estimate the horizontal E–W dimension, we take twice the distance from the eastern edge (where the isotherms level off) to the centre, yielding a distance of 530 km. We obtain an estimate of the N–S extent in the same way from combined CTD and XBT sections (Fig. 5b and c) of 180 km. These sections revealed a surface mixed layer of 19°C down to a depth of 100 m across the centre of the ring.

The vertical salinity sections from the two CTD transects (Fig. 6) show an isohaline upper mixed layer of 35.66 psu to a depth of 100 m. These sections indicate a difference of 0.6 psu between the ring core water and the surrounding water at 400 m depth.

The vertical nutrient distribution (Fig. 7) measured on the S–N CTD transect through

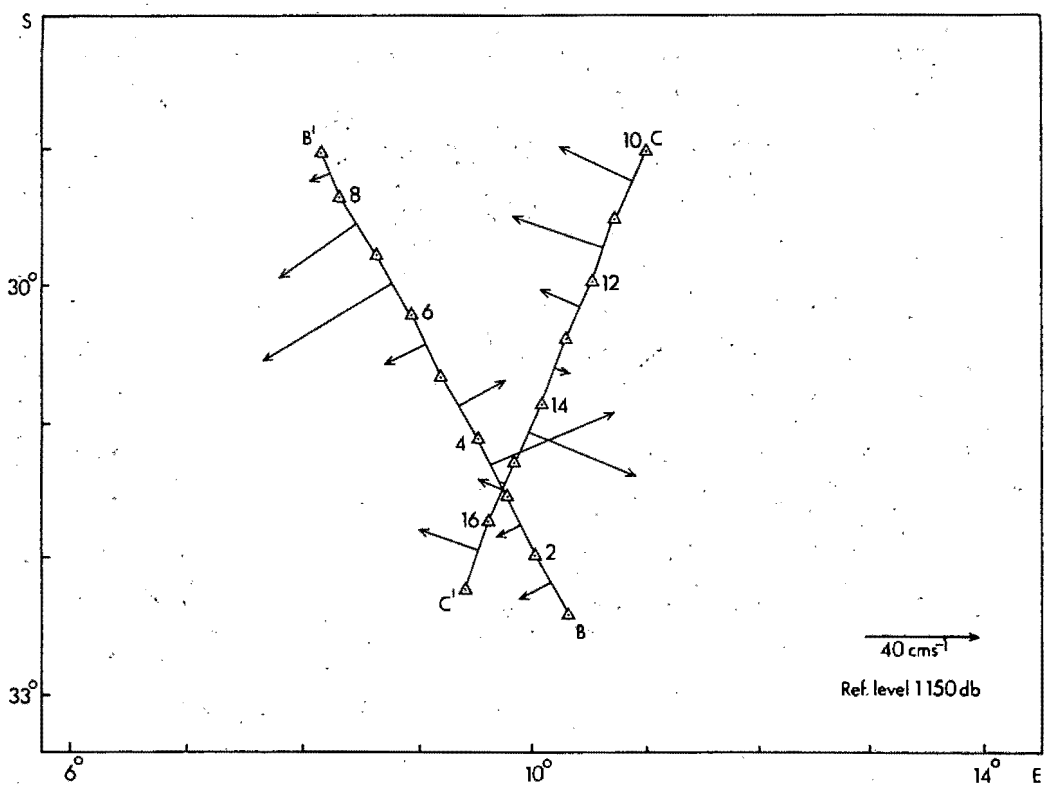

Fig. 3. Surface geostrophic current speeds (cm s^{-1}) referenced to 1150 db. The lengths of the vectors are proportional to the current speed. Even-numbered CTD stations are indicated.

the ring (line B..B′ on Fig. 2) shows that the concentrations of silicate, phosphate and nitrate in the surface water surrounding the ring are typical of oligotrophic Atlantic Ocean water. Water within the ring has even lower nutrient concentrations, typical of the Agulhas Current (CHAPMAN *et al.*, 1987), particularly in the upper 300 m. However, use of these nutrient values to assist in differentiating Agulhas (Indian Ocean) water from Atlantic water can be problematic (CHAPMAN *et al.*, 1987) due to mixing at the Agulhas retroflection of Agulhas water with both Atlantic water and water south of the Subtropical Front during the ring separation. The silicate distribution is similar to that reported by GORDON *et al.* (1987b) for the ring they examined.

The potential density sections (Fig. 8) computed via the equation of state (e.g. GILL, 1982) from the potential temperature and salinity for the two CTD transects of the ring show most of the features discussed in the temperature and salinity sections. From the potential density data the geopotential anomalies (GPA) were calculated relative to 1150 db, enabling the calculation of geostrophic velocities between CTD stations through the water column relative to that depth (Fig. 9). For these stations, the volume flux in Sverdrup (1 Sv = 10^6 m^3 s^{-1}) was also calculated and is indicated below the reference level in Fig. 9.

If the depth of an isotherm can be statistically correlated to the geopotential anomaly relative to some depth, then there exists a large quantity of useful data in the XBT casts.

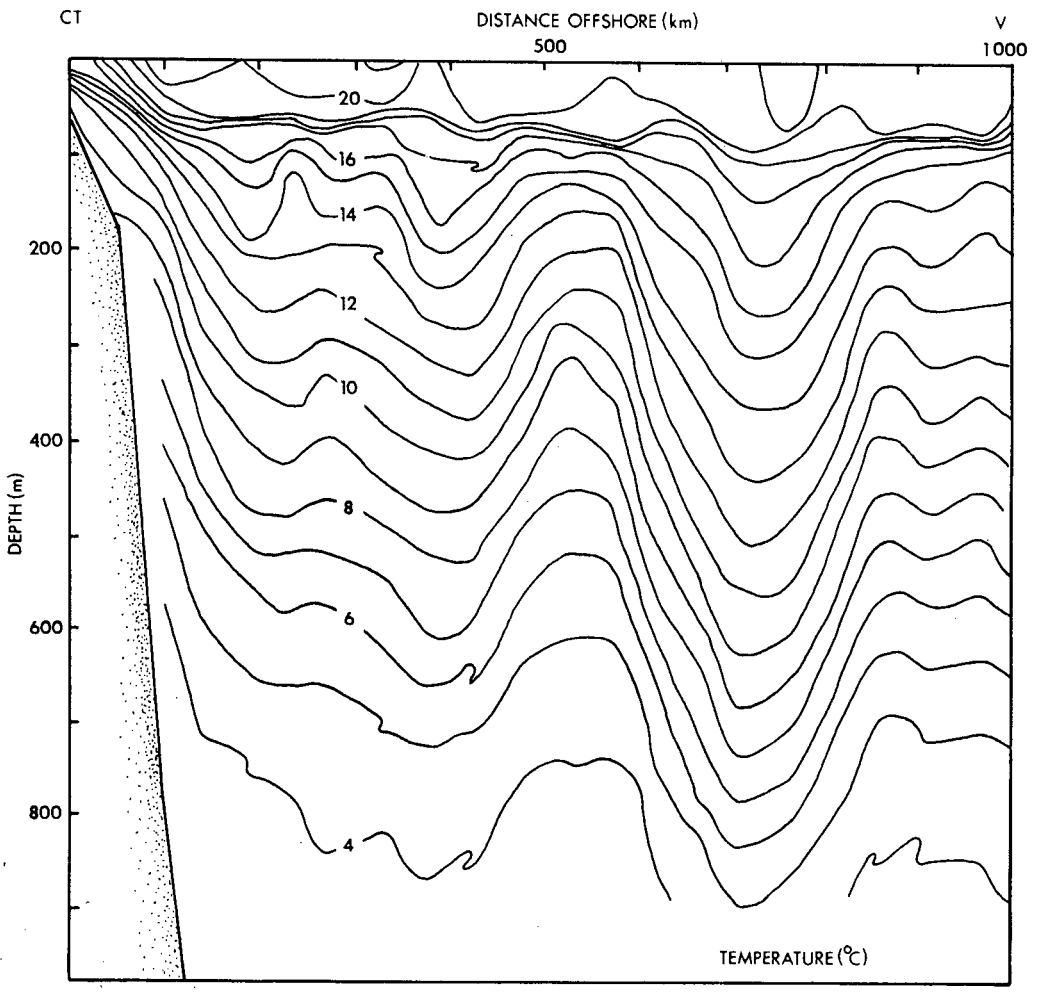

Fig. 4. Vertical temperature section derived from XBT measurements taken from F.R.S. *Africana* in April 1989 on a cruise between Cape Town (CT) and Vema Seamount (V).

Following OLSON *et al.* (1985) and OLSON and EVANS (1986), we plotted the regression of the depth of even-numbered isotherms (8, 10, 12, 14°C) with the geopotential anomaly (GPA) relative to 1150 db, the deepest CTD data available for all stations. The depth of the 10°C isotherm (h_{10}) gave the best fit ($r^2 = 0.982$) so that the GPA (D_{1150}) can be estimated from the relation

$$D_{1150} = 0.01513\ h_{10} + 7.7585.$$

Using Olson *et al.*'s two-layer model with $g' = 0.01513$ (standard error in g' of ± 0.0005) to obtain GPAs from the XBT traces, we could calculate the surface geostrophic velocities from both the CTD and XBT data. In spite of the good correlation between the depth of the isotherm and the GPA, the velocity distribution shows greater horizontal shear than one would expect from the distribution obtained from the CTD traces alone. This reflects

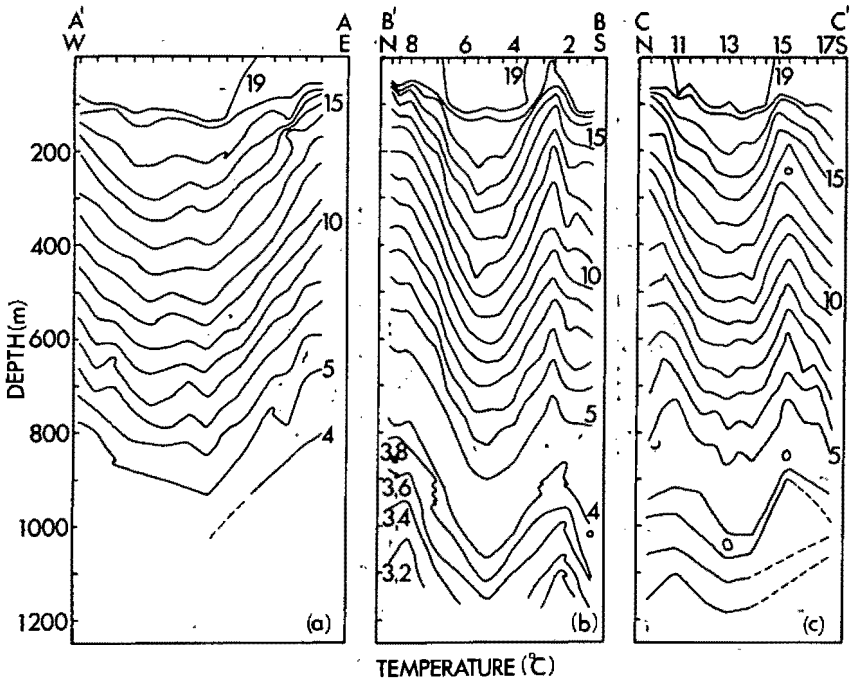

Fig. 5. Temperature sections from XBT and CTD measurements from R.S. *Benguela* in May 1989. (a) E–W XBT section A..A′, (b) S–N XBT and CTD section B..B′, (c) N–S XBT and CTD section C..C′ (see Figs 1 and 2 for cruise track details).

the greater detail evident in the temperature, and hence density, structure revealed by the XBT data.

Following Olson and Evans (1986) we plotted the depth of the 10°C isotherm (h_{10}) against the distance from the ring centre (d) and fitted a normal curve to the data ($h_{10} = h_\infty + a_1 \exp(a_2 d^2)$; where h_∞ is the depth of h_{10} far from the ring) to model the ring. Integrating over the model we obtained values of 38.8×10^{15} J for the available potential energy (APE) and 2.3×10^{15} J for the kinetic energy (KE) of the ring.

In order to determine water mass characteristics of the ring water, temperature–salinity (T–S) sections were compiled for all the stations. From these T–S diagrams it became clear that there was something very unusual about the NW corner of the first CTD transect (line B..B′, Stas 8 and 9). The salinity between depths of 50–150 m was much lower (35.2 psu) than that of the other edge stations. In other "edge" stations, this low salinity is normally found at about 200 m, and associated with a temperature of about 13.20°C.

Water with such characteristics ($T = 13.20$°C; $S = 35.2$ psu) is commonly found in the Benguela upwelling frontal region much closer inshore, and has recently been observed in a decaying filament off Lüderitz (Shillington *et al.*, 1990). The contrast between this low-salinity near-surface layer and the water in the centre of the ring is shown in the T–S diagram in Fig. 10. This water is evident in Fig. 6a as the low salinity (35.20 psu) 100 m thick layer from 50 to 150 m depth at the NW edge of the ring.

The only plausible explanation for this low salinity water being present in this region near the surface is that it is mature upwelled frontal water from the Benguela upwelling

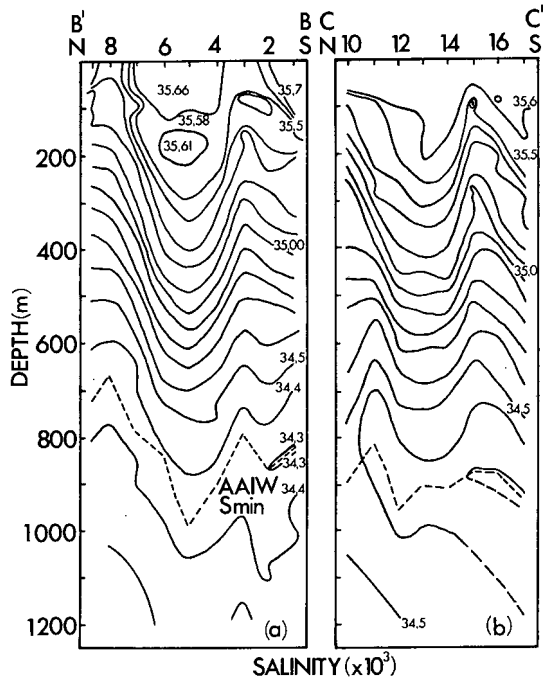

Fig. 6. Salinity sections for the two CTD transects across the ring: (a) S–N leg B'..B (Stas 1–9), (b) N–S leg C..C' (Stas 10–17). The mid-water salinity minimum (S_{min}) indicating Antarctic Intermediate Water (AAIW) is shown by the dotted line.

region (SHILLINGTON *et al.*, 1990), as confirmed in the NOAA satellite imagery of the cool filament surrounding the northern edge of the ring (Fig. 11).

(b) *Remote sensing*

1. *NOAA imagery*. The NOAA satellite image from 15 June 1989 shows the origin of the anomalous edge water described above to be a filament captured from the Benguela upwelling system (Fig. 11a). The ring was first observed in contact with the filament in satellite infra-red images from 24 and 30 April. From feature-tracking between the two images from 15 and 16 June 1989, velocity vectors were constructed on the perimeter of the ring showing anticyclonic motion with speeds up to a maximum of 70 cm s^{-1} to the north-east of the ring (Fig. 11b). Elsewhere speeds were of the order of 50 cm s^{-1}. At the base of the filament current speeds were of the order of 25 cm s^{-1}. The filament was 50 km wide and 550 km long, extending from the edge of the Benguela upwelling front. The water within the filament originated in the current associated with the upwelling front (AGENBAG, submitted).

2. *GEOSAT altimetry*. From the snapshot pictures obtained from the GEOSAT altimeter data, a region of elevated sea surface can be identified in the region of the Agulhas retroflection, to the south-west of Cape Town. This region remains relatively static over several cycles, within a few hundred kilometres of the area marked "14 February" in the composite (Fig. 12). On the snapshot representing 1 March, a feature

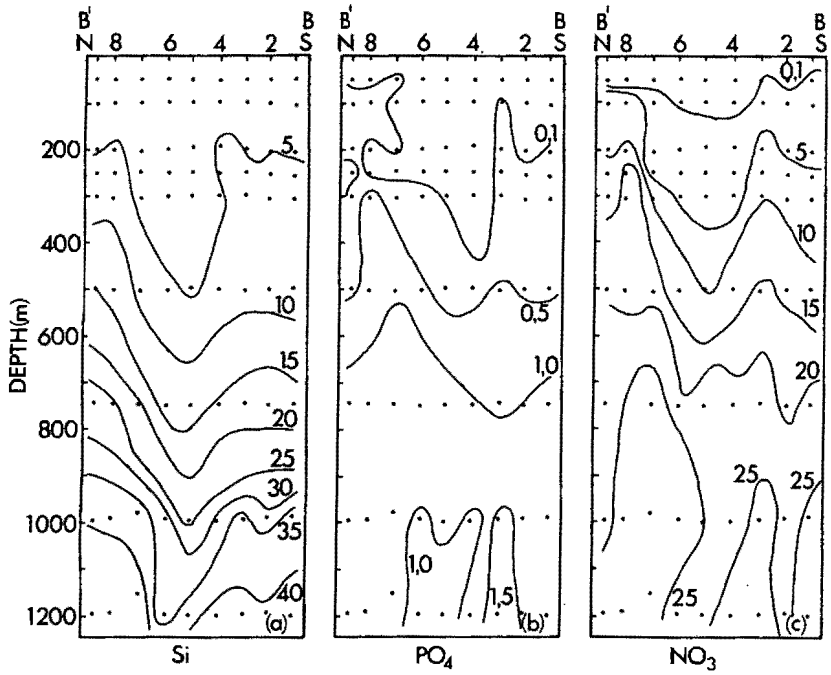

Fig. 7. Vertical nutrient sections for S–N leg B..B′ (Stas 1–9). (a) Silicate, (b) phosphate, (c) nitrate. Concentrations are in mmol l^{-1}.

of markedly greater elevation than the surroundings appears to bud off from this elevated region and moves north-westwards approximately along ascending ground track A158. The positions of this feature on 14 March and 14 April in the weekly snapshots are indicated.

No data were available after the end of April. This is unfortunate as the three sets of data (altimeter, hydrographic and infra-red) do not overlap in time to any great extent. However, some corroboration is obtained: the position of the ring centre on 6 April (determined by hydrography from the *Africana* XBT data) is in the same region as the sea surface elevation revealed by the altimeter data at about the same time (14 April). Using earlier altimeter data, the structure can be tracked back to the region of the Agulhas retroflection two months earlier (late January 1989).

The averaged altimeter data depict spatially smoothed sea surface elevations and are thus quite difficult to interpret if the features are of the same order of magnitude as the grid spacing of the satellite ground-track. It is easier to identify features and to follow their progress along individual tracks as sampled by the GEOSAT altimeter.

Along ascending pass A158 the ring appeared to move NW and can be seen (Fig. 13) in successive cycles 52, 53, and 54 (24 March–27 April). For this pass (A158), GEOSAT data are bad or missing for cycles 50 and 51 (before 24 March) and for cycles after 27 April 1989. The region of sea–surface elevation corresponding to the Agulhas retroflection is evident between 36°S and 38°S. The anticyclonic Agulhas ring is seen to move progressively equatorwards, as indicated by the dashed line in Fig. 13, at a speed of 6.8 cm s^{-1}. The sea surface elevation relative to the general background sea level (assumed to be 0 cm on Fig.

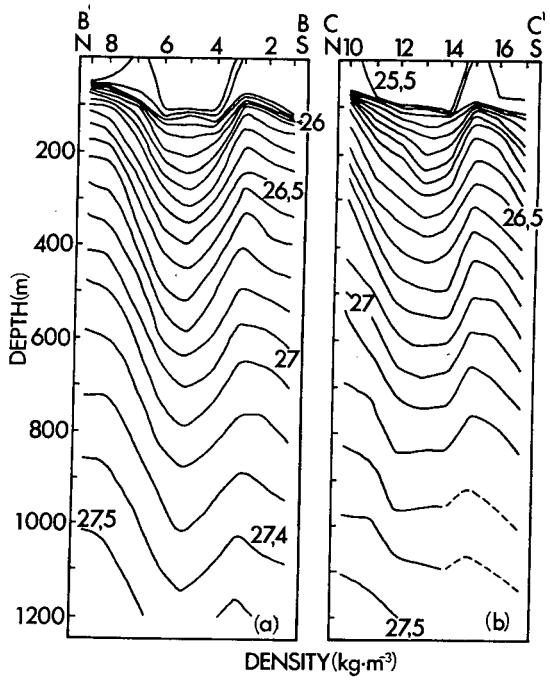

Fig. 8. Vertical potential density (σ_t) structure for the two CTD lines on the R.S. *Benguela* cruise: (a) Leg B..B′ (Stas 1–9). (b) Leg C..C′ (Stas 10–17). Units are kg m^{-3}.

13) was about 30 cm and the north–south diameter was between 200–300 km. Sea surface slopes were calculated from Fig. 13 to be 3.2×10^{-6}. From the geostrophic balance (e.g. GILL, 1982) this corresponds to speeds of 40 cm s^{-1}.

DISCUSSION

The general direction of translation of the ring, the NOAA imagery before the hydrographic cruises from January to May 1989 (DUNCOMBE RAE *et al.*, 1989) and the distribution of similar rings followed using satellite altimetry (GORDON and HAXBY, 1990) suggest that the ring originated at the Agulhas retroflection. This hypothesis has been confirmed from GEOSAT altimetry during and prior to the period of the cruises.

At the retroflection, Agulhas water with a temperature above 16°C is isohaline and less saline (35.6 psu) than the South Atlantic thermocline water. The ring centre exhibited two isohaline layers: one of 35.66 psu with temperature greater than 19°C near the surface and another of 35.61 psu with a temperature of 17.5°C at 150 m (Fig. 6a). Water in the surrounding South Atlantic had a salinity greater than 35.7 psu at temperatures greater than 17°C. The more saline water of the ring centre near the surface could be due to evaporation increasing the salinity in the wind mixed layer.

These features confirm the Agulhas origin of the ring. Further confirmation of the Agulhas origin of the ring is given by the sections of silicate, phosphate and nitrate which show the concentrations of these nutrients to be depressed relative to the surrounding water (Fig. 7).

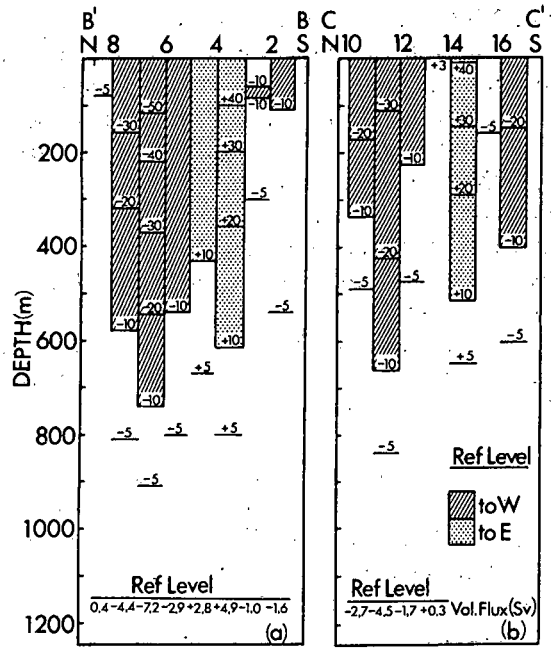

Fig. 9. Vertical geostrophic velocity structure for the two CTD lines on the R.S. *Benguela* cruise: (a) Leg B..B′ (Stas 1–9). (b) Leg C..C′ (Stas 10–17). The reference depth level for each station pair is indicated. Below the reference level the volume flux in Sverdrup (1 Sv = 10^6 m^3 s^{-1}) is indicated.

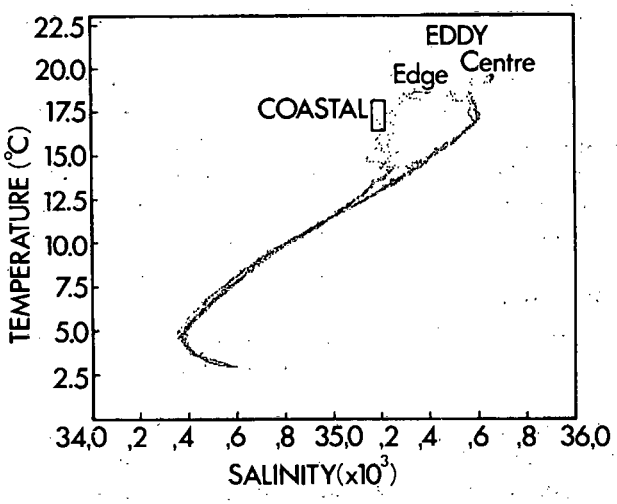

Fig. 10. Temperature–salinity (T–S) diagram for stations representative of the centre of the ring (5 and 6 on leg B..B′) and of the NW edge of the ring (Stas 8 and 9 on leg B..B′). Typical surface Benguela frontal water (SHILLINGTON *et al.*, 1990) is boxed and indicated as "COASTAL". The apparent splitting of the thermocline water between 5° and 10°C is not related to the salinity differences near the surface.

From the two measured XBT sections (one from the F.R.S. *Africana* and the other from the R.S. *Benguela*) we inferred that the ring translated 230 km in 42 days. The measurements give a velocity of 6.4 cm s^{-1} in a northwesterly direction. An error of 50 km in the first ring location (e.g. due to the first transect not exactly bisecting the ring) would imply an uncertainty in the speed estimate of about 1 cm s^{-1}. From the GEOSAT altimetry data presented in Fig. 13, the ring is seen to move 200 km in 34 days, a speed of 5.9 km day^{-1} (6.8 cm s^{-1}) immediately prior to the *Africana* cruise, which is in good agreement with the speed deduced from the hydrographic data.

CUSHMAN-ROISIN *et al.* (1990) show theoretically that rings of the dimension seen here should have a westward translation of some 2 cm s^{-1} due to the planetary beta effect. (They use a one-moving-layer model for their main result, and in attempts to generalize to a two-layer system, suggest that there will be an additional equatorward component.) OLSON and EVANS (1986) obtained theoretical westward values of 1.6 and 2.1 cm s^{-1} for the rings they studied, while observed westward values were 7.5 and 3.8 cm s^{-1}. Our theoretical westward translation is consistent with these results (2.1 cm s^{-1}, calculated following NOF (1981) and FLIERL (1984)). The observed westward component was 2.1 cm s^{-1} calculated between the ring positions in May and June. Although this is similar to the theoretical value, extrapolating back to the retroflection region requires the use of a higher value of the westward velocity. Note that OLSON and EVANS (1986) also observed drift speeds higher than the theoretically determined values.

The speed obtained from observations for the ring reported here implies that the background flow must be an important additional effect to drive the ring in a northwesterly direction at a speed three times the theoretical rate. The only other known case of an Agulhas ring drifting along a very similar path to the one taken by the ring discussed here is described in detail by GORDON and HAXBY (1990). They described a ring which GEOSAT data showed was moving at 8.4 cm s^{-1}. The continuation of the ring path described by GORDON and HAXBY (1990) has been evaluated from subsequent GEOSAT data by WAKKER *et al.* (1990a). They found the ring had a mean speed of 4 cm s^{-1} and stalled somewhat as it passed over the Walvis Ridge. Most rings observed recently in the South Atlantic (e.g. OLSON and EVANS, 1986; GORDON and HAXBY, 1990; WAKKER *et al.*, 1990a) have a more westerly direction. OLSON and EVANS (1986) found the speed of translation from drifter data for the two rings they observed to be 4.8 and 8.5 cm s^{-1}.

DUNCOMBE RAE *et al.* (1989) calculated that the heat loss of the upper mixed layer to the atmosphere between the XBT temperature sections from the two cruises was of the order of 1.8×10^{19} J. (The time between the sections was 42 days.) This is consistent with an estimated heat loss of 80 W m^{-2}, which is considered to be the climatic mean for this region (HÖFLICH, 1984). DUNCOMBE RAE *et al.* (1989) also estimated that the volume flux of the ring per annum was about 1.2×10^6 m^3 s^{-1} per ring per year, whilst the ring injected a heat energy flux of 2×10^{14} J s^{-1} and excess salt amounting to 2×10^{13} kg into the South Atlantic.

In addition to the thermal energy input we have calculated the APE and KE associated with this ring (38.8 and 2.3×10^{15} J, respectively). These values are of the same order as those obtained for similar rings by OLSON and EVANS (1986) and also an order of magnitude greater than similar Gulf Stream rings. The kinetic energy of the ring under consideration here is slightly lower, suggesting that some of this energy has already been lost by friction to the South Atlantic, due to the longer time elapsed since shedding from the Agulhas.

(a)

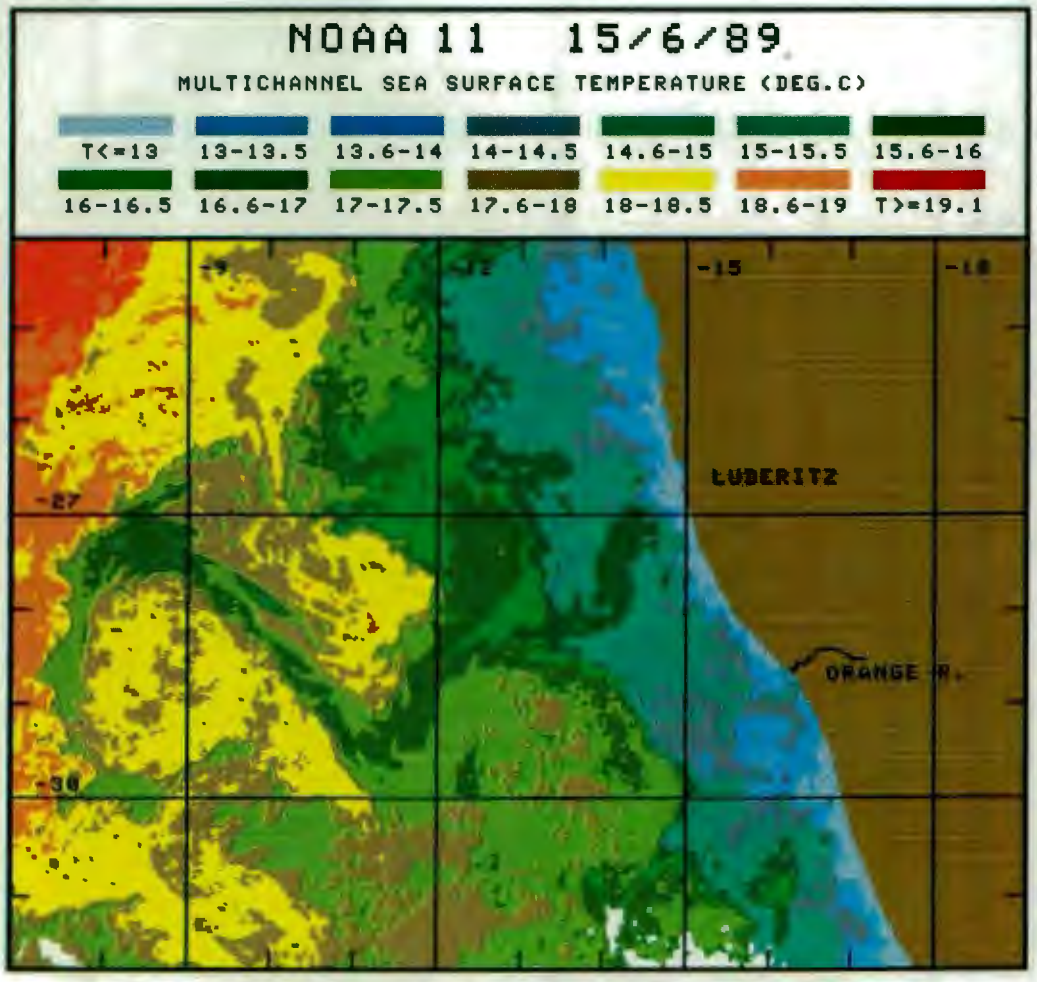

Fig. 11. (a) NOAA-11 multichannel sea surface temperatures for 15 June 1989 showing the extent of the filament drawn in from the Benguela system and the relationship of the ring with the coast. (b) NOAA-11 single channel infra-red image for 15 June 1989 with surface current vectors from feature tracking with two images approximately 24 h apart.

(b)

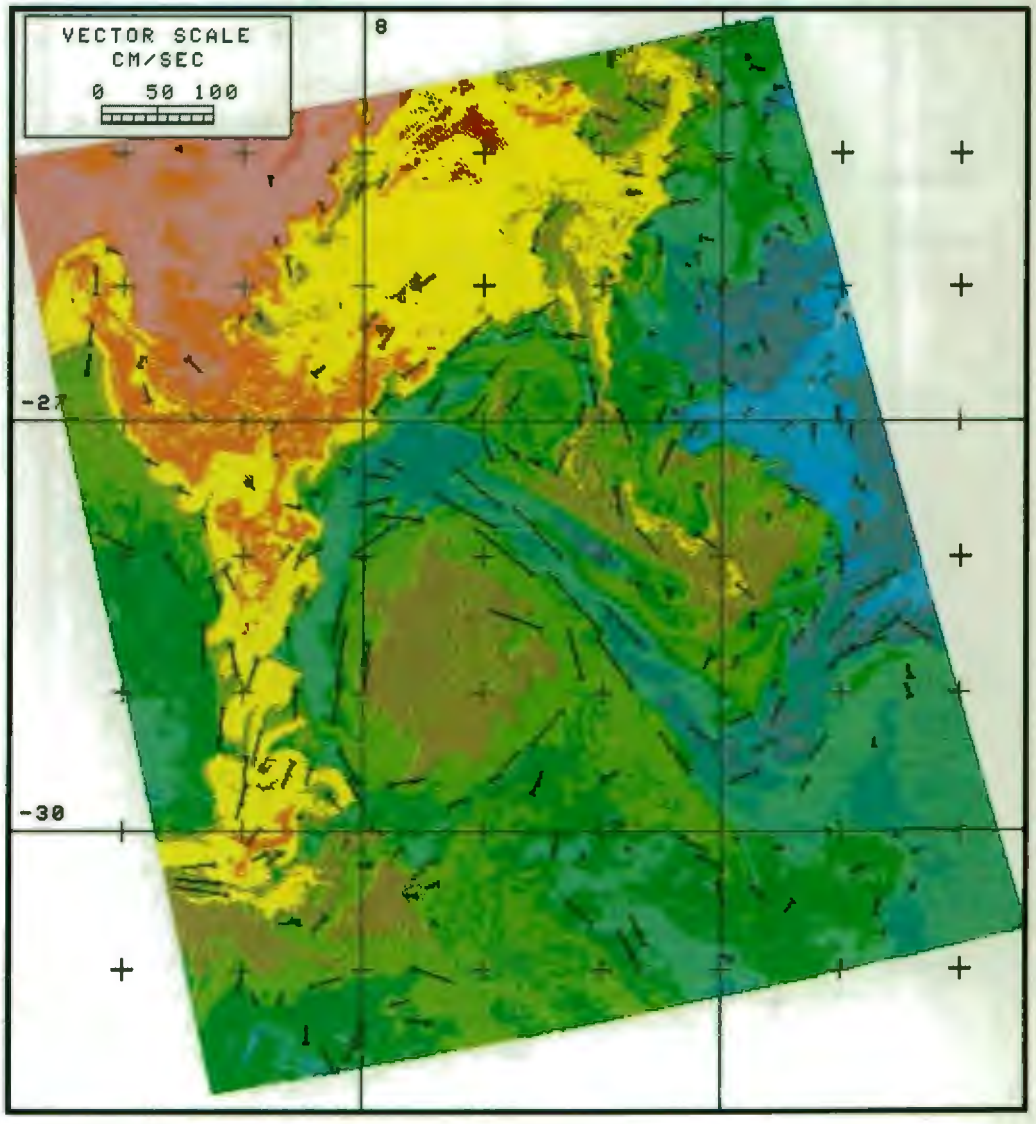

Fig. 11. *Continued.*

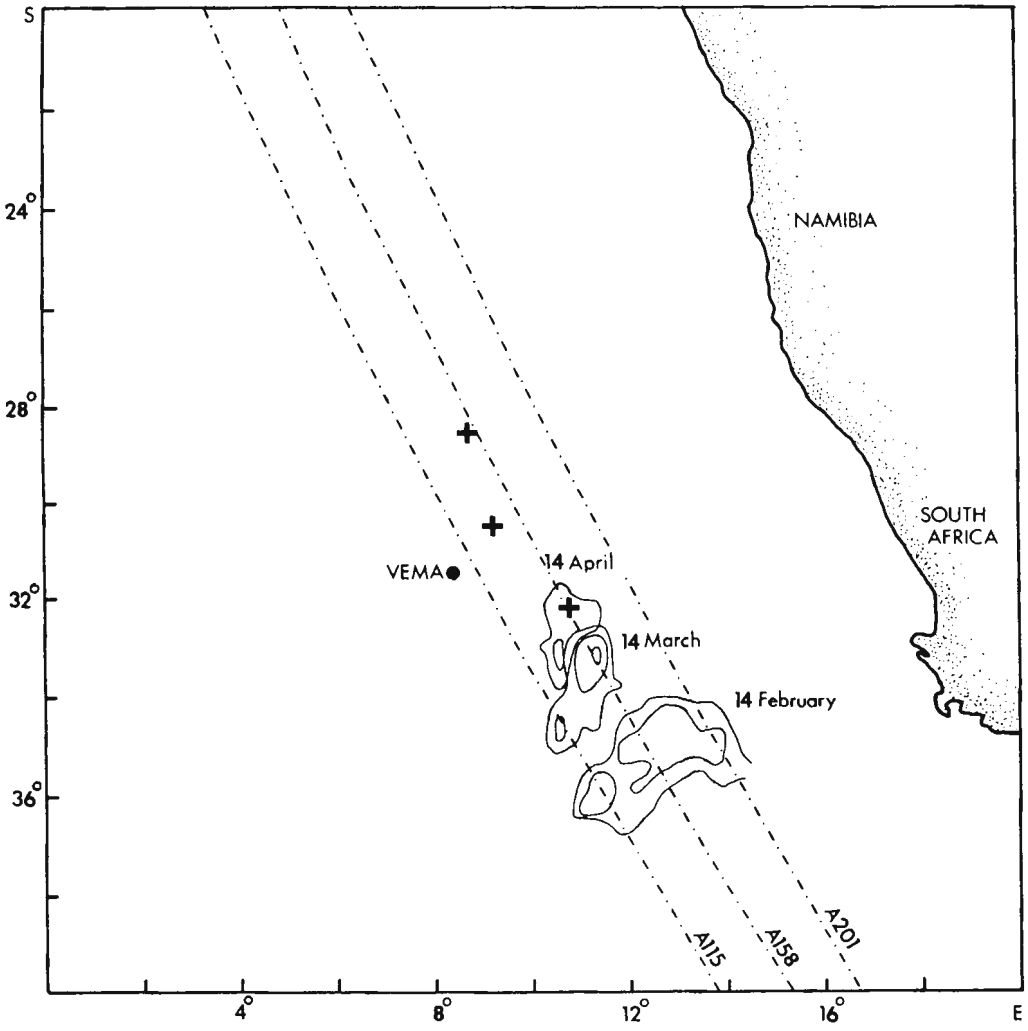

Fig. 12. Composite of snapshot sea elevations from mid-February to mid-April. Contours less than 20 cm and elevations away from the features of interest have been omitted. The relevant ascending satellite ground track over the ring path (A158) is marked. Adjacent ground-tracks (A115, A201) are shown to indicate ground-track spacing. The approximate positions of the ring centre on 6 April and 20 May determined by hydrography and on 15 June by NOAA imagery are indicated by crosses. A dot indicates Vema Seamount.

Of considerable interest to fisheries and biological applications is the apparent connection between the ring and the Benguela upwelling front. Coastal upwelling zones are well-known features of eastern boundary currents (SHANNON, 1985). Large volumes of cool deep water are transported away from the coast, often in the form of narrow filaments or jets extending perpendicular to the coast (FLAMENT *et al.*, 1985). In the Benguela region, LUTJEHARMS *et al.* (1991) have identified several extremely long filaments extending hundreds of kilometres from the coast, allowing interaction with passing rings.

We have two sources of information which reveal that the ring entrained mature

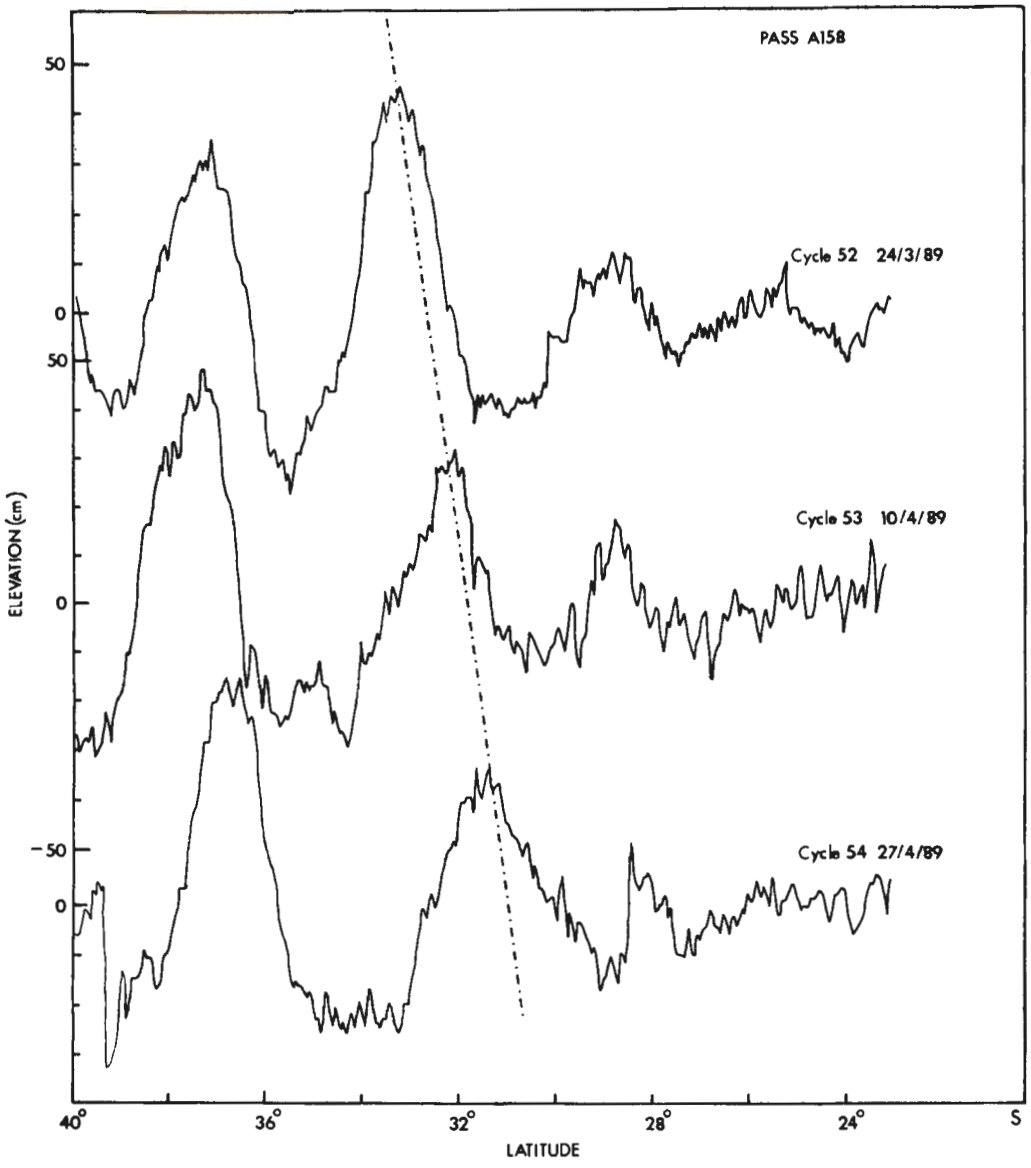

Fig. 13. Along-track elevations from three successive cycles (52, 53, 54) along pass A158 in March and April 1989. The progress of the sea surface elevation corresponding to the ring is indicated by the dashed line.

upwelled water from the Benguela front. The first is the NOAA-11 satellite imagery both before and after the CTD transects (24 and 30 April 1989, not shown, and 15 June 1989, Fig. 11), and the second is the appearance of low salinity (35.2 psu) water at the NW corner of the CTD transect (Stas 8 and 9). Referring first to the satellite imagery from 15 June 1989 (Fig. 11a), it can be seen that a cool filament of surface water with a temperature of 16.6–17°C had been entrained by the ring. Using feature-tracking (AGENBAG and SHANNON, 1988), surface velocity vectors of the order of 50 cm s^{-1} were derived in the vicinity of

the cool filament and the outer edge of the ring (Fig. 11b). The low salinity water (35.2 psu) in Stas 8 and 9 between 50 and 150 m can be satisfactorily explained by noting that SHANNON (1985) found a salinity minimum of 35.2 psu for T–S curves in the region 20°–30°S, 7°–18°E in the upper surface layer near the coast.

SHILLINGTON *et al.* (1990) reported that the filament they investigated (26°S, 12.5°E) had surface water with temperatures of 13° to 18°C and a salinity of 35.2 psu (between 0 and 130 m). The westward extremity of their filament extended to 27°S, 12°E, some 340 km east of the centre of the ring being discussed here, or 160 km north of the base of the filament entrained by the ring (Fig. 11a). Unfortunately we have no simultaneous T–S measurements from the Benguela frontal region at the time of these cruises, but from the evidence presented above, the source region of the low salinity water is assumed to be the Benguela frontal region.

Assuming that the filament is continuous around the ring, its length is approximately 1000 km. If the entire volume of water (5×10^{12} m^3) within this annulus 50 km wide, 300 km diameter and 100 m deep, has its origin in the current associated with the Benguela upwelling front, the possible effects on the Benguela ecosystem could be profound. The shelf-edge frontal jet is responsible for the transport of eggs and larvae from the spawning grounds of certain species to their nursery areas along the west coast of South Africa. Removal of these larvae from the ecosystem by the ring may be detrimental to the commercial fisheries of these species as suggested by DUNCOMBE RAE *et al.* (1992).

To judge the significance of this interaction with the Benguela ecosystem, we need to know the frequency of the juxtaposition of rings with the Benguela upwelling front. Although it is difficult to determine how often this interaction with passing rings occurs, GORDON and HAXBY's (1990) data from a ring in a similar location in 1987 (about 250 km further west) show no obvious entrainment of Benguela upwelling frontal water by the ring. On the other hand, LUTJEHARMS *et al.* (1991) discuss other extended filaments from the Benguela upwelling front and suggest that at least some of these extreme extensions are caused by Agulhas rings.

Acknowledgements—Discussions on drafts of this paper with colleagues at the University of Cape Town and the Sea Fisheries Research Institute, particularly Geoff Brundrit of U.C.T., were very helpful. We are grateful to the Captains and crews of the F.R.S. *Africana* and the R.S. *Benguela* for assistance in obtaining the data. Parts of this research were supported by the Foundation for Research Development and the Benguela Ecology Programme. Ships' time was made available by the Department of Environment Affairs (DEA, SFRI).

REFERENCES

AGENBAG J. J. A procedure for the computation of sea-surface advection velocities from satellite thermal band imagery, with application to the south-east Atlantic Ocean. Unpublished Ph.D. Thesis, University of Cape Town, 394 pp.

AGENBAG J. J. and L. V. SHANNON (1988) A suggested physical explanation for the existence of a biological boundary at 24°30′S in the Benguela system. *South African Journal of Marine Science*, **6**, 119–132.

BANG N. D. (1970) Dynamic interpretations of a detailed surface temperature chart of the Agulhas Current retroflexion and fragmentation area. *South African Geographical Journal*, **52**, 67–76.

BENNETT S. L. (1988) Where three oceans meet: the Agulhas retroflection region. Unpublished Ph.D. Thesis, MIT/WHOI, WHOI-88-51, xxvii + 367 pp.

BOUDRA D. B. and E. P. CHASSIGNET (1988) Dynamics of Agulhas retroflection and ring formation in a numerical model. I. The vorticity balance. *Journal of Physical Oceanography*, **18**, 280–303.

CHAPMAN P., C. M. DUNCOMBE RAE and B. R. ALLANSON (1987) Nutrients, chlorophyll and oxygen relationships in the surface layers at the Agulhas Retroflection. *Deep-Sea Research*, **34**, 1399–1416.

CHASSIGNET E. P. and D. B. BOUDRA (1988) Dynamics of Agulhas retroflection and ring formation in a numerical model. II. Energetics and ring formation. *Journal of Physical Oceanography*, **18**, 304–319.

CUSHMAN-ROISIN B., E. P. CHASSIGNET and B. TANG (1990) Westward motion of mesoscale eddies. *Journal of Physical Oceanography*, **20**, 758–768.

DUNCOMBE RAE C. M., L. V. SHANNON and F. A. SHILLINGTON (1989) An Agulhas ring in the South Atlantic ocean. *South African Journal of Science*, **85**, 747–748.

DUNCOMBE RAE C. M., A. J. BOYD and R. J. M. CRAWFORD (1992) "Predation" of anchovy by an Agulhas ring: a possible contributory cause of the very poor yearclass of 1989. In: *Benguela trophic functioning*, A. I. L. PAYNE, K. H. BRINK, K. H. MANN and R. HILBORN, editors, *South African Journal of Marine Science*, **12**,163–167.

FLAMENT P., L. ARMI and L. WASHBURN (1985) The evolving structure of an upwelling filament. *Journal of Geophysical Research*, **90**, 11765–11778.

FLIERL G. R. (1984) Model of the structure and motion of a warm-core ring. *Australian Journal of Marine and Freshwater Research*, **35**, 9–23.

GILL A. E. (1982) *Atmosphere–ocean dynamics*. Academic Press, London, 662 pp.

GORDON, A. L. (1985) Indian–Atlantic transfer of thermocline water at the Agulhas retroflection. *Science*, **227**, 1030–1033.

GORDON A. L. (1986) Interocean exchange of thermocline water. *Journal of Geophysical Research*, **91**, 5037–5046.

GORDON A. L. and W. F. HAXBY (1990) Agulhas eddies invade the South Atlantic: evidence from Geosat altimeter and shipboard conductivity–temperature–depth survey. *Journal of Geophysical Research*, **95**, 3117–3125.

GORDON A. L., J. R. E. LUTJEHARMS and M. L. GRÜNDLINGH (1987a) Stratification and circulation at the Agulhas retroflection. *Deep-Sea Research*, **34**, 565–599.

GORDON A. L., J. R. E. LUTJEHARMS and M. L. GRÜNDLINGH (1987b) *Select hydrographic sections from the Agulhas research cruises of the research vessels* Knorr *and* Meiring Naude—1983. Technical Report LDGO-87-1, Lamont-Doherty Geological Observatory Columbia University, N.Y., 28 pp.

HARRIS T. F. W. and D. VAN FOREEST (1978) The Agulhas Current in March 1969. *Deep-Sea Research*, **25**, 549–561.

HÖFLICH O. (1984) Climate of the South Atlantic ocean. In: *Climates of the oceans*, *World Survey of Climatology*, Vol. 15, H. VAN LOON, editor, Elsevier Science Publishers, pp. 1–191.

LEWIS L. (1990a) Satellite Altimetry Data System (SADS). Part 1: The design of SADS. *Council for Scientific and Industrial Research, South Africa*, Report EMA-T 8905/01, 15 pp.

LEWIS L. (1990b) Satellite Altimetry Data System (SADS). Part 2: Programmers reference manual. *Council for Scientific and Industrial Research, South Africa*, Report EMA-T 8905/02, 40 pp. plus source code listing.

LEWIS L. and U. V. ST ANGE (1990) Satellite Altimetry Data System (SADS). Part 3: User's manual. *Council for Scientific and Industrial Research, South Africa*, Report EMA-T 8905/03, 20 pp.

LUTJEHARMS J. R. E. (1987) Die subtropiese konvergensie en Agulhasretrofleksievaart (SCARC). *South African Journal of Science*, **83**, 454–456.

LUTJEHARMS J. R. E. and A. L. GORDON (1987) Shedding of an Agulhas ring observed at sea. *Nature*, **325**, 138–140.

LUTJEHARMS J. R. E., F. A. SHILLINGTON and C. M. DUNCOMBE RAE (1991) Observations of extreme upwelling filaments in the South East Atlantic Ocean. *Science*, **253**, 774–776.

LUTJEHARMS J. R. E. and R. C. VAN BALLEGOOYEN (1988) The Retroflection of the Agulhas Current. *Journal of Physical Oceanography*, **18**, 1570–1583.

MCCARTNEY M. S. and M. E. WOODGATE-JONES (1991) A deep-reaching anticyclonic eddy in the subtropical gyre of the eastern South Atlantic. *Deep-Sea Research*, **38**, S411–S443.

MOSTERT S. A. (1983) Procedures used in South Africa for the automatic photometric determination of micronutrients in sea-water. *South African Journal of Marine Science*, **1**, 189–198.

NOF D. (1981) On the β-induced movement of isolated baroclinic eddies. *Journal of Physical Oceanography*, **11**, 1662–1672.

OLSON D. B. and R. H. EVANS (1986) Rings of the Agulhas current. *Deep-Sea Research*, **33**, 27–42.

OLSON D. B., R. W. SCHMITT, M. KENNELLY and T. M. JOYCE (1985) A two-layer diagnostic model of the long-term physical evolution of Warm-Core Ring 82B. *Journal of Geophysical Research*, **90**, 8813–8822.

SHANNON L. V. (1985) The Benguela ecosystem. I. Evolution of the Benguela, physical features and processes. In: *Oceanography and marine biology. An annual review*, **23**, M. BARNES, editor, University Press, Aberdeen, pp. 105–182.

Shannon L. V., J. J. Agenbag, N. D. Walker and J. R. E. Lutjeharms (1990) A major perturbation in the Agulhas retroflection area in 1986. *Deep-Sea Research*, **37**, 493–512.

Shannon L. V., D. E. Pollock, P. Chapman and A. A. Robertson (1989) South-east Atlantic expedition of R.S. *Africana*. April 1989: Some preliminary results. *South African Journal of Science*, **85**, 665–669.

Shillington F. A., W. T. Peterson, L. Hutchings, T. A. Probyn, H. N. Waldron and J. J. Agenbag (1990) A cool upwelling filament off Namibia, southwest Africa: preliminary measurements of physical and biological properties. *Deep-Sea Research*, **37**, 1753–1772.

Wakker K. F., M. C. Naeije, R. Scharroo and B. A. C. Ambrosius (1990a) Extraction of mesoscale ocean current information from GEOSAT altimeter data. *Proceedings of the Space and Sea Colloquium, Paris*, 24–26 *September* 1990, ESA SP-312, 221–226.

Wakker K. F., R. C. A. Zandbergen, M. C. Naeije and B. A. C. Ambrosius (1990b) Geosat altimeter data analysis for the oceans around South Africa. *Journal of Geophysical Research*, **95**, 2991–3006.